CNRS
Centre National de la Recherche Scientifique

INFN
Instituto Nazionale di Fisica Nucleare

Calibration status in September 2009

L. Rolland

VIR-0576A-09

October 13, 2009

VIRGO * A joint CNRS-INFN Project
Project office: Traversa H di via Macerata - I-56021 S. Stefano a Macerata, Cascina (PI)
Secretariat: Telephone (39) 50 752 521 – Fax (39) 50 752 550 – e-mail virgo@pisa.infn.it

Contents

1 Introduction

This note gives the status of the Virgo calibration in September 2009 for the first months of VSR2. The calibration data were taken during the week before the run, from June 29th to July 3rd 2009, and during the run to monitor the parameter stability. The calibration period is from GPS 930290000 to 937000000.

2 Dark fringe sensing

A synoptic of the general sensing of the dark fringe channels is shown in the figure 1. The laser beam is sensed through photodiodes. Their signals are sent through a pre-amplifier and demodulated before being digitized in an ADC board. The raw signals are then directly sent to the DAQ to be stored in the data. Some processing is computed in the Pr process to generate channels sent to the DAQ and stored in the data.

Different channels are used at the level of the dark fringe sensing:

- $Pr\_B1p\_\{d1,d2\}\_\{DC,ACp,ACq\}$ raw channels, sampled at 20 kHz without emphasis filter, are used to reconstruct ΔL in free swinging Michelson data. They are the base for the actuation calibration.
- Pr_B1_ACp channel, sampled at 20 kHz without emphasis filters. It is the reference for the timing of the dark fringe channels.
- $Pr\_B1\_ACp\_40K$ channel, sampled at 40 kHz with emphasis filters. The raw channels $Pr_B1_d\{2,3\}_ACp_40K$are planned to be used in the h(t) reconstruction.

Their differences are highlighted in the following sections.

The timing has been computed from the time series stored in FrVect objects setting the value of sample i at the time $startX[0]+i\times dx[0]$ where $startX[0]$ is the time of the beginning of the FrVect and $dx[0]$ is the sampling period.

2.1 Pr_B1_ACp channels

The sensing and timing of the raw channels $Pr\_B1\_d\{2,3\}\_ACp$ are first studied. The sensing of the combined channel Pr_B1_ACp is then discussed.

2.1.1 Readout of the raw channels $Pr\_B1\_d\{2,3\}\_ACp$

The readout of the raw channels $Pr\_B1\_d\{2,3\}\_ACp$, sampled at 20 kHz, are done through the following path, without emphasis filters:

- photodiode sensing,

- demodulation electronics (analog),
- digitization by an ADC. The ADC board has an analog filter (a 6th order Butterworth filter cutting at 100 kHz, in the so-called mezzanine) which induces a measured delay of $(6 \pm 0.5)\,\mu$s. The signal is then sampled at 800 kHz. An analog 8th order Butterworth anti-alias filter[1] ($f_0 = 7503.65$ Hz) is used before the signal is subsampled at 20 kHz, picking 1 sample over 40 (the last sample over the 40 of the window is kept).
- the DAQ where some delay can be adjusted before the data are stored: no delay is set for these channels[2].

The 8th order Butterworth filter is defined[3] as function of $s = \mathrm{j} \times \frac{f}{f_0}$ by:

$$H(s) = \frac{1}{(s^2 + 0,3902s + 1)(s^2 + 1,1111s + 1)(s^2 + 1,6629s + 1)(s^2 + 1,9616s + 1)} \quad (1)$$

The transfer function (TF) of the Butterworth filter for $f_0 = 7503.65$ Hz is shown in the figure 2.

For one filter i: $\frac{1}{s^2+\alpha_i s+1}$, the phase for $f << f_0$ is: $\phi_i \sim \arctan(\alpha_i \frac{f}{f_0}) \sim \alpha_i \frac{f}{f_0}$. It is proportionnal to f and can thus be approximated by a delay t_d^i: $\phi_i \sim 2\pi f t_d$ with $t_d = \frac{\alpha_i}{2\pi f_0}$. The phase of a 8th order Butterworth filter at low frequency is thus equivalent to a delay: $t_d \sim \sum_{i=0}^{3} t_d^i = \sum_{i=0}^{3} \alpha_i \frac{1}{2\pi f_0} \sim 108.7\,\mu$s for $f_0 = 7503.65$ Hz.
The delay equivalent to the phase of the TF is shown in the figure 2 and agrees with the expectation: below 2 kHz, the Butterworth filter is equivalent to a pure delay of (109 ± 1) μs.

2.1.2 Measurement of the delay of the sensing of $Pr\_B1\_d\{2,3\}\_ACp$

In this section, the delay introduced by the Virgo timing system, ADC board and DAQ on the dark fringe readout related to the absolute GPS time is estimated.

The estimation is based on the measurement of the delay between the frame start and the time of the 1 PPS signal generated by the GPS receiver and sampled in the same ADC board as the dark fringe channels. The estimation principle is the following:

- measurement of the delay when the data are sampled at 800 kHz, without the effects of the Butterworth filter nor the subsampling. The measurements are compared to the expected delay in order to estimate the systematic errors. Such measurements are used as the absolute timing calibration.

[1] The Butterworth frequency is set such that the signal is attenuated by a factor 10 at half the sampling frequency, i.e. at 10 kHz.

[2] The DAQ PAGE_DELAY parameter is set to -50 μs but it has no effect on the 20 kHz channels, see data from logbook entry 24634.

[3] Also as function of $S = \mathrm{j} \times \Omega$, the Butterworth is a cascade of 4 filters defined as $\frac{a_2 \times S^2 + a_1 \times S + a_0}{b_2 \times S^2 + b_1 \times S + b_0}$ with $(a_2, a_1, a_0\,;\, b_2, b_1, b_0)$ being $(0, 0, 1; 4.499 \times 10^{-10}, 8.276 \times 10^{-6}, 1)$, $(0, 0, 1; 4.499 \times 10^{-10}, 2.357 \times 10^{-5}, 1)$, $(0, 0, 1; 4.499 \times 10^{-10}, 3.527 \times 10^{-5}, 1)$, $(0, 0, 1; 4.499 \times 10^{-10}, 4.161 \times 10^{-5}, 1)$.

- measurement of the delay with the data sampled at 20 kHz after a 8th order Butterworth filter. The systematic effects of the digital processing are reproduced offline: they can be accounted for. Such measurements are used as a monitoring of the delay.

Measurement setup - A monitoring system of the delay induced by the sensing of the raw channels $Pr\_B1\_d\{2,3\}\_ACp$ has been setup on July 21st 2009 (logbook entry 23852). A synoptic of the installation is given in the figure 3. The 1 PPS signal generated by a receiver GPS is sent to the main Timing Distibution Box (TDBox) and then sent through an optical fiber to the of the detection crate TDBox. The propagation time of the 1 PPS signal is estimated to less than 200 ns (53 ns in the two TDBox and ~ 100 ns in the optical fiber). The 1 PPS signal is sent to a ramp generator [1][4] through a BNC cable : a ramp is generated at each pulse and then sampled by the same ADC used for the $Pr\_B1\_d\{2,3\}\_ACp$ readout at 20 kHz. The ramp generation introduces a delay of 50 ns to 80 ns. The ADC output is then sent to the DAQ and stored in the data. The 1 PPS signal is sent to the ADC short after its generation by the GPS receiver (< 500 ns): it thus tags the absolute GPS time.

The delay between the start of the frame and the start of the readout ramp signal permits to measure the absolute delay of the acquisition path.

Ramp sampled at 800 kHz without Butterworth filter: results - An example of such a 800 kHz digitized ramp[5] is shown in the figure 4(a) along with the fitted line[6]. In order to avoid border effects, the line is fitted excluding the first 10% of the ramp (in amplitude) and excluding 40 μs of data before the maximum of the ramp. The pedestal (level without ramp) is estimated from 10 ms of data on each side of the ramp exluding the first 2 ms before and after the ramp. The intersection between the fitted line and the pedestal level determines the time of the pulse as stored in the data. The difference between this time and the start of the frame gives the delay introduced by the ramp readout and timing system. The distribution of the measured delays shows that the ramp readout introduces a delay of -113.6 ± 0.05 μs.

On the same data, only the beginning of the ramp has been fitted as shown in figure 4(b) (excluding only the first 0.1% of the ramp in amplitude and excluding 400 μs of data before the maximum of the ramp). Such analysis results in a delay of -111.1 ± 0.05 μs. Looking at the start of the ramp, as in figure 4(c), one can see that the start of the fitted ramp looks properly determined within one sample (1.25 μs) since the ramp is slightly distorted at the beginning

[4] Two ramps are observed (see figure 6). This is due to the duration of the 1 PPS pulse which is longer than the ramp duration. The ramp generator is thus triggered a second time. Only the first ramp gives information about the 1 PPS start time.

[5] GPS 938790930, for 10 minutes (October 5th, 2009, 15h15m20s UTC).

[6] The samples from the time-serie FrVect are stored in a TGraph from ROOT at the time of the sample i: $startX[0] + i \times dx[0]$. It results an offset of half a sample (25 μs) from the same fits performed from dataDisplay since there TH1 histograms are used, with the bin center placed in-between two samples. Fitting plots from dataDisplay, delays of ~ 70 μs are found.

due to the ramp genrator itself and/or the ADC board analog anti-alias filter. The check of the fit using the zoomed plot close to the start of the ramp gives more confidence in this last measurement.

As a conclusion, the delay from the ramps sampled 800 kHz without Butterworth filter is estimated to -111 μs, with systematic erors of the order of 3 μs.

Ramp sampled at 800 kHz without Butterworth filter: understanding of the measured delay - In this paragraph, the expected delay between the readout ramp signal and the frame is estimated after a brief description of the Virgo timing reference.

As shown figure 3, the timing system is based on the IRIG-B signal generated every second by the master GPS receiver and sent to the main TDBox [2]. It is then sent to the detection crate TDBox through an optical fiber. The lenght of the optical fiber has been adjusted such that the delay to all the buildings is the same: 16.041 μs. The IRIG-B signal is sent from the detection TDBox to the ADC through a RJ45 cable in order to synchronise the ADC clock every second.
It has been checked[7] that the 1 PPS signal and the IRIG-B signal are synchronised within ~ 100 ns at the GPS receiver output.

Compared to the IRIG-B signal that defines the Virgo timing, the 1 PPS signal, sampled at 800 kHz, sees:

- an advance of 16 μs due to the propagation time from the timing crate TDBOX to the detection crate TDBOX [2],
- the time to propagate the 1 PPS signal (~ 0.15 μs) and to generate of the ramp: ~ 0.1 μs,
- the delay from the ADC analog mezzanine[8]: 5.7 ± 0.2 μs,
- the delay from the DAQ[9]: -100 μs.

Their sum gives the expected delay: $-16+0.25+5.7-100 = -110 \pm 2$ μs. This is in agreement within better than 4 μs with the measurements. It gives an estimation of the timing systematic errors.

Note that the ramp generator might introduce some systematic errors of ± 2 μs due to some offset at the beginning of the ramp (see[1], p.14). The effect of such offset cannot be estimated

[7] by Alain Masserot

[8] For the $Ti\_1PPS\_GPSMaster$ signal, the delay introduced by the mezzanine number 83 has been measured to 5.68 ± 0.12 μs.

[9] It has been checked that the DAQ parameter $PAGE\_DELAY$ of -50 μs results in an advance of 100 μs on the 800 kHz channel.

from the data. It could be responsible for a part of the discrepancy between the measured and expected delay.

Ramp sampled at 20 kHz with Butterworth filter: results - When sampling the ramp signal at 20 kHz, the same 8th order Butterworth filter as for the dark fringe readout at 20 kHz is used in the ADC.

An example of such a 20 kHz digitized ramp[10] is shown in the figure 5(a) along with the fitted line. The same algorithm as previously described has been used to estimated the delay between the frame and the 1 PPS pulse. The distribution of the measured delays is shown in the figure 5(b): the ramp readout introduces a delay of $45.1 \pm 0.1\,\mu$s.

The ramp sampled at 20 kHz has 10 points. Only the 8 central points are used in the standard algorithm. Modifying it to use the first or the last 9 points, or to use all the 10 points results in measured delays between 41 μs and 50 μs.

Ramp sampled at 20 kHz with Butterworth filter: digital processing effect - In this paragraph, the effect of the digital processing is studied.

The ramp sampled at 800 kHz without Butterworth filter from previous paragraph has been used as an input for offline simulations of the ADC digital processing:

- the 800 kHz ramp has been passed through a 8th order Butterworth filter with $f_0 = 7503.65\,$Hz using SIESTA [3],
- the 800 kHz filtered ramp has been sub-sampled to 20 kHz, picking the last sample out of 40 (39th sammple, starting at 0),
- a delay of 100 μs has been added since the 800 kHz channel is advanced of 100 μs compared to the 20 kHz channel by the DAQ.

The ramps of the output 20 kHz signal has analysed as previously described to determine the delay between the frame and the start of the ramp.

A delay of 45.1 μs has been found, as in the raw data sampled at 20 kHz. This proves that the digital part of the ADC and DAQ processing is well understood.

The comparison of the data at 20 kHz to the data at 20 kHz computed offline from the 800 kHz data is shown figure 6. The offline computation reproduces properly the data: it confirms that the digital processing in the ADC (Butterworth filter and subsampling) is well understood.

[10] Standard configuration of channel $Ti\_1PPS\_GPSMaster$.

Ramp sampled at 20 kHz with Butterworth filter: understanding of the measured delay - In this paragraph, the expected delay between the readout ramp signal and the frame is estimated.

Compared to the IRIG-B signal that defines the Virgo timing, the 1 PPS signal, sampled at 20 kHz, sees:

- an advance of 16 μs due to the propagation time from the timing crate TDBOX to the detection crate TDBOX [2],
- the time to propagate the 1 PPS signal (~ 0.15 μs) and to generate of the ramp: ~ 0.1 μs,
- the delay from the ADC analog mezzanine: 5.7 ± 0.2 μs,
- the delay from the ADC anti-alias Butterworth filter: 109 ± 1 μs,
- the delay to subsample the signal from 800 kHz to 20 kHz: -48.75 μs (advance of 39 samples at 800 kHz),
- the delay from the DAQ[11]: 0 μs.

Their sum gives the expected delay: $-16 + 0.25 + 5.7 + 109 - 48.75 = 50.2 \pm 2$ μs. This is in agreement within 5 μs with the measurements. It gives an estimation of the systematic errors on the delay when using the channel sampled at 20 kHz.

Ramp sampled at 800 kHz and 20 kHz: discussion - It has been shown in the previous paragraphs that:

- the delay of the analogic part has been measured and is well understood, with systematic error below 4 μs.
- including the digital part, the systematic error seems to increase. Since the digital processing in the ADC board is well understood and reproduced offline, the additionnal delay discrepancy must not be taken into account.

To conclude, the delay of the dark fringe readout will be based on the measurements computed at 800 kHz -111 μs adding the delays from the well understood digital ADC and DAQ processing: $109 - 48.75 + 100 = 160.25$ μs. The delay of the dark fringe readout at 20 kHz is thus estimated to 49.25 with systematic errors of 4 μs.

[11] It has been checked that the DAQ parameter *PAGE_DELAY* of -50 μs has no effect on the 20 kHz channel.

Delay stability - The ramped 1 PPS signal is permanently digitized at 20 kHz and analysed online: the channel $TiMoni\_Ti\_1PPS\_GPSMaster\_t0$ contains the delay between the frame and the start of the ramp computed online. The estimated delay has systematic errors larger than 4 μs as shown above, but it can be used to monitor the time stability of the system. As shown in the figure 5(c), the monitored delay is stable within 0.2 μs from July 25rd to September 9th 2009.

Conclusion - Except for some analog electronics with negligible delays, the path used to read the 1 PPS ramped signal is the same as the one to read the dark fringe signals at 20 kHz. The total delay of the acquisition channel of the raw dark fringe signals at 20 kHz, $Pr\_B1\_d\{2,3\}\_ACp$, is thus estimated to 49.3 $\pm$ 4 μs.

2.1.3 Models of $Pr\_B1\_\{d2,d3\}\_ACp$ sensing

To conclude about the raw channel sensing, two models can be defined. They are given in the table 1.

Model up to 20 kHz - The readout of the $Pr\_B1\_\{d2,d3\}\_ACp$ channel up to 20 kHz can be modeled by:

- a 8th order Butterworth filter with frequency 7503.65 Hz,
- a delay of -59.7 ± 5 μs (49.3 – 109 μs)

Simple model up to 2 kHz - Considering this response only below $\sim$ 2 kHz, it can be modeled by a simple delay of 49.3 $\pm$ 4 μs as measured above.

2.1.4 The sensing of the Pr_B1_ACp dark fringe channel

The Pr_B1_ACp channel readout, at 20 kHz, is computed from the raw channels $Pr\_B1\_d\{2,3\}\_ACp$ taken at the output of the ADC:

- the signals from the two photodiodes are summed in the Pr process,
- a delay can be adjusted in the DAQ before the channel is stored in the data. This delay is set to compensate for the duration of the Pr process (100 μs).

The TF

$$\frac{Pr\_B1\_ACp}{0.000446 \times Pr\_B1\_d2\_ACp + 0.000538 \times Pr\_B1\_d3\_ACp}$$

(the gains are the same as used in the Pr process to compute Pr_B1_ACp) computed with data in step 12 is shown in the figure 2.6. As expected, no additionnal delay is found between Pr_B1_ACp and the raw channels. The same models as given in section 2.1.3 can thus be used for the sensing of Pr_B1_ACp.

2.2 The sensing of the channels $Pr\_B1p\_\{DC, ACp, ACq\}$

The Pr_B1p raw channels are used to reconstruct ΔL in free swinging Michelson data. The knowledge of its sensing is thus very important since it is included in the raw measurements of the mirror actuation TF and has to be subtracted to get the mirror actuation itself. Two photodiodes $d1$ and $d2$ are used to measure the Pr_B1p signals but their signals are not summed. The channels $Pr\_SW\_B1p\_DC$ and $Pr\_SW\_B1p\_AC$ indicate what photodiode is used to compute the channels $Pr\_B1p\_\{DC, ACp, ACq\}$: 0 means $d1$, 1 means $d2$.

2.2.1 The sensing of the raw channels $Pr\_B1p\_\{d1, d2\}\_\{DC, ACp, ACq\}$

The Pr_B1p raw channels ($d1$ and $d2$) are sampled at 20 kHz by the same ADC as the Pr_B1 raw channels at 20 kHz described in the section 2.1.3. A similar readout path is defined, also without emphasis filter. The same models can thus be defined (see table 2.1.3).

2.2.2 The sensing of the channels $Pr\_B1p\_\{DC, ACp, ACq\}$

Only one photodiode, $d1$ or $d2$, is used to compute the channels $Pr\_B1p\_\{DC, ACp, ACq\}$, depending on values of switches. The signal of the photodiode is subsampled to 10 kHz in the Pr process. The decimation is done averaging the current sample with the next one. This introduces a delay of the processed channel compared to the raw channel of -25 μs (advance).

The figure 8 shows different TFs (such as $\frac{Pr\_B1p\_DC}{Pr\_B1p\_d1\_DC}$) for the DC, ACp signals and for the $d1$ and $d2$ photodiodes during data in free swinging Michelson [12]. The DC signal is read through the $d1$ photodiode while the AC signals are read through the $d2$ photodiode. The phase of the TFs have been fitted by a delay of -25.0 μs, in agreement with the expectation[13].

2.3 $Pr\_B1\_ACp\_40k$ channels

The 40 kHz dark fringe channels are not used for the ITF control but are aimed to be used for the $h(t)$ reconstruction since they have more dynamic and should be less noisy due to the use of emphasis filters in their sensing.

2.3.1 The raw 40 kHz dark fringe channels $Pr\_B1\_d\{2, 3\}\_ACp\_40K$

The synoptic of the raw channels $Pr\_B1\_d\{2, 3\}\_ACp\_40K$ readout at 40 kHz is shown on the upper part of the figure 9. The signal processes through:

[12] Note that the same photodiodes are used in step 12. No delay between the raw channels and final ones was found in step 12 neither.

[13] Warning: this effect is lost when the 10 kHz channel Pr_B1p_DC is extended to 20 kHz copying each sample twice. Since the extension of the data introduces a delay of 25 μs, the phase of the TF is flat. This is what is done in dataDisplay (v9r12p7). When computing TFs between signals with different sampling rates, the FrVect extension was also done in the Cali module up to version v0r3p6

- photodiode sensing,
- demodulation electronics (analog),
- analog filter with a measured delay of $(8 \pm 0.5)\,\mu$s (in the mezzanine of the ADC board),
- analog emphasis filter (in the mezzanine of the ADC board),
- after digitization by the ADC at 800 kHz, 8th order Butterworth filter ($f_0 = 15007.3$ Hz),
- decimation to 40 kHz: pick-up of 1 sample over 20 (the last one),
- the DAQ where some delay can be adjusted: no delay is set for these channels.

For $f_0 = 15007.3$ Hz and below ~ 5 kHz, the Butterworth filter is equivalent to a pure delay of $(55 \pm 1)\ \mu$s.

When the ITF is in step 12, the photodiode signals are recorded in both channels $Pr\_B1\_d\{2,3\}\_ACp$ and $Pr\_B1\_d\{2,3\}\_ACp\_40K$ at 20 kHz and 40 kHz respectively as shown in the figure 9. Since they measure the signal from the same photodiode through two different electronics, the TF of

$$\frac{Pr\_B1\_d2\_ACp}{Pr\_B1\_d2\_ACp\_40K}$$

permits to measure the differences between both channels.

The measurements are shown in the figures 10 and 11 for the two photodiodes $d2$ and $d3$ respectively (at GPS 931843000, for 1 hour). The full model given in the table 1 has been used for the $Pr\_B1\_\{d2,d3\}\_ACp$ readout at 20 kHz. A model containing the Butterworth filter at 15007.3 Hz, an emphasis filter and a delay has been used for the $Pr\_B1\_\{d2,d3\}\_ACp\_40k$ raw photodiode readout at 40 kHz. The gain has been fixed to 1. The five free parameters of the fit are thus the delay and the emphasis filter pole, zero and quality factors (2). The data points with coherence higher than 95% between 1 Hz and 10 kHz have been used in the fit. The fitted models for the sensing of the channels $Pr\_B1\_\{d2,d3\}\_ACp\_40K$ is given in the table 2. The fit results and residuals are also shown on the figures. The phase residuals are within 30 mrad from 1 Hz to 10 kHz. The modulus residuals are within 3% from 20 Hz to 10 kHz and within 6% from 1 Hz to 20 Hz.

Note that the coherence is low ($\sim$ 85%) around 10 Hz. This must be explained by the high gain of the loop of the ITF: most of the longitudinal motion signal is subtracted by the controls: the control signals thus contain most of the information about the z-motion while the dark fringe signal has a non-negligible contribution of ADC noise. At frequencies higher than 300 Hz, the coherence also decreases to 95%: it indicates that the ADC noise starts to contribute to a few % to the dark fringe signal sampled at 20 kHz

Understanding of the time delay - The expected delay (not including the Butterworth filter delay) is $-31.75\ \mu$s, coming from (i) $-16\ \mu$s from the frame time delay, (ii) $< 1\ \mu$s from the analog electronics, (ii) $8\ \mu$s from the mezzanine anti-alias filter, (iv) $-23.75\ \mu$s from the decimation from 800 kHz to 40 kHz (keeping the last sample over a 20 sample window: $19 \times 1.25\ \mu$s), (v) 0 from the DAQ. The fitted delay for the 40 kHz channels is $-32.2\ \mu$s. Both delays are in agreement within the $4\ \mu$s timing systematic errors estimated in the previous sections.

Time stability - The time stability of the dark fringe readout has been checked. The parameterization given in the table 2 has been computed on data measured on July 17th, 2009. It has been compared to data measured on September 5th, 2009.

The figure 12 shows the models from July 17th superposed to the TFs measured on September 5th as well as the residuals between both. The residuals are compatible with the one obtained during the fit process on July 17th data. This indicates that the response of the dark fringe did not change between July 17th to September 5th.

2.3.2 Sensing of the channel $Pr\_B1\_ACp\_40K$

The $Pr\_B1\_ACp\_40K$ channel is computed from the raw channels $Pr\_B1\_d\{2,3\}\_ACp\_40K$ after the ADC.

- de-emphasis filters are applied to both channels in the Pr process,
- the two signals are then summed in the Pr process,
- a delay can be adjusted in the DAQ before the channel is stored in the data.

From the TF

$$\frac{\mathrm{Pr}\_B1\_ACp\_40K}{0.000446 \times Pr\_B1\_d2\_ACp\_40k + 0.000538 \times Pr\_B1\_d3\_ACp\_40k}$$

computed in step 12, a delay of $99.2 \pm 1.6\ \mu$s is found. It is the $100\ \mu$s delay from the Pr process that is not compensated in the DAQ. The model is thus the same as in table 2 but with delay of $\sim 67.8\ \mu$s.

2.4 Time jitter of the timing system

2.4.1 Measurement setup

The monitoring of the timing system phase noise has been setup on May 7th, 2009 (logbook entry 22842). It permits to monitor the phase noise of the 10 MHz clock generated by the ADC and used to sample the data. This clock is enslaved on the IRIG-B signal from the GPS receiver.

The reference clock is the 10 MHz clock generated by an atomic clock in the DAQ room. It is sent to the ADC7674 SN30 in the detection lab through a BNC cable. The 10 MHz clock of the ADC is demodulated by the 10 MHz clock of the atomic clock. The two output signals are sampled at 20 kHz by the ADC7674 SN30 (applying a Butterworth filter): Ti_10MHz_ACp and Ti_10MHz_ACq.

Note that the ADC is the one used to measure the dark fringe channels at 40 kHz, $Pr\_B1\_d2\_ACp\_40K$ and $Pr\_B1\_d3\_ACp\_40K$.

2.4.2 Timing jitter estimation

The relative dephasing of the two clocks is computed from the phase and quadrature signals:

$$\phi = \mathrm{atan}\Big(- \frac{Ti\_10MHz\_ACq}{Ti\_10MHz\_ACp}\Big) \; + \; n\pi$$

where n is an integer set to have a continuous phase ϕ as function of time.

The time series of the two demodulated signals and of the reconstructed phase are shown figure 13(a) and 13(b). Since the atomic clock is independent of the Virgo timing system, it is slowly drifting related to the ADC clock (it can be estimated to ~ 4 μs per day).

In order to measure the timing jitter, the measured phase ϕ is translated into a delay:

$$t_d = \frac{\phi}{2\pi f_0} \qquad \text{where } f_0 \; = \; 10\,\mathrm{MHz}$$

The spectrum of the delay is shown figure 13(c). The interested part to be looked at is above 1 Hz since the ADC clock is synchronise on the IRIG-B clock every second. Above 1 Hz, the estimated timing jitter is below $0.1\,\mathrm{ns}/\sqrt{\mathrm{Hz}}$, orders of magnitude below the calibration timing uncertainties.

Note that at high frequency, the timing jitter is dominated by the jitter of the Virgo timing system while at low frequency, the timing jitter is dominated by the drift of the independent atomic clock used for the measurement: in this case, the measurement gives only an upper limit of the timing jitter of the Virgo timing system. The frequency where the two contributions are similar has not been estimated.

2.5 Tables

Parameters	Full model ($f < 20\,\mathrm{kHz}$)	Simple model ($f < 2\,\mathrm{kHz}$)
Gain	1	1
Φ_0 (rad)	0	0
Delay (μs)	-59.7	49.3
Butterworth frequency (Hz)	7503.65	–

Table 1: ***Models for the sensing of the*** $Pr\_B1_{\{}d2, d3\}$***,*** Pr_B1 ***and*** $Pr\_B1p\_\{d1, d2\}$ ***channels at 20 kHz.*** *The delays are given related to the absolute GPS time.* **Simple model***: the delay has been measured with the ramped 1 PPS. It is valid up to 2 kHz.* **Full model***: the delay is the simple model delay subtracted for the Butterworth equivalent delay. It is valid up to 20 kHz. Systematic errors are* ± 4 μs *on the delay.*

Parameters	$Pr\_B1\_d2\_ACp\_40K$	$Pr\_B1\_d3\_ACp\_40K$
Gain	1	1
Φ_0 (rad)	0	0
Delay (μs)	-32.28 ± 0.0001	-32.16 ± 0.0001
8th order Butterworth frequency (Hz)	15007.30	15007.30
Zero frequency (Hz)	2.38939 ± 0.00011	2.37568 ± 0.00014
Zero quality factor	0.48340 ± 0.00006	0.47822 ± 0.00006
Pole frequency (Hz)	14.4088 ± 0.0007	14.4365 ± 0.0009
Pole quality factor	0.49653 ± 0.00002	0.49592 ± 0.00002
χ^2ndf	451480./167021	271480./77103

Table 2: ***Models for the sensing of the raw channels*** $Pr\_B1\_\{d2, d3\}\_ACp\_40K$*, valid up to 40 kHz. The delays are given related to the absolute GPS time. Systematic errors are:* $\pm 3\%$ *on the modulus and* ± 30 *mrad on the phase from the fit residuals, and* ± 4 μs *on the delay.*

2.6 Figures

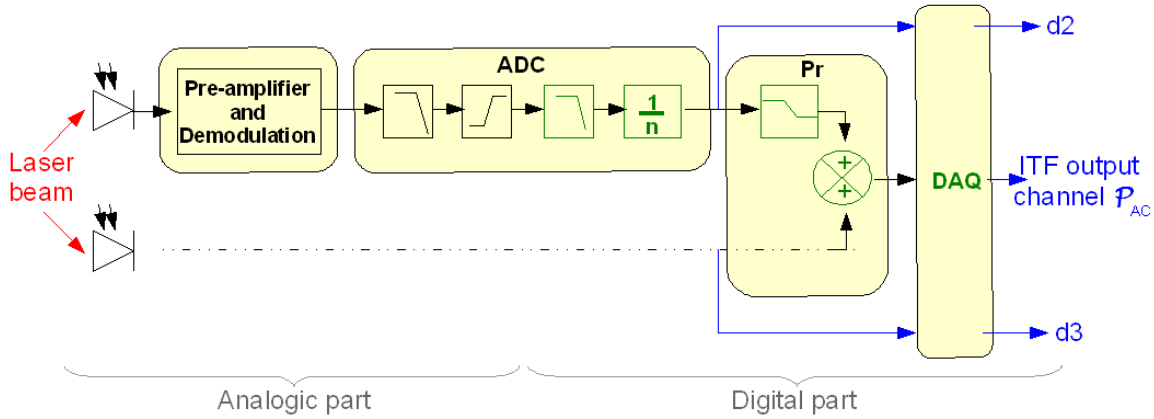

Figure 1: ***Synoptic of the photodiode general readout.*** *Differences between the different channels are described in the text.*

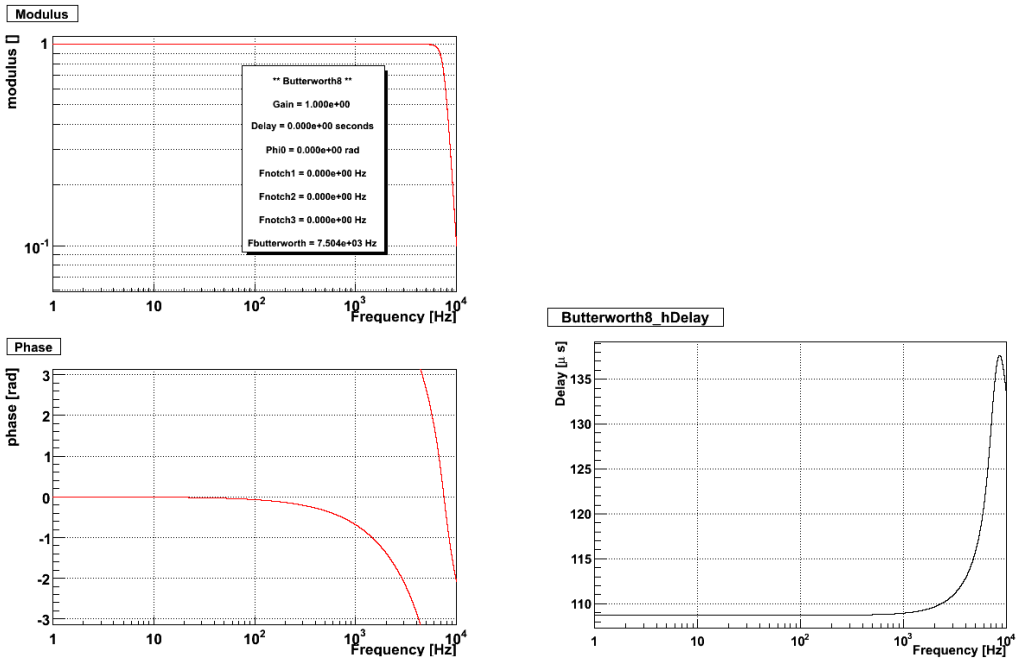

(a) Modulus and phase.

(b) Phase-equivalent delay ($\phi/(2\pi f)$).

Figure 2: ***TF of 8th order Butterworth filter with*** $f_0 = 6503.65$ ***Hz.***

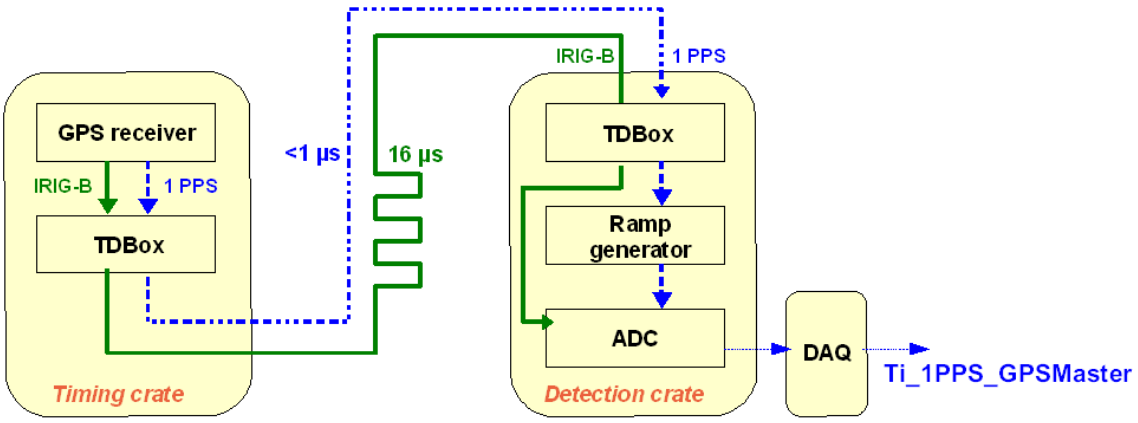

Figure 3: ***Synoptic of the measurement of the delay induced by the*** Pr_B1_ACp ***readout.***

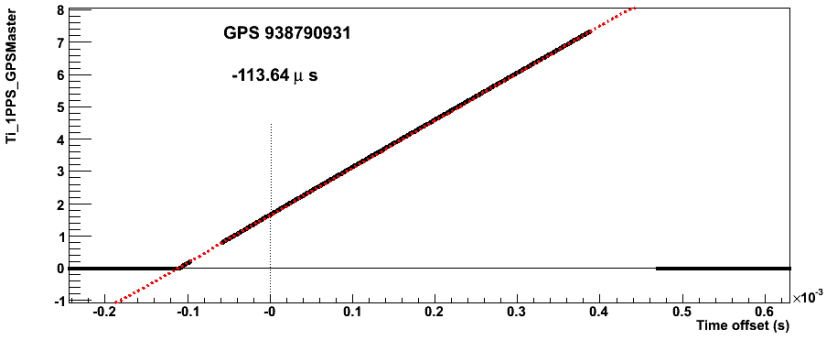

(a) Standard fit of the ramp

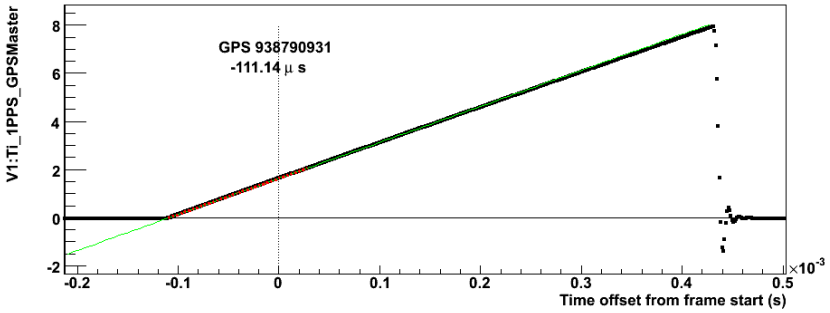

(b) Fit of the beginning of the ramp

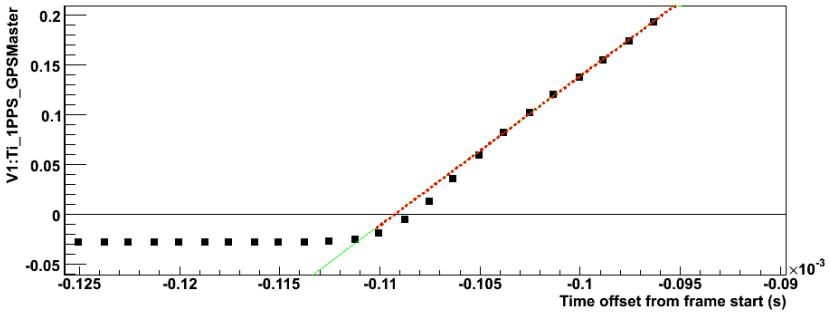

(c) Fit of the beginning of the ramp, zoomed

Figure 4: ***Ramp triggered by the 1PPS signal from the GPS receiver and sampled at 800 kHz without digital filter in the detection ADC.*** *The name of the channel is Ti_1PPS_GPSMaster, in V. The sampled data are the black squares (around GPS 938790931). The red dashed line is the fit of the ramp. The green dashed line is the extrapolation of the fit outside the fitted range. The time of the 1PPS signal as stored in the data is the time of the intersection between the ramp fit and the pedestal level. The vertical dotted line indicates the start of the frame.*

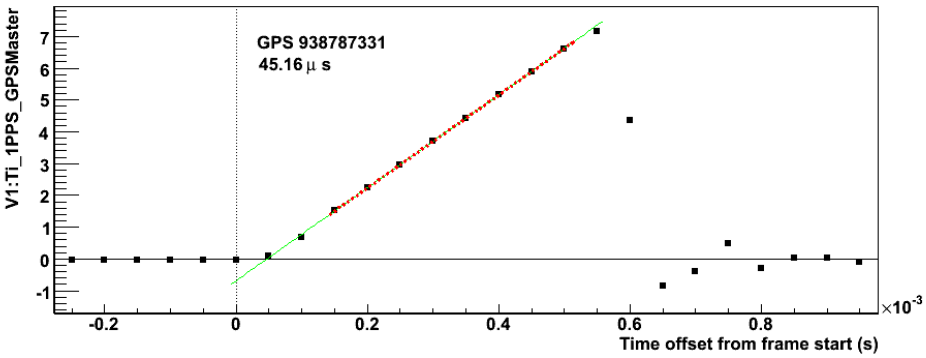

(a) Ramp sampled at 20 kHz (signal $Ti\_1PPS\_GPSMaster$)

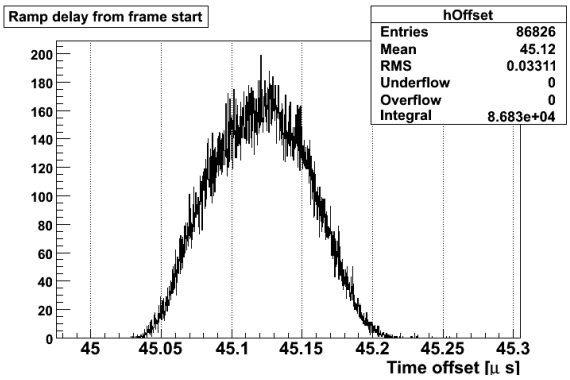

(b) Delay distribution.

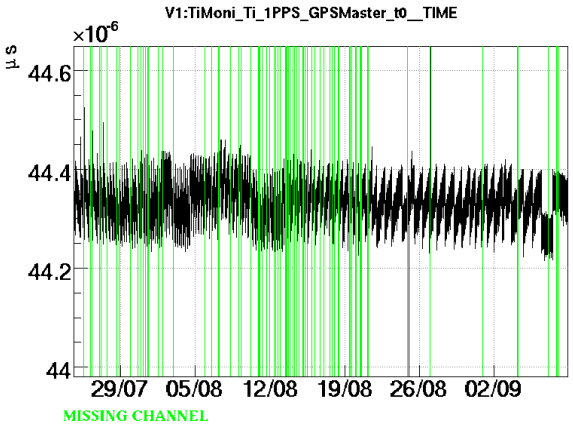

(c) Delay monitoring.

Figure 5: ***Measurement of the delay between the start of the frame and the start of the ramped 1 PPS signal sampled at 20 kHz.*** *(a) Ramp triggered by the 1PPS signal from the GPS receiver and sampled at 20 kHz in the detection ADC. The name of the channel is $Ti\_1PPS\_GPSMaster$, in V. The sampled data are the black squares (GPS 938787331). The red dashed line is the fit of the ramp. The green dashed line is the extrapolation of the fit. The time of the 1PPS signal as stored in the data is the time of the intersection between the ramp fit and the pedestal level. The vertical dotted line indicates the start of the frame. The delay from the frame start to the ramp start is* $45.16\,\mu$s*. (b) Distribution of the measured delays on July 24th 2009 (GPS 932428815), during 24 hours. (c) Monitoring channel $TiMoni\_1PPS\_GPSMaster\_t0$ vs time.*

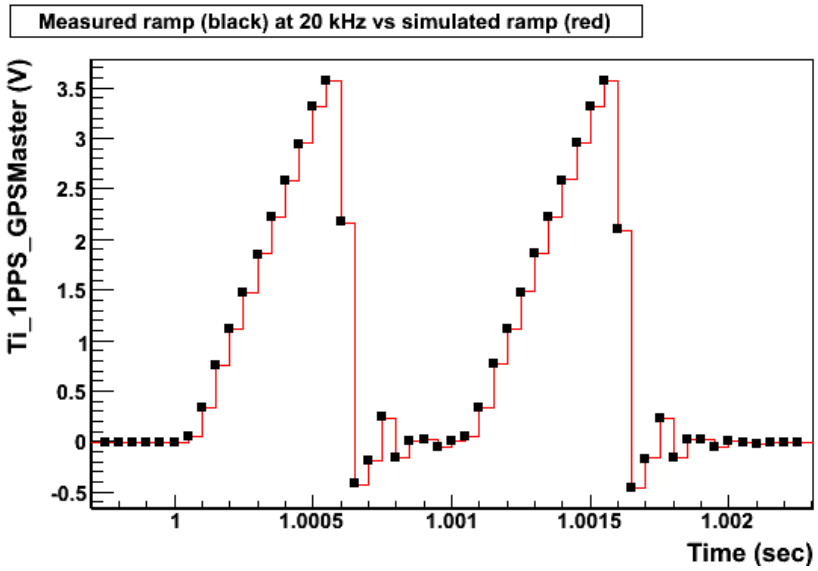

Figure 6: ***Data vs offline computation of the 20 kHz signal*** $Ti\_1PPS\_GPSMaster$. *The black points are the data. The red histogram is the 20 kHz signal computed from the* $Ti\_1PPS\_GPSMaster$ *sampled at 800 kHz. The timestamps of the histogram are put at the lower edge of each bin. The two triggered ramps are visible.*

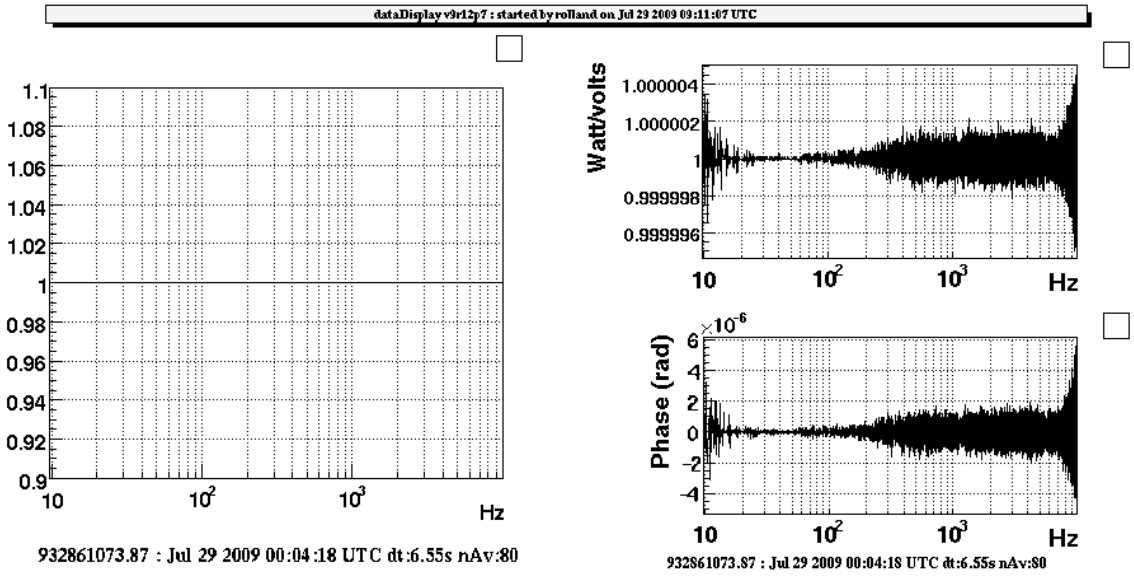

Figure 7: ***Coherence and TF of*** Pr_B1_ACp ***over the computed sum*** $0.000446 \times Pr\_B1\_d2\_ACp + 0.000538 \times Pr\_B1\_d3\_ACp$ ***of the raw channels.***

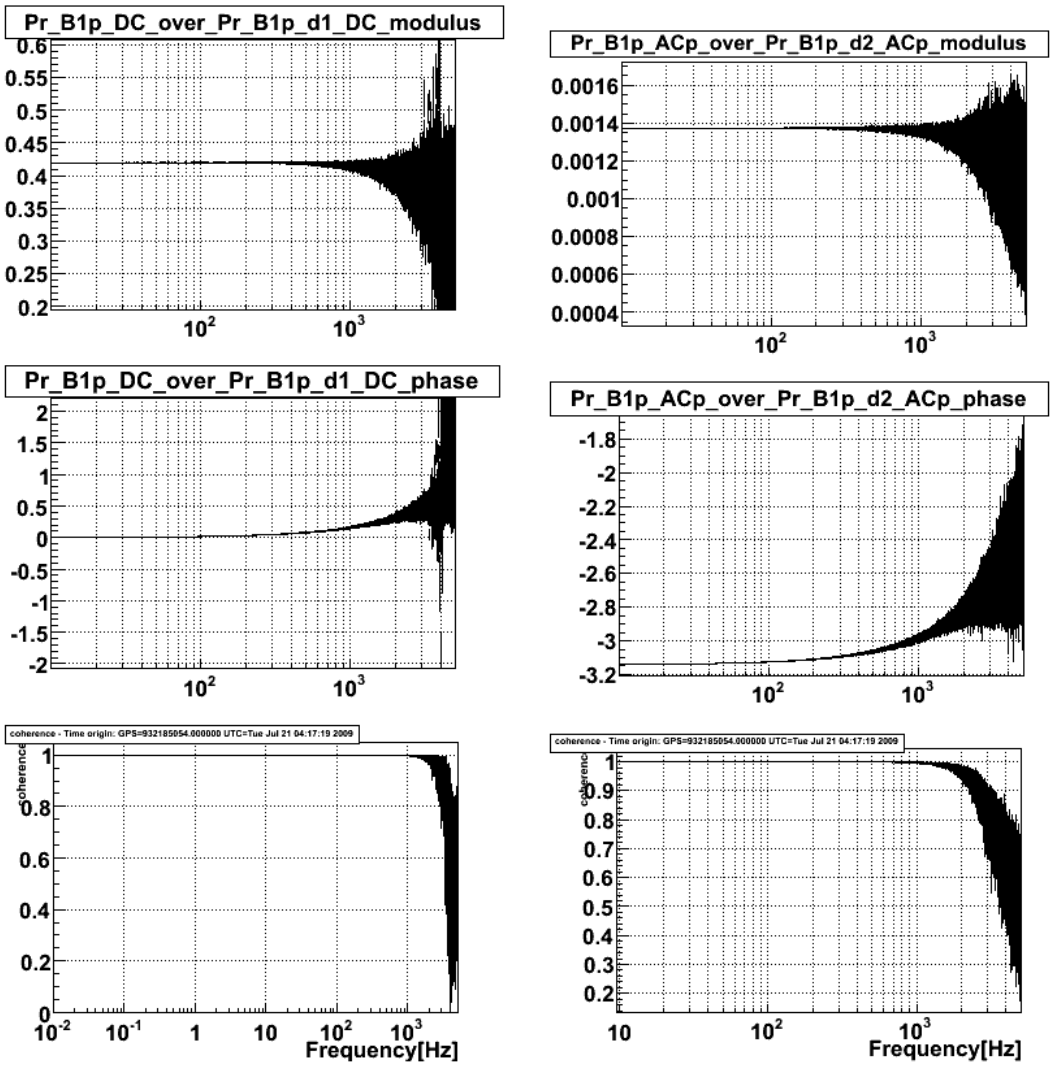

(a) $\frac{Pr\_B1p\_DC}{Pr\_B1p\_d1\_DC}$ (b) $\frac{Pr\_B1p\_ACp}{Pr\_B1p\_d2\_ACp}$

Figure 8: ***TF of*** Pr_B1p ***channels over*** $Pr\_B1p\_\{d1, d2\}$ ***raw channels.*** *The rows correspond to the modulus, the phase (rad) and the coherence of the TFs respectively.*

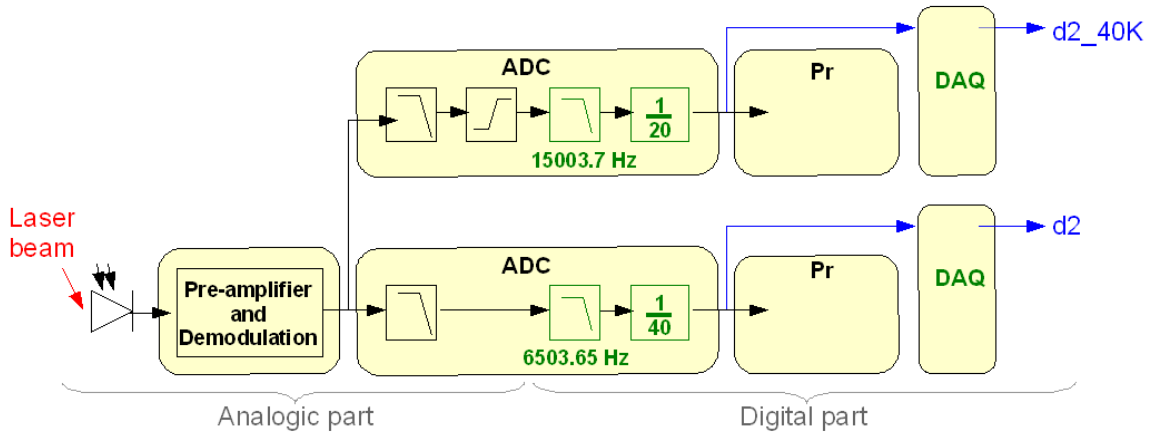

Figure 9: ***Synoptic of the measurement of the 40 kHz as function of the 20 kHz dark fringe channels.***

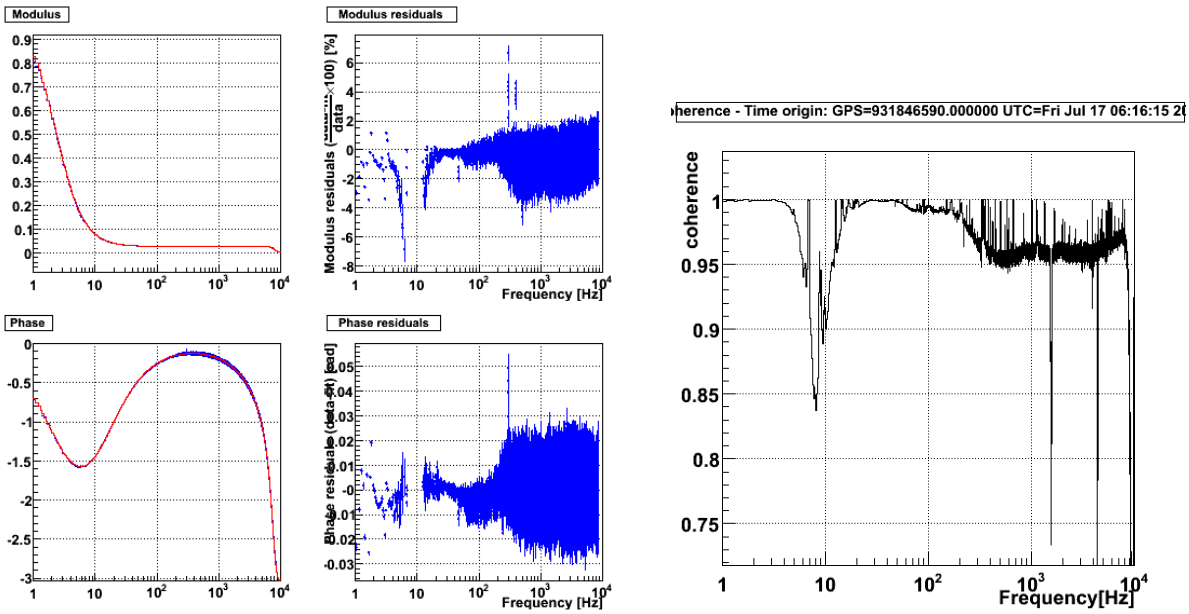

(a) TF, fit and residuals

(b) Coherence

Figure 10: ***TF of*** *Pr_B1_d2_ACp* ***over*** *Pr_B1_d2_ACp_40K. The data points with coherence above 95% are shown on the left plots (blue points), along with the fit result (red curve) from 1 Hz to 10 kHz. The fit residuals are shown on the right column. Data from GPS 931843000 (July 17th 2009), for 1 hour.*

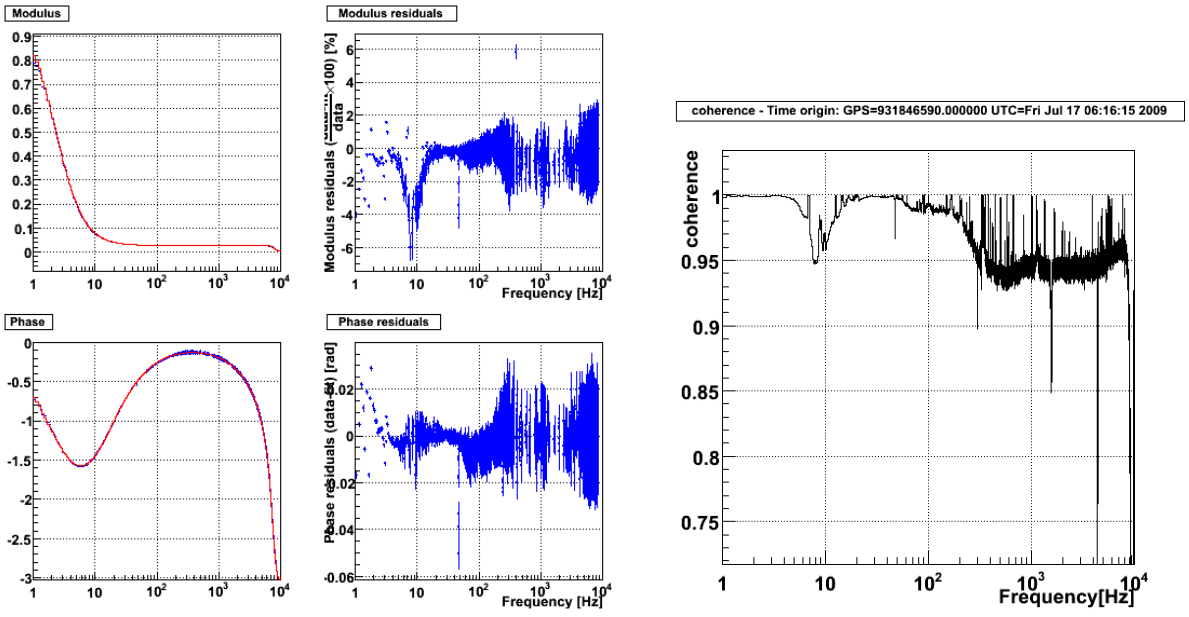

(a) TF, fit and residuals

(b) Coherence

Figure 11: ***TF of*** *Pr_B1_d3_ACp* ***over*** *Pr_B1_d3_ACp_40K. The data points with coherence above 95% are shown on the left plots (blue points), along with the fit result (red curve) from 1 Hz to 10 kHz. The fit residuals are shown on the right column. Data from GPS 931843000 (July 17th 2009), for 1 hour.*

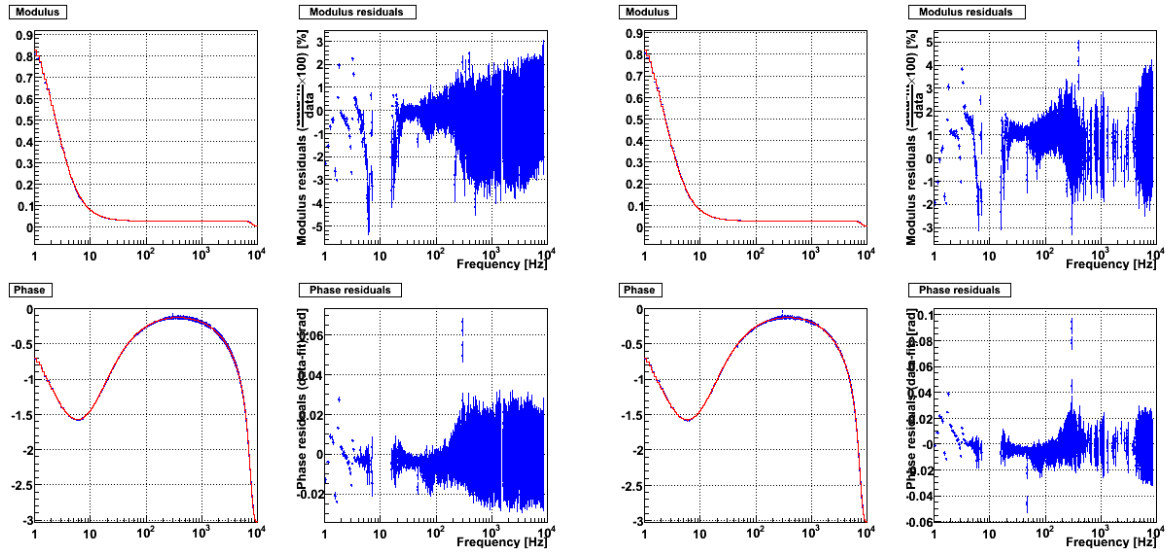

(a) $Pr\_B1\_d2\_ACp\_40K$ (b) $Pr\_B1\_d3\_ACp\_40K$

Figure 12: ***TFs of*** $Pr\_B1\_d2\_ACp$ ***over*** $Pr\_B1\_d2\_ACp\_40K$ ***and*** $Pr\_B1\_d3\_ACp$ ***over*** $Pr\_B1\_d3\_ACp\_40K$ *measured on September 5th, 2009 and compared to the model from table 2 computed on July 17th, 2009. The data points with coherence above 95% are shown on the left plots (blue points) from 1 Hz to 10 kHz. The red curve is the sensing model. The residuals between the data and the model are shown on the right column: they show the stability of the readout. Data from GPS 936200000, for 1 hour.*

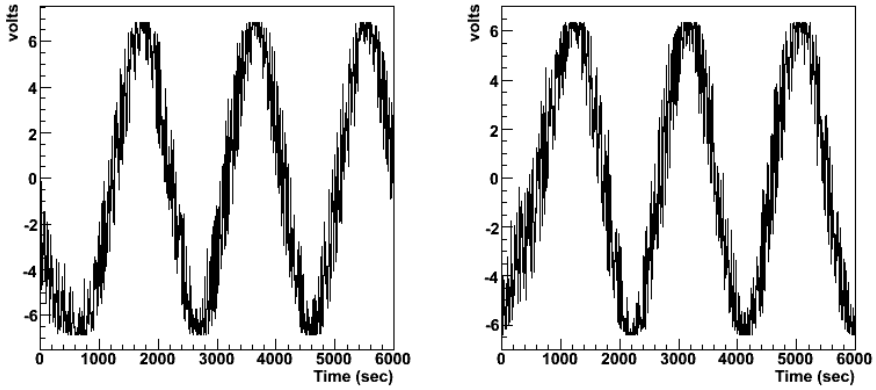

(a) Demodulated signals vs time (left: Ti_10MHz_ACp, right: Ti_10MHz_ACq)

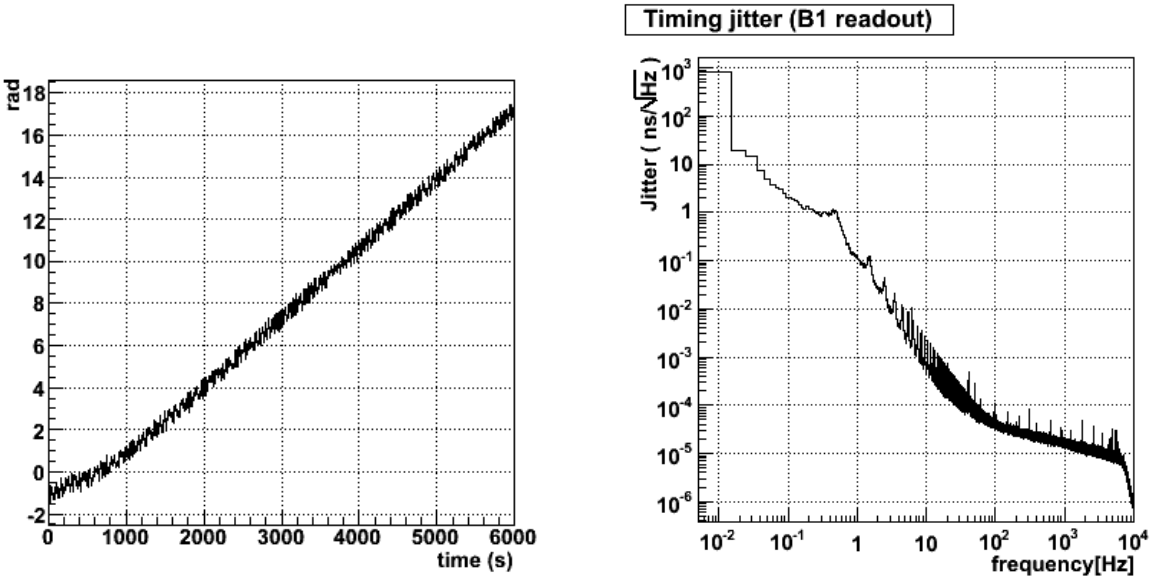

(b) Phase vs time

(c) Timing jitter spectrum

Figure 13: ***Timing jitter measurement.*** *The time series of the raw signals Ti_10MHz_ACp and Ti_10MHz_ACq are used to reconstruct the phase between the clocks and then to estimate the delay spectrum. The time series have been decimated from 20 kHz to 100 Hz in the plots. Data from GPS 933001200, for 1.7 hours.*

3 Calibration of the mirror actuation

The mirror actuation is defined as the TF (with modulus in m/V) from the correction signal to the induced mirror motion. The time reference is the GPS time.

In the plots that are shown, the actuation is corrected for the mechanical model of the pendulum, defined as a 2nd order low-pass filters with $f_0 = 0.6\,\mathrm{Hz}$ and $Q = 1000$.

3.1 Description of the measurements

3.1.1 Actuation in HP mode: Free Michelson data

The mirror actuation is measured in High Power (HP) mode using free swinging Michelson data.

The injected noise (lines) follows this path:

- the noise $zMir$ (channels such as $Ca\_WE\_zMir\_UD\_lines$) is generated in the PrCa process (rtpc06) and stored in the DAQ. It is sent to the actuation DSP through a gateway. It takes $100\,\mu$s for the noise to be sent to the DSP[14],
- the mirror actuation A (DSP+DAC+coil driver) and pendulum mechanical response P,
- a possible delay between the force applied to the magnets and the mirror motion,
- the ITF laser propagates the mirror motion to the dark fringe with some delay due to the light propagation time in the arms,
- the signals $Pr\_B1p\_\{d1, d2\}\_\{DC, ACp, ACq\}$ are readout at 20 kHz and used to reconstruct the ΔL of the free swinging Michelson [4][15].

Two examples of ellipse $Pr\_B1p\_d2\_ACp, ACq$ vs $Pr\_B1p\_d1\_DC$ and of ΔL spectrum are shown in the figure 14.

The measured TF is then $\Delta L/zMir$. Only the data with coherence higher than 90% have been used. Since one wants to measure the mirror actuation A from the correction signal (i.e. Sc_WE_zCorr) to the mirror motion, this TF is corrected for (see note [5]):

1. the pendulum mechanical response P: a second order low-pass filter[16] with frequency $f_0 = 0.6$ Hz and quality factor $Q = 1000$,

[14] This delay has been checked from the TF $\frac{Sc\_NI\_LoopIn}{Ca\_NI\_noise\_lines}$ at the frequencies of the lines injected in free Michelson data.

[15] The processed channels $Pr\_B1p\_\{DC, ACp, ACq\}$ are sampled at 10 kHz after decimation in the Pr process that adds some delay.

[16] The mechanical response of the pendulum is modeled by: $P(f) = \frac{-f_0^2(f^2-f_0^2)-j\frac{f_0^3 f}{Q}}{(f^2-f_0^2)^2+(\frac{f f_0}{Q})^2}$. It is equivalent to write it as function of $s = \mathrm{j}\omega$ as: $P(s) = \frac{\sum_{i=0}^{2} a_i \times s^i}{\sum_{k=0}^{2} b_k \times s^k}$ with $a_2 = a_1 = 0$, $a_3 = 14.2122$, $b_2 = 1$, $b_1 = 0.00376991$ and $b_0 = 14.2122$.

2. the light propagation time: 0 μs for NI and WI, 10 μs for NE and WE, 0 μs for BS in NE-WI configuration and 10 μs for BS in WE-NI configuration,

3. the delay from PrCa to the mirror actuation DSP: 100 μs,

4. the delay induced by the readout of $Pr\_B1p\_\{d1,d2\}\_\{DC,ACp,ACq\}$. The absolute delay is 49.3 μs below 2 kHz (see table 1).

The first two corrections are done automatically in the calibration code. In the following, the plots of A are corrected for these two effects only. In the tables, this delay is given as the "raw delay". The last two delays ($100 + 49.3 = 149.3$ μs) are taken into account afterwards to get the true delay of the actuation A, also given in the tables. The delay is thus the absolute delay between the correction signal as stored in the Virgo data and the GPS time.

About 15 lines have been injected from 6 Hz to 2 kHz. They have been injected with different amplitudes in order to check the linearity of the measurement. They have been injected every two weeks since the start of VSR2 in order to check the stability of the measurements.

3.1.2 LN1/HP actuation ratio measurements

To translate the mirror actuation A measured in HP to the actuation in Low Noise 1 (LN1) mode (for the NE, WE and BS mirrors), a noise $zMir$ is injected to the mirrors and the current flowing in the coils (i.e. Ca_WE_RM_CoilU) is readout in HP and then in LN1 modes. Only the data with coherence higher than 99% in both datasets have been used. The ratio of both TFs $\frac{\text{Ca\_WE\_RM\_CoilU}/zMir_{LN1}}{\text{Ca\_WE\_RM\_CoilU}/zMir_{HP}}$ is then computed.

From the noise to the output channel, the signal follows the path:

- the noise is generated in PrCa (rtpc06) or in the HInjectors (rtpc19) and stored in the DAQ. It is sent to the actuation DSP with some delay: 100 μs from PrCa and 200 μs from the HInjectors[17],

- the mirror actuation A (DSP+DAC+coil driver) that generates the current in the coils,

- the readout of the current in the coils and the DAQ that stores the channels such as Ca_WE_RM_CoilU.

Since the readout of the Ca_WE_RM_CoilU channels is the same both in HP and in LN1 mode, its shape cancels in the TF ratio. Since the noise $zMir$ injected in HP and in LN1 modes is generated by the same process[18] in the data used to measure the ratio, the delay from the noise generator to the mirror actuation cancels in the TF ratio. Thus the ratio is only sensitive to the difference of the actuation A itself between LN1 and HP modes.

[17] This delay has been checked from the TF Sc_WE_zCorr/Ca_WE_zMirUD measured during white noise injections for the LN1/HP ratio.

[18] Pr_Ca is used to inject lines. CaNoise, CaInjection and CaBlind are used to inject white noise.

Two types of measurements have been done: (i) injection of lines at the same frequencies as the free Michelson line injection and (ii) injection of white noise from a few Hz to a few kHz. The line injections allow to have precise measurements at the frequencies where the actuation is known in HP mode. The white noise injections are used to check the behaviour of the ratio at all frequencies. The noise has been injected with different amplitudes to check the TF linearity.

3.1.3 Mirror actuation in LN1 mode

The mirror actuation in LN1 mode is obtained multiplying the mirror actuation in HP mode (measured in free swinging Michelson data) by the LN1/HP ratio. The multiplication is done using the data points measured at the free Michelson line frequencies. The data are then fitted by a model including poles and zeros.

As for the actuation in HP mode, the plots of A are not corrected for some delays. Both the "raw delay" (only corrected for the light propagation time) and the corrected delay are given in the tables with the model parameters.

3.2 Actuation calibration

The parameters of the parameterizations fitted on the mirror actuation measurements are given in the table 3 for the configurations used in the longitudinal controls and in the table 4 for the configurations used for the hardware injections.

The figures of the different data and fit are shown in the section 3.4.

3.2.1 Actuation in HP mode

Free swinging Michelson data were analysed to extract the actuation response A in HP mode. The results were checked for variations as function of time and of injected amplitude. The modulus and the phase are compatible with constants. Longer monitoring will be performed during VSR2 to better estimate possible time variations.

The analysis of the data in free Michelson for the **NE mirror actuation using the L-R coils** show strange behaviour at high frequency (around 800-900 Hz). It has been found using other measurements that the NE, coil L, is not well fixed and induces a resonance of the mirror motion (around 800-900 Hz in free Michelson data and around 1100-1200 Hz in step 12 data). See logbook entries 24332, 24353 and 24532 for more details.

3.2.2 LN1 to HP TF ratio

Shape of the ratio - In HP mode, the voltage input is converted in a current in the coil through a trans-conductance amplifier. It response is not well known but is expected to be rather flat up to a few kHz. Introduce a delay ?

In LN modes, the voltage input is converted to a current through serie resistors. These resistors R_s are in serie with the inductance $L_c \sim 3.3\,\mathrm{mH}$ of the coil. The conversion voltage to current by the coil driver is thus a pole at frequency $f_p = \frac{R_s}{2\pi L_c}$. In LN1 mode, the serie resistors include the so-called serie resitors themselves ($300\,\Omega$), the protection resistor ($10\,\Omega$) and the coil internal resistor ($\sim 10\,\Omega$). The pole is thus around 15 kHz, far above the measurements. Below a few Hz, it is equivalent to a delay of $\sim 6\,\mu$s.

Different DACs are used in HP and in LN1 modes. The anti-imaging filters might be slightly different between both channels. The cut-off being around 3 kHz, it should not be visible below 1 kHz in the modulus. Below 1 kHz, the equivalent delay of the DAC filters is $177 \pm 5\,\mu$s. Differences of the order of $10\,\mu$s could arise between different DACs [6].

The ratio is thus expected to be close to flat up to 1 kHz. Some mistuning in the compensation of the de-emphasis filters (0.9 Hz and 9Hz) can explain a few percent variations in modulus ratio below a few tenth of Hz and of the order of 30 mrad variations in phase difference below a hundred Hz.

The modulus of the LN1 to HP ratio are flat within 5% up to 1 kHz. The phase difference shows some behaviour below 100 Hz that must be due to the filter compensation tuning. At higher frequency, it can be interpreted as a delay. For the **WE-CoilL, WE-CoilR and WE-CoilD**, the equivalent delay is negative (decreasing phase), $\sim 10\,\mu$s, while it is positive (increasing phase), ~ -5 to $-20\,\mu$s, for all the other coils. Such differences are compatible with the variations between the DAC filters.

LN1 to HP TF ratio as function of injected amplitude - Different levels of injections have been done. The maximum value of the current flowing in the coil (i.e. $Ca\_WE\_RM\_CoilU$) in LowNoise mode has been choosen as reference for the injection level. The modulus and phase as function of this amplitude are shown in the different figures at the injected frequency around 116 Hz. It is also shown at different amplitudes for the WE, coilU, in the figure 21.

In the latter case (**WE, coilU**), some variations of the ratio is observed as function of the amplitude. At lower current, the modulus ratio is higher by $\sim 3\%$ than at the higher currents. Concerning the phase, the differences between different datasets seem to increase when the frequency increases. Interpreting this evolution as a delay gives an uncertainty of $\sim 5\,\mu$s.

For the other coils, the modulus and ratio are much more constant as function of the amplitude, within $\sim$1% in modulus and $\sim$10 mrad in phase.

BS, coil DL - The measurements are different by 6% when injecting lines than when injected white noise. Note that this coil has some noise issues in HP mode, coming from the DAC or the coil driver: see logbook entry 25006.

Comparing the data when injecting white noise and when injecting lines:

- in HP mode, the coil current $Ca\_BS\_RM\_CoilDL$ varies between ± 0.15 V and between ± 6 V when injecting white noise and lines respectively,
- in LN1 mode, the coil current varies between ± 0.004 in both cases (white noise and lines).

The plots given in figure 37 gives the modulus of the LN1/HP ratio as function of the amplitude in LN1 mode: no dependency is observed. The figure 40(a) gives the modulus of the LN1/HP ratio as function of the amplitude in HP mode: the modulus clearly decreases by $\sim 6\%$ when the HP amplitude increases by a factor of 20. For comparison, the same plot done on the coil UR is shown figure 40(b): the modulus is independent on the HP amplitude in all the range.

BS, coil DR - Nothing special to report concerning this coil in the calibration measurements. However, some issues with the current sensing (channel $Ca\_BS\_RM\_CoilDR$) has been found: see logbook entries 24860 and 25006.

Difference between coils - The ratio is different for the up and down coils. This might induce systematic errors since their average is used when computing the WE actuation in LN1 mode from the actuation in HP mode.

Mirror actuation of NE using L-R coils - NE, coil L, is not well fixed and induces a resonance of the mirror motion. See logbook entries 24332, 24353 and 24532 for more details.

3.3 Tables

		WE, U-D coils	NE, U-D coils	BS, four coils
HP	Gain (μm/V)	12.772 ± 0.004	13.44 ± 0.01	89.2 ± 0.01
	Raw delay (μs)	(597.8 ± 1.0)	(610.1 ± 0.8)	(624.8 ± 0.04)
	Φ_0 (rad)	0	0	π
	Pole frequency (Hz)	56.6 ± 3.4	53.6 ± 4.5	38.483 ± 0.038
	Zero frequency (Hz)	61.5 ± 4.3	59.1 ± 5.6	39.126 ± 0.038
	Pole frequency (Hz)	201.7 ± 16	206.2 ± 19	–
	Zero frequency (Hz)	239.5 ± 18	247.6 ± 20	–
	Pendulum	One 2nd order low-pass filter: $f_0 = 0.6\,\text{Hz}$, $Q = 1000$		
	χ^2/ndf	19.63/30	29.86/30	41581.6/36
LN1	Gain (μm/V)	13.486 ± 0.009	13.76 ± 0.012	87.722 ± 0.005
	Raw delay (μs)	(553.9 ± 4.2)	(560.3 ± 3.4)	(556.7 ± 0.2)
	Delay (μs)	404.6 ± 4.2	411.0 ± 3.4	407.4 ± 0.2
	Φ_0 (rad)	0	0	π
	Pole frequency (Hz)	22.48 ± 1.6	34.26 ± 0.46	3568.1 ± 11
	Zero frequency (Hz)	23.45 ± 1.8	36.40 ± 0.51	–
	Pole frequency (Hz)	139.67 ± 6.4	175.04 ± 4.3	–
	Zero frequency (Hz)	171.33 ± 8.4	217.18 ± 5.7	–
	Pole frequency (Hz)	3212 ± 329	3773 ± 346	–
	Pendulum	One 2nd order low-pass filter: $f_0 = 0.6\,\text{Hz}$, $Q = 1000$		
	χ^2/ndf	23.0/29	34.16/29	13345.9/31

Table 3: ***WE (U-D coils), NE (U-D coils) and BS (four coils) mirror actuation parameterizations****, in HP mode and LN1 mode. The models are valid up to 1.5 kHz. The* χ^2/ndf *of the fits are given. The raw delay is the measured delay that includes the delay from the injection path to the DSP and the delay from the* Pr_B1p *channels sensing. The corrected delay takes as reference the correction channel in the DSP (i.e.* Sc_WE_zCorr*) and does not contain the B1 sensing delay nor the delay for the injection part (raw delay with 100* μs *less for the PrCa to DSP delay and* 49.3 μs *less from the dark fringe sensing: delay =* $raw\_delay - 100 - 49.3$ μs*). Applying these TFs to zCorr should enable to estimate the induced motion at absolute GPS time.*

		WE, L-R coils	NE, L-R coils
HP	Gain (μm/V)	12.956 ± 0.008	12.768 ± 0.012
	Raw delay (μs)	(590.7 ± 1.3)	$(637.8 \pm 3.6$
	Φ_0 (rad)	0	0
	Pole frequency (Hz)	65.9 ± 5.0	56.27 ± 4.9
	Zero frequency (Hz)	72.6 ± 6.5	60.5 ± 5.3
	Pole frequency (Hz)	240.8 ± 32	133.2 ± 10
	Zero frequency (Hz)	280.8 ± 36	149.6 ± 13
	Pendulum	One 2nd order low-pass filter: $f_0 = 0.6\,$Hz, $Q = 1000$	
	χ^2/ndf	10.438/28	2.412/14
LN1	Gain (μm/V)	13.51 ± 0.014	14.08 ± 0.023
	Raw delay (μs)	(543.4 ± 3.2)	(563.7 ± 17.4)
	Delay (μs)	594.1 ± 3.2	614.4 ± 17.4
	Φ_0 (rad)	0	0
	Pole frequency (Hz)	9.557 ± 0.06	9.629 ± 0.117
	Zero frequency (Hz)	9.896 ± 0.06	9.877 ± 0.119
	Pole frequency (Hz)	116.5 ± 1.8	87.79 ± 1.61
	Zero frequency (Hz)	142.0 ± 2.5	104.0 ± 2.0
	Pole frequency (Hz)	2450 ± 139	2146 ± 540
	Pendulum	One 2nd order low-pass filter: $f_0 = 0.6\,$Hz, $Q = 1000$	
	χ^2/ndf	23.55/27	2.79/13

Table 4: ***WE (L-R coils), NE (L-R coils) mirror actuation parameterizations****, in HP mode and LN1 mode. The WE actuations model are valid up to 1.5 kHz. The NE actuations in HP and in LN1 mode have been fitted from 5 Hz to 400 Hz only. The* χ^2/ndf *of the fits are given. The raw delay is the measured delay that includes the delay from the injection path (from PrCa) to the DSP and the delay from the* Pr_B1p *channels sensing. The corrected delay takes as reference the channels sent by the CaInjectors (i.e.* Ca_WE_zMirLR*) and does not contain the B1 sensing delay (raw delay with 100* μs *more since the hardware injections are done from the CaInjectors and* 49.3 μs *less from the dark fringe sensing:* $delay = raw\_delay + 100 - 49.3$ μs*). Applying these TFs to* Ca_WE_zMirLR *channels should enable to estimate the induced motion at absolute GPS time.*

3.4 Figures

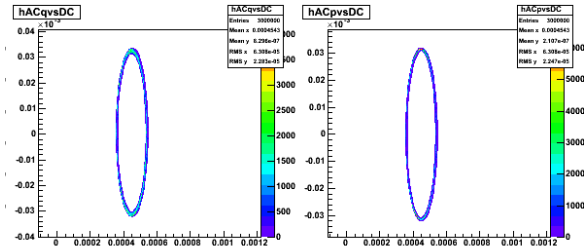

(a) GPS 930344269, 5 min.

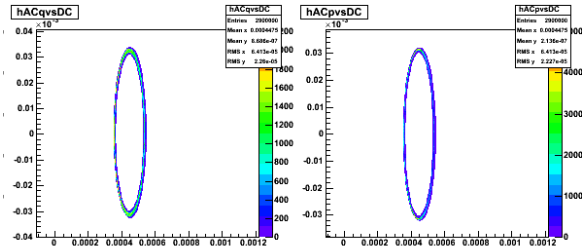

(b) GPS 930346691, 5 min.

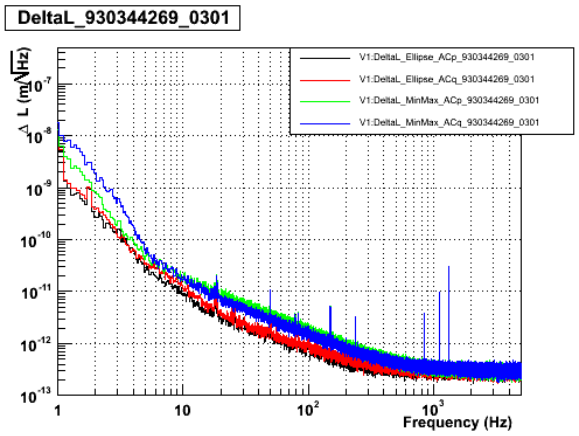

(c) GPS 930344269, 5 min.

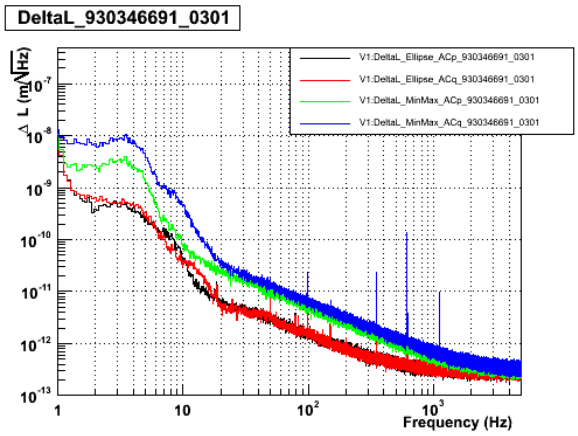

(d) GPS 930346691, 5 min.

Figure 14: ***Left: typical measured ellipses*** *Pr_B1p_d2_ACq* ***vs*** *Pr_B1p_d1_DC* ***and*** *Pr_B1p_d2_ACp* ***vs*** *Pr_B1p_d1_DC.* ***Right: typical reconstructed*** ΔL ***from free swinging Michelson data.*** *The channel* ΔL*_Ellipse_ACq (red) is used for the actuation calibration.*

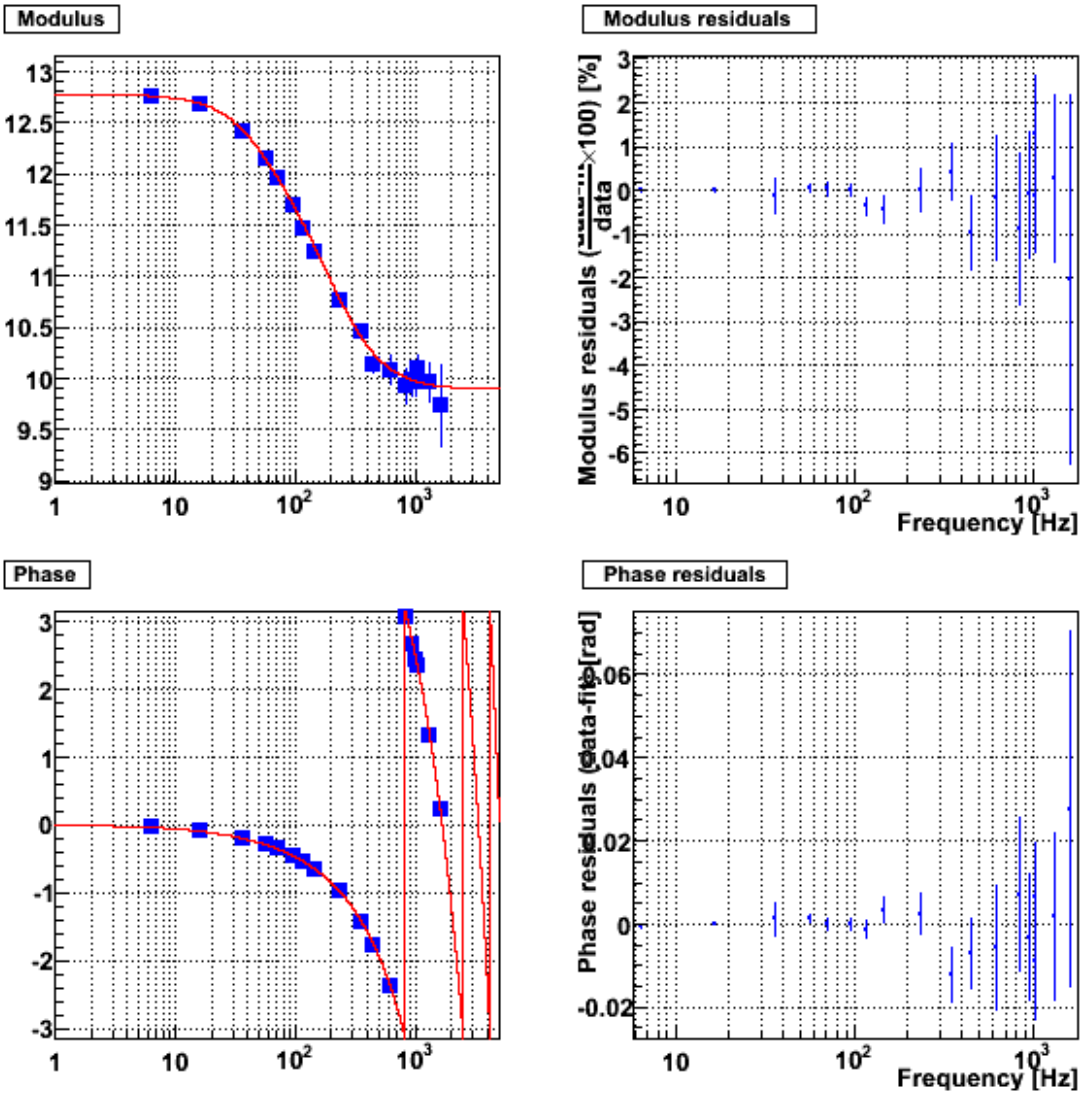

Figure 15: ***Measured actuation of the WE mirror using the U-D coils in HP mode****, fitted model and residuals.*

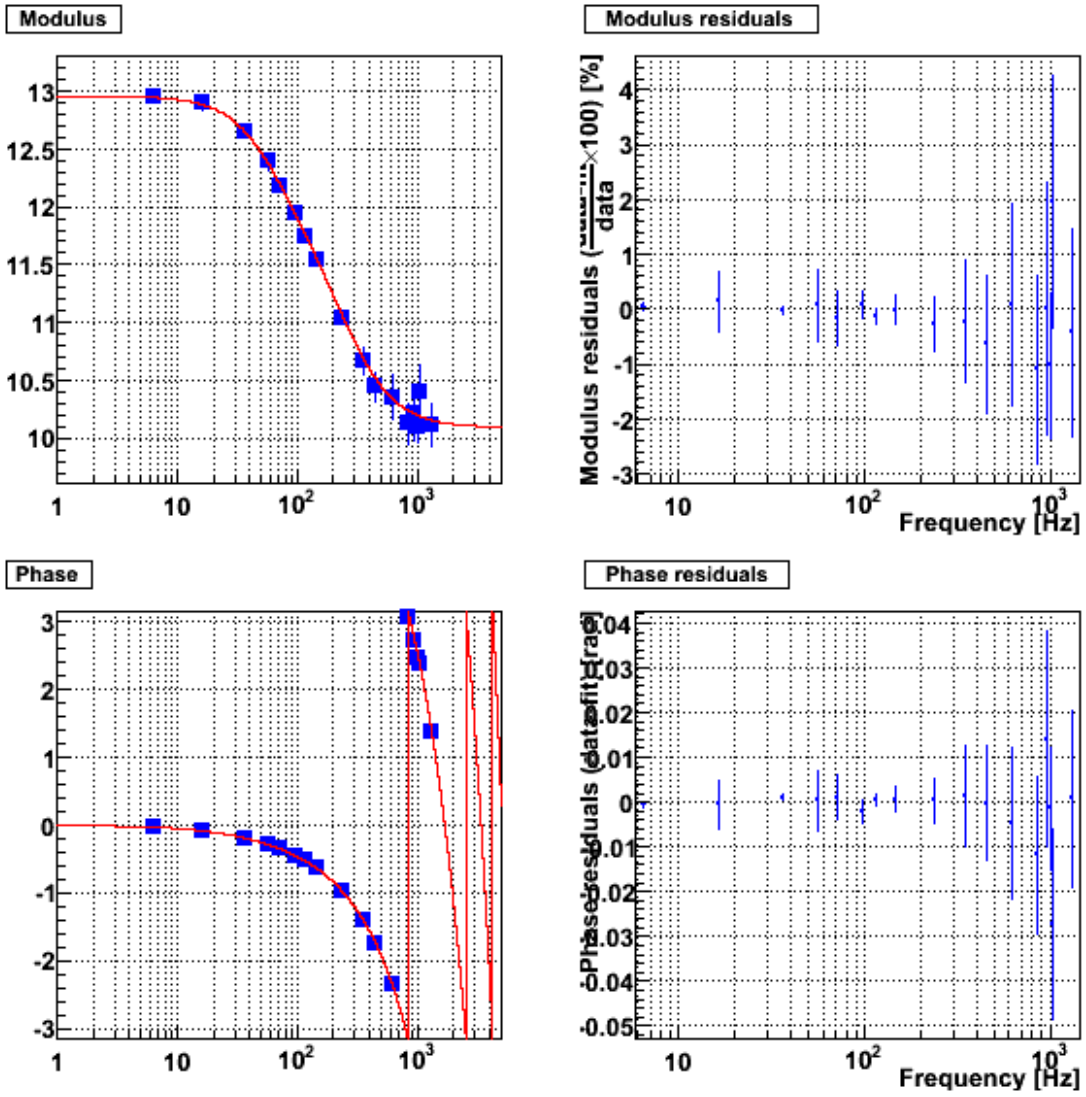

Figure 16: ***Measured actuation of the WE mirror using the L-R coils in HP mode****, fitted model and residuals.*

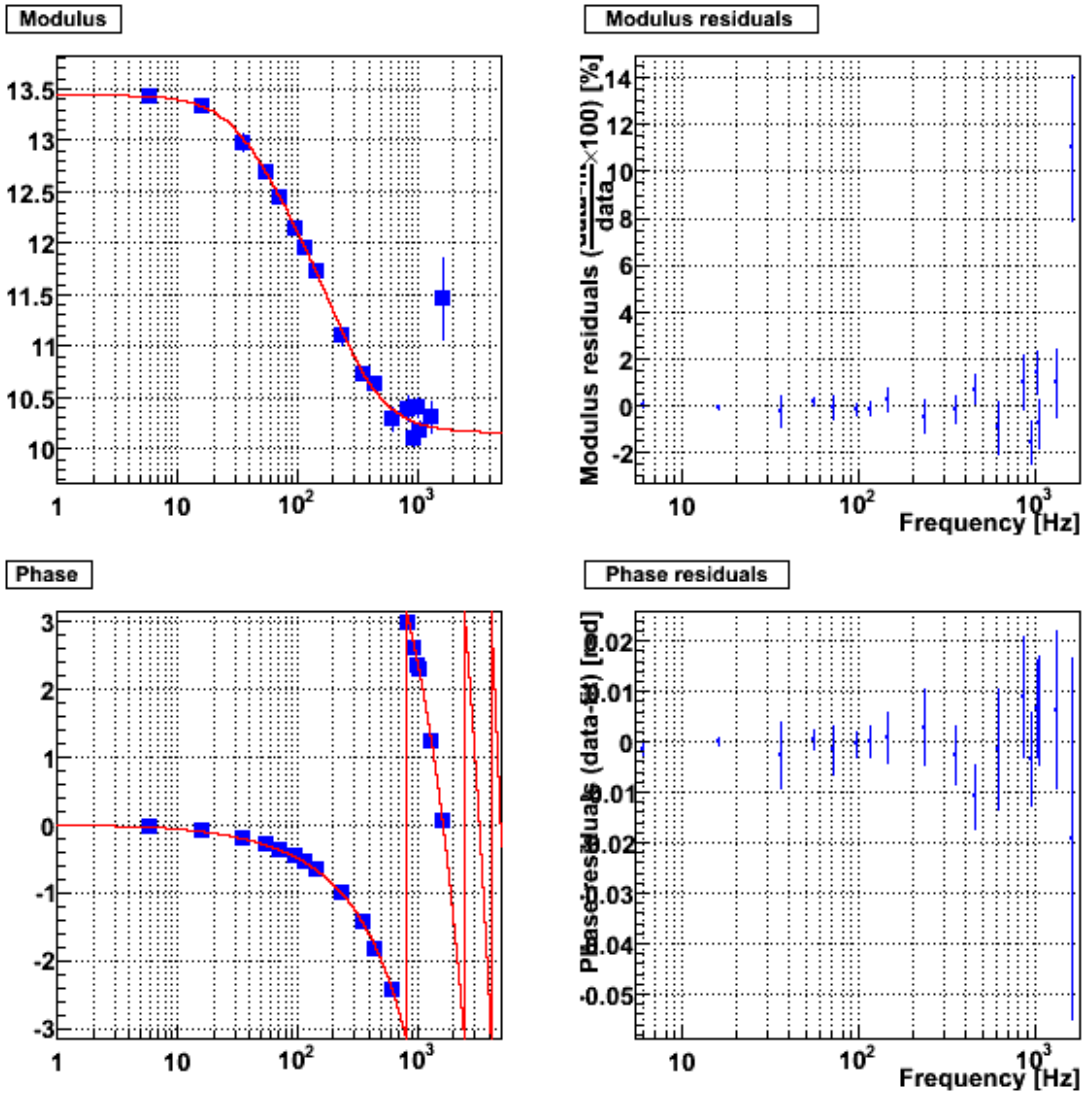

Figure 17: ***Measured actuation of the NE mirror using the U-D coils in HP mode****, fitted model and residuals.*

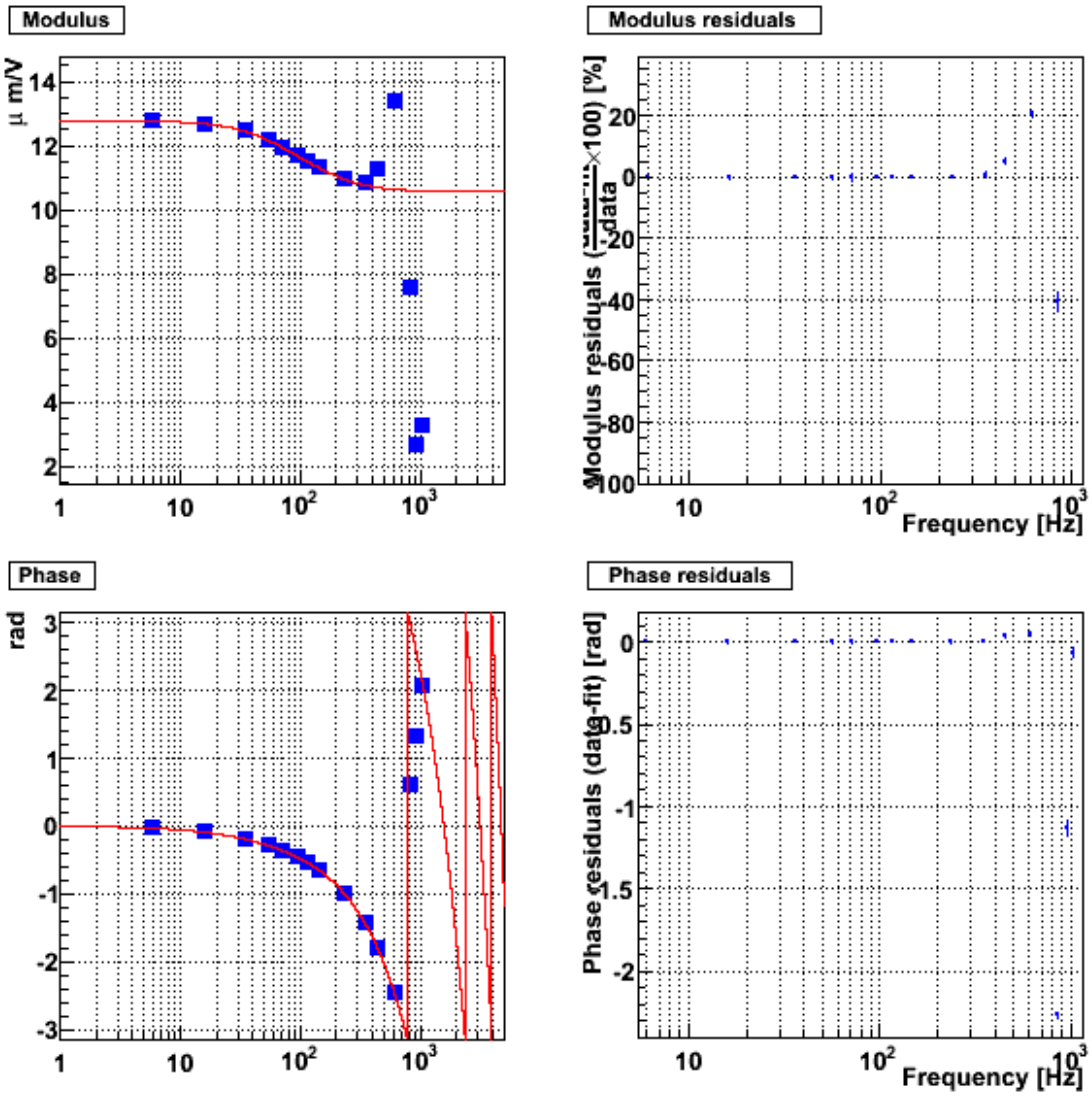

Figure 18: ***Measured actuation of the NE mirror using the L-R coils in HP mode****, fitted model and residuals. The data have been fitted up to 400 Hz only.*

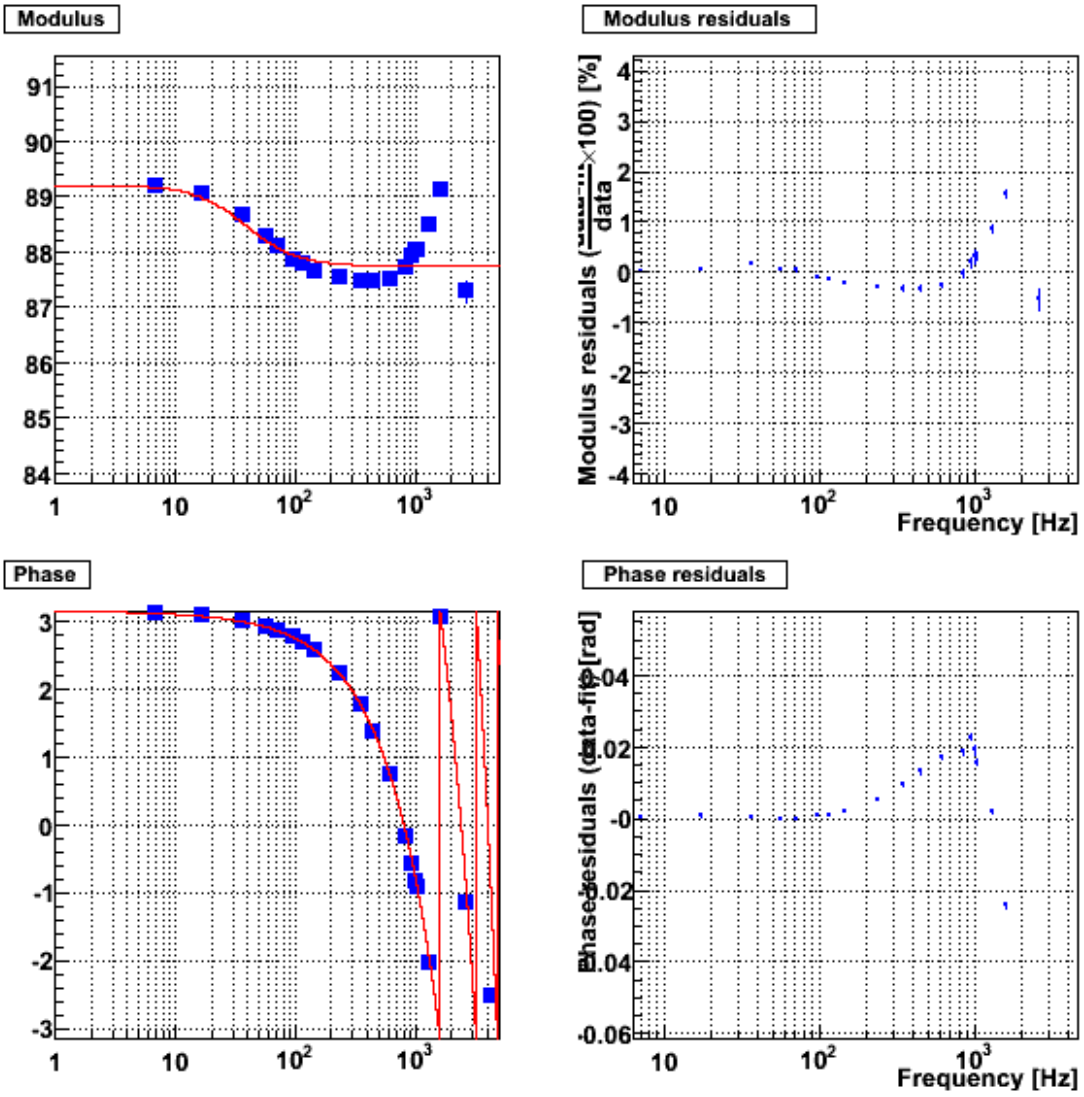

Figure 19: ***Measured actuation of the BS mirror using the four coils in HP mode****, fitted model and residuals.*

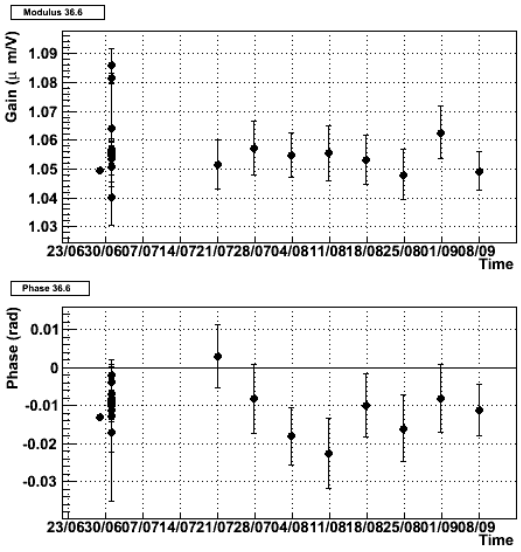

(a) 36.5 Hz

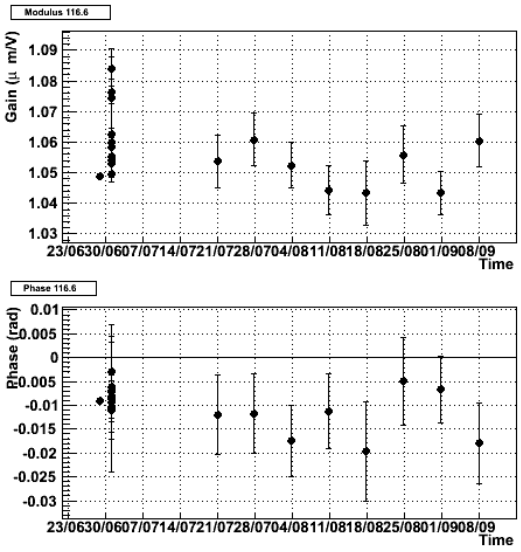

(b) 116.5 Hz

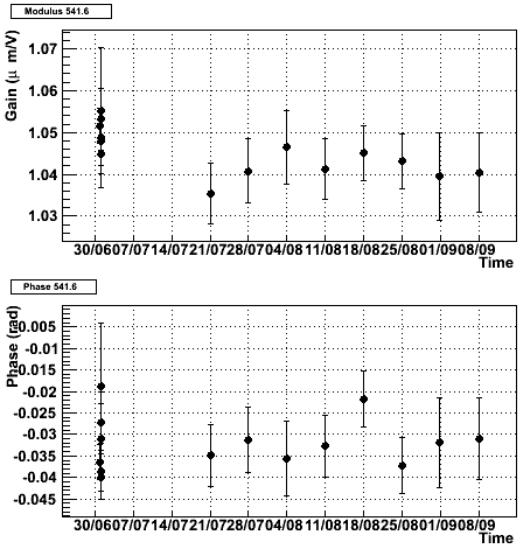

(c) 451.5 Hz

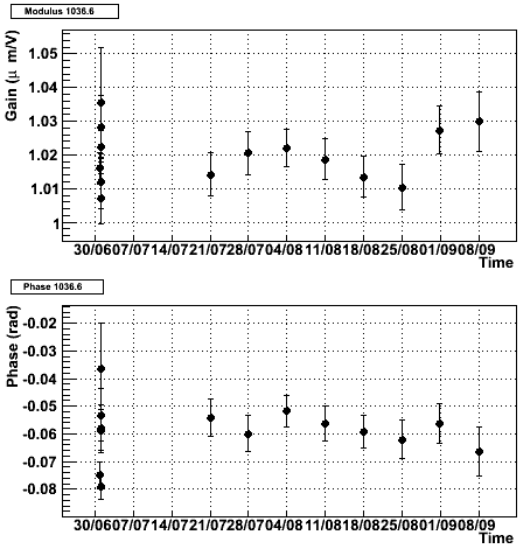

(d) 1036.5 Hz

Figure 20: ***Evolution as function of time (June to September 2009) of the measured actuation TF ratio (LN1/HP) for the up coil of the WE mirror*** *at four different frequencies.*

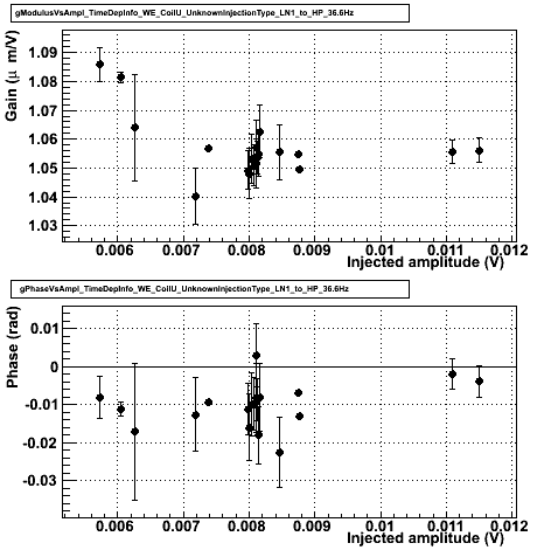

(a) 36.5 Hz

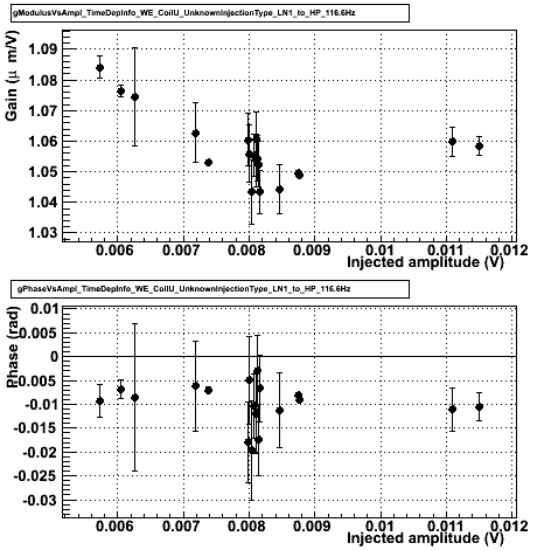

(b) 116.5 Hz

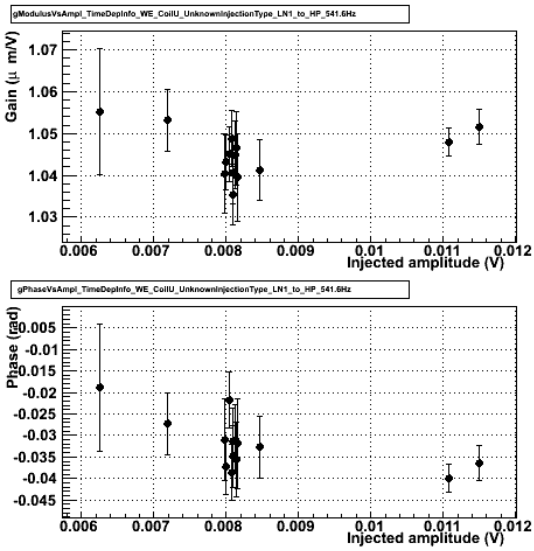

(c) 451.5 Hz

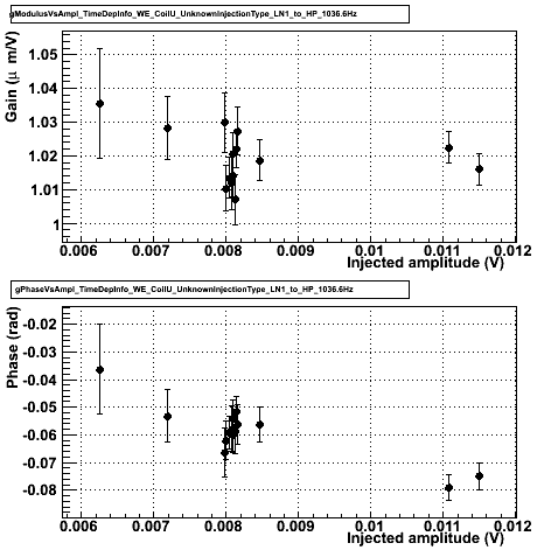

(d) 1036.5 Hz

Figure 21: ***Evolution as function of the signal amplitude of the measured actuation TF ratio (LN1/HP) for the up coil of the WE mirror*** *at four different frequencies. The amplitude in the x-axis is the amplitude of* $V1 : Ca\_WE\_RM\_CoilU$ *during the injections in LowNoise mode.*

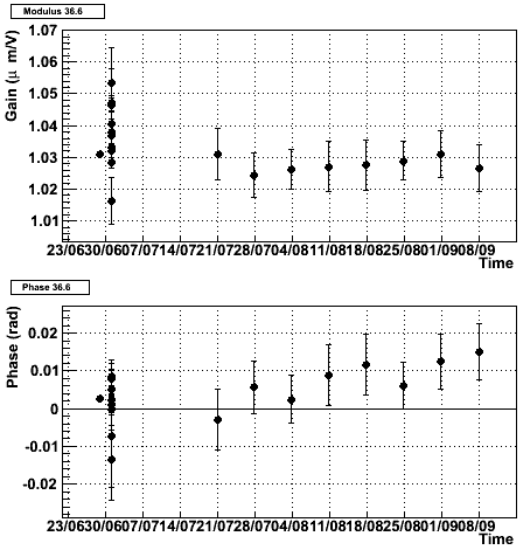

(a) 36.5 Hz

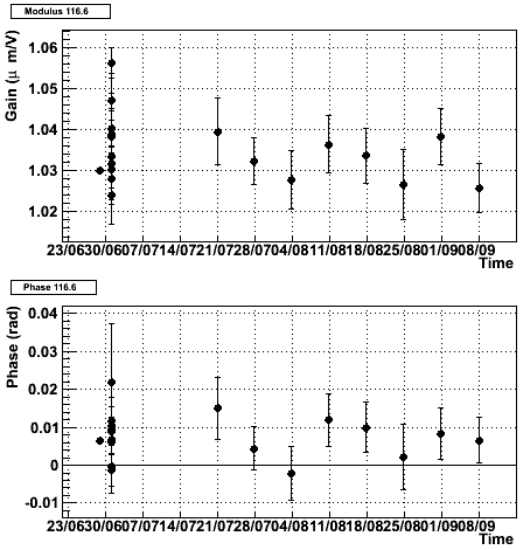

(b) 116.5 Hz

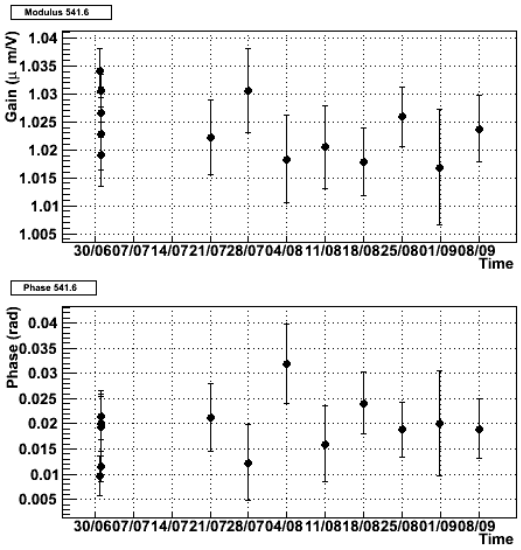

(c) 451.5 Hz

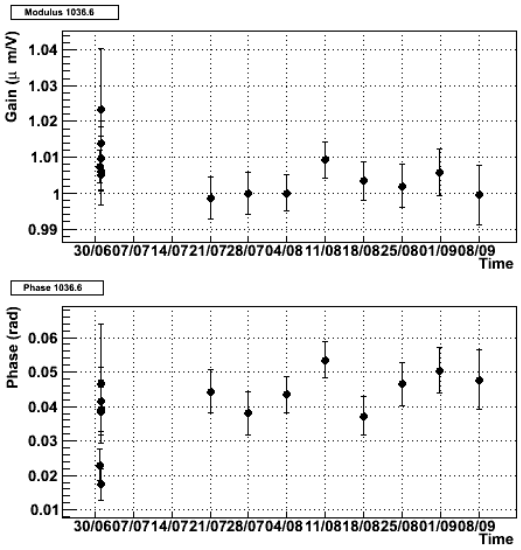

(d) 1036.5 Hz

Figure 22: ***Evolution as function of time (June to September 2009) of the measured actuation TF ratio (LN1/HP) for the down coil of the WE mirror*** *at four different frequencies.*

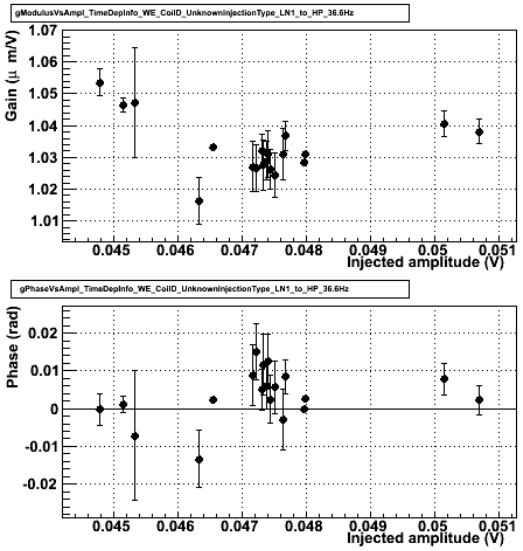

(a) 36.5 Hz

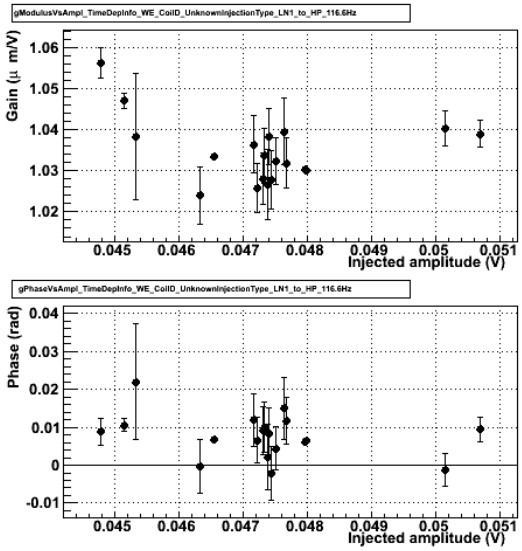

(b) 116.5 Hz

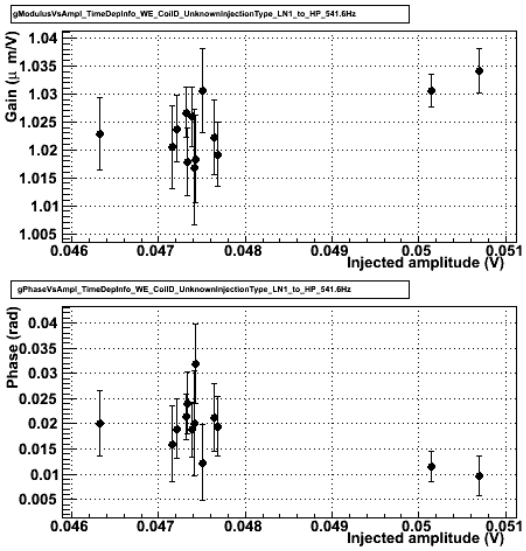

(c) 451.5 Hz

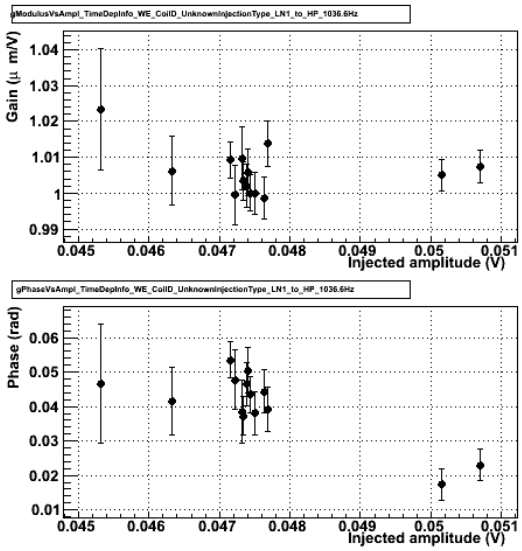

(d) 1036.5 Hz

Figure 23: ***Evolution as function of the signal amplitude of the measured actuation TF ratio (LN1/HP) for the down coil of the WE mirror*** *at four different frequencies. The amplitude in the x-axis is the amplitude of* $V1 : Ca\_WE\_RM\_CoilD$ *during the injections in LowNoise mode.*

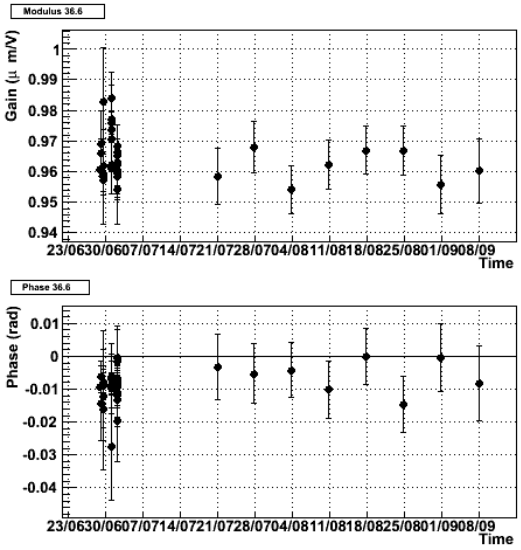

(a) 36.5 Hz

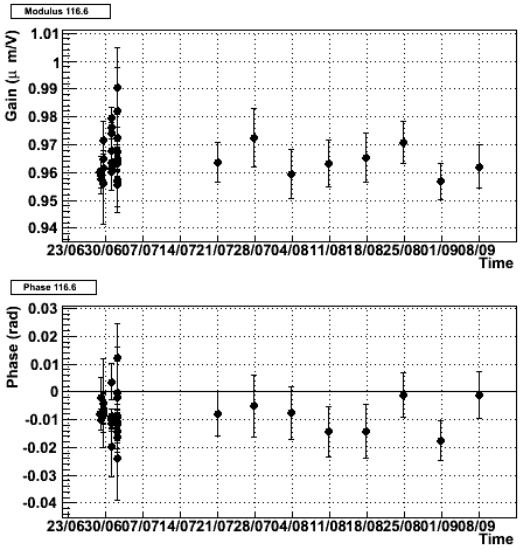

(b) 116.5 Hz

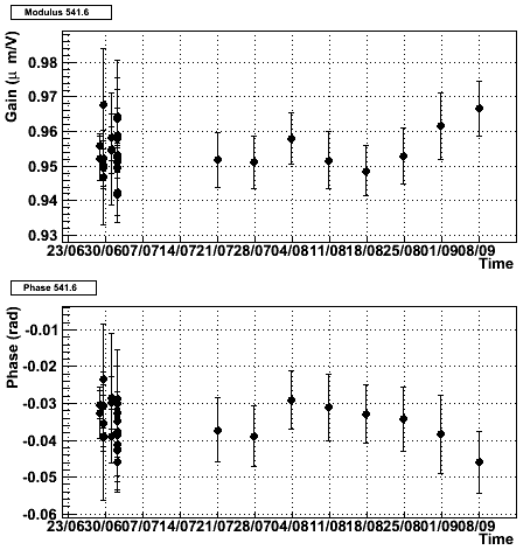

(c) 451.5 Hz

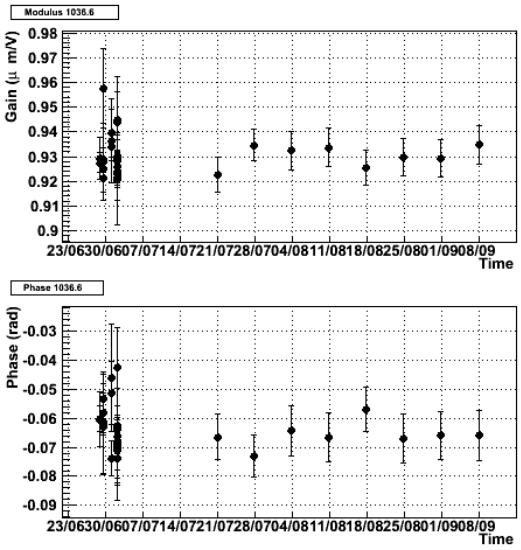

(d) 1036.5 Hz

Figure 24: ***Evolution as function of time (June to September 2009) of the measured actuation TF ratio (LN1/HP) for the left coil of the WE mirror*** *at four different frequencies.*

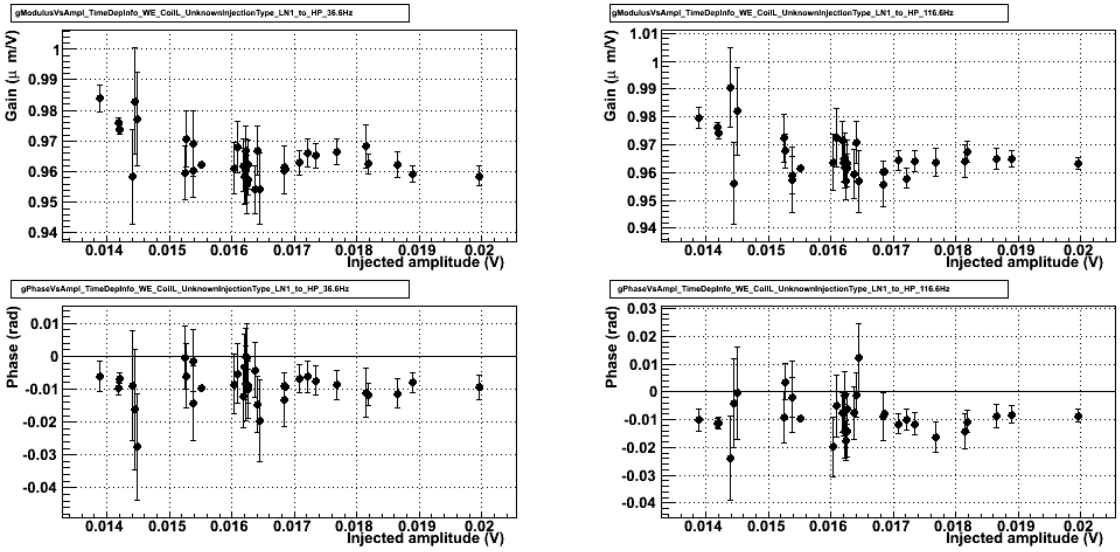

(a) 36.5 Hz (b) 116.5 Hz

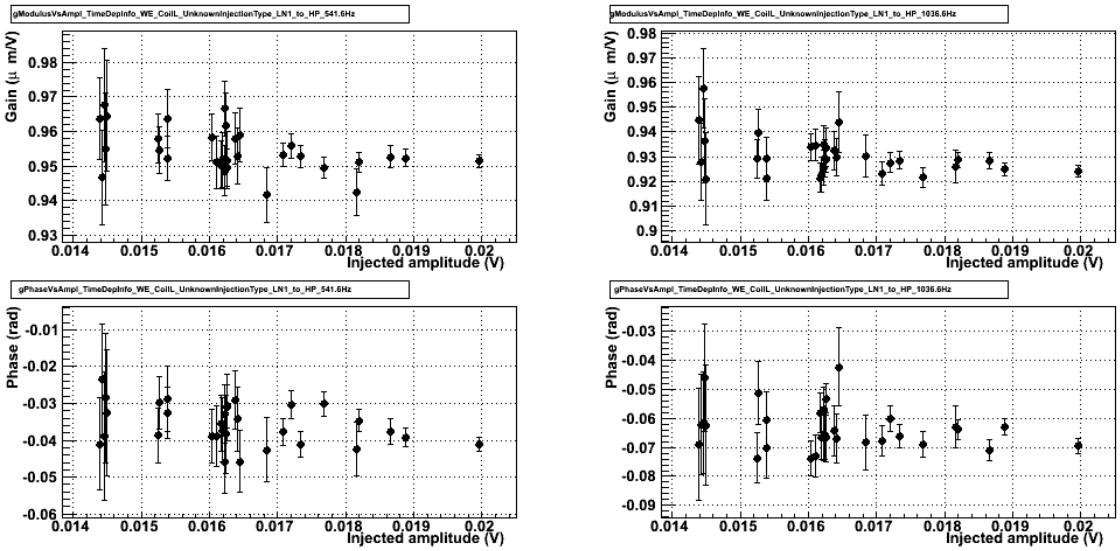

(c) 451.5 Hz (d) 1036.5 Hz

Figure 25: ***Evolution as function of the signal amplitude of the measured actuation TF ratio (LN1/HP) for the laft coil of the WE mirror*** *at four different frequencies. The amplitude in the x-axis is the amplitude of* $V1 : Ca\_WE\_RM\_CoilL$ *during the injections in LowNoise mode.*

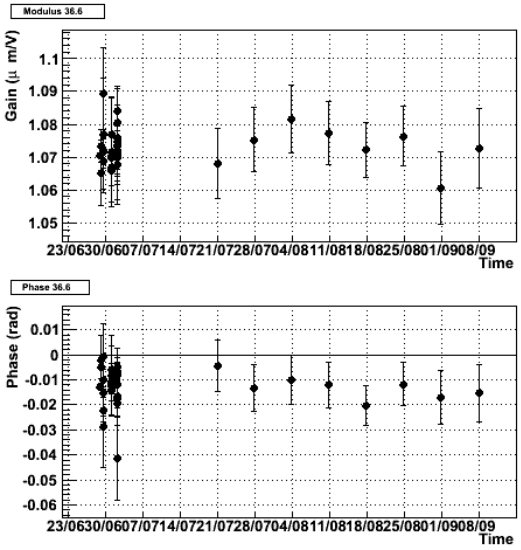

(a) 36.5 Hz

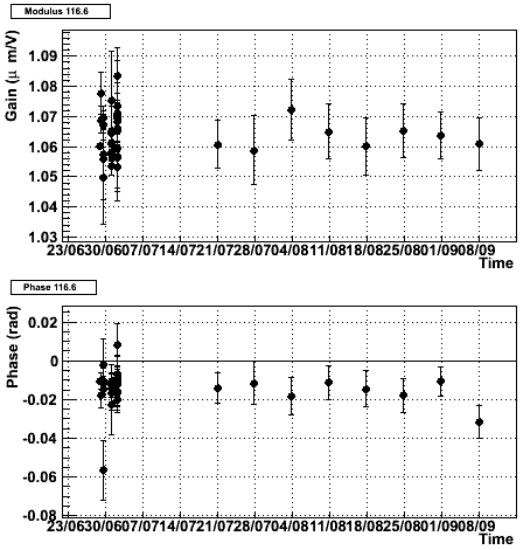

(b) 116.5 Hz

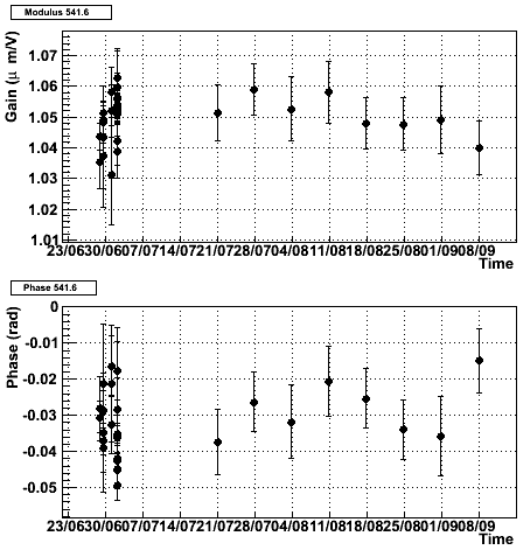

(c) 451.5 Hz

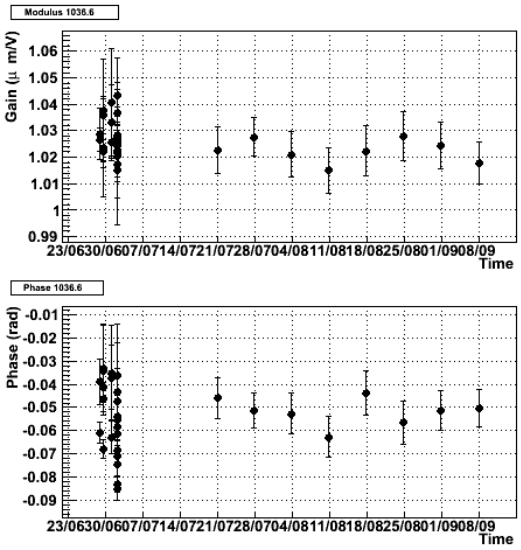

(d) 1036.5 Hz

Figure 26: ***Evolution as function of time (June to September 2009) of the measured actuation TF ratio (LN1/HP) for the right coil of the WE mirror*** *at four different frequencies.*

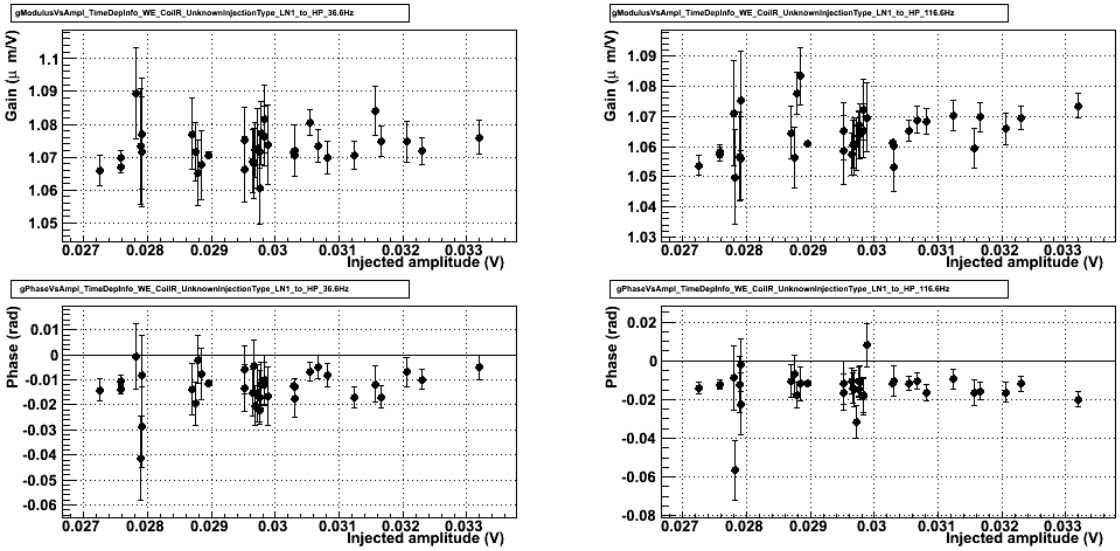

(a) 36.5 Hz

(b) 116.5 Hz

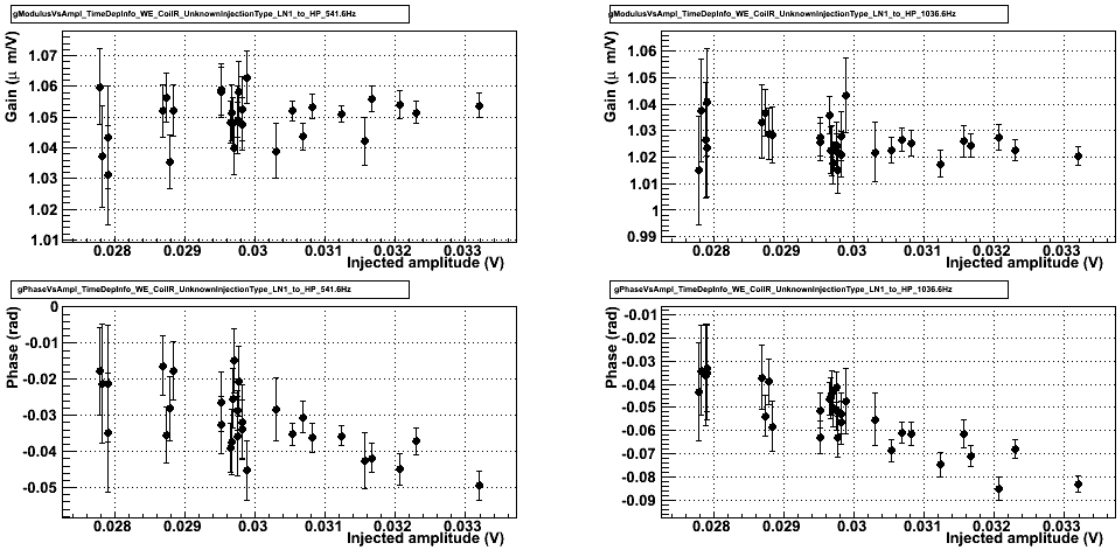

(c) 451.5 Hz

(d) 1036.5 Hz

Figure 27: ***Evolution as function of the signal amplitude of the measured actuation TF ratio (LN1/HP) for the right coil of the WE mirror*** *at four different frequencies. The amplitude in the x-axis is the amplitude of* $V1 : Ca\_WE\_RM\_CoilR$ *during the injections in LowNoise mode.*

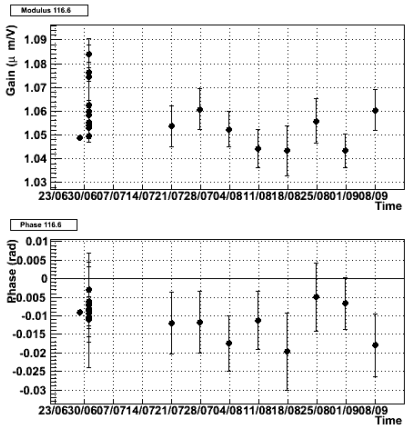

(a) Coil Up, 116.5 Hz.

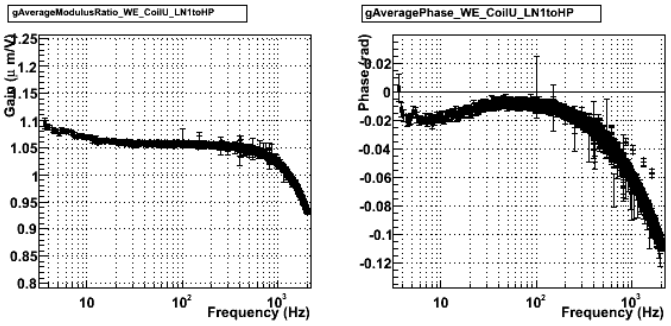

(b) Coil Up, averaged

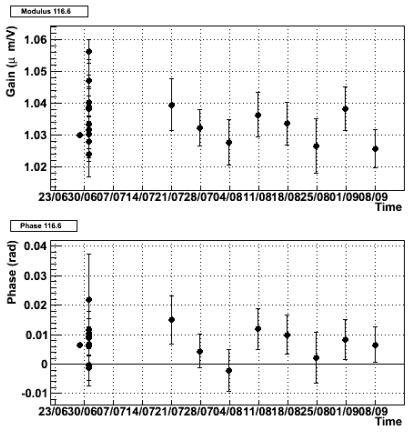

(c) Coil Down, 116.5 Hz

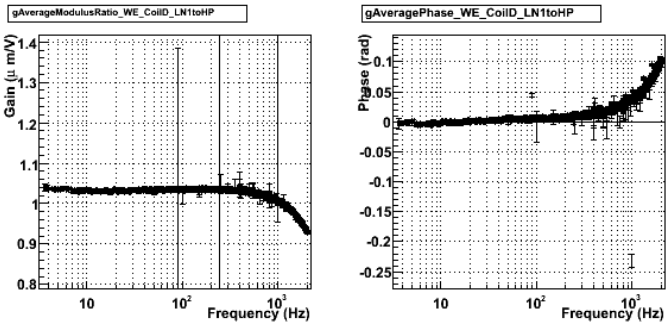

(d) Coil Down, averaged

Figure 28: ***Measured actuation TF ratio (LN1/HP) for the up and down coils of the WE mirror.***

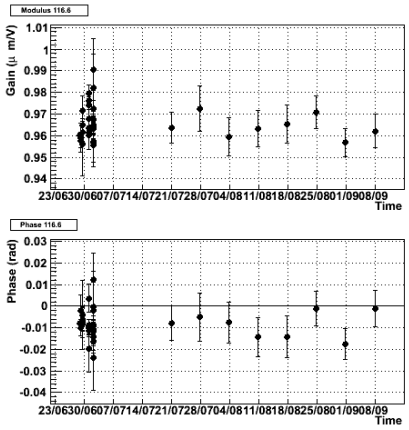

(a) Coil Left, 116.5 Hz

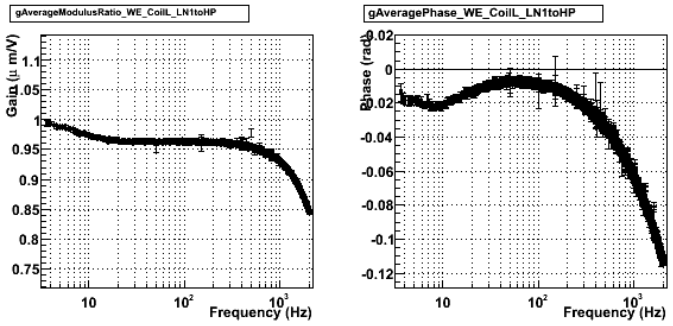

(b) Coil Left, averaged

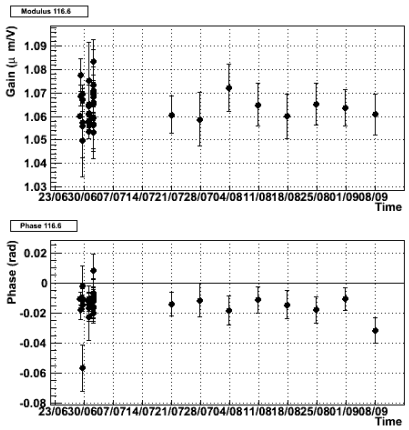

(c) Coil Right, 116.5 Hz

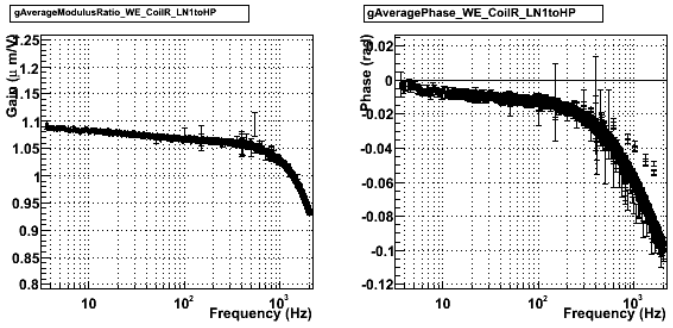

(d) Coil Right, averaged

Figure 29: ***Measured actuation TF ratio (LN1/HP) for the left and right coils of the WE mirror.***

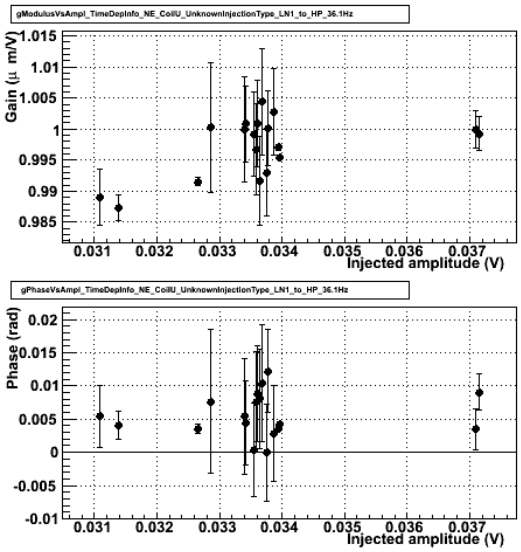

(a) 36.5 Hz

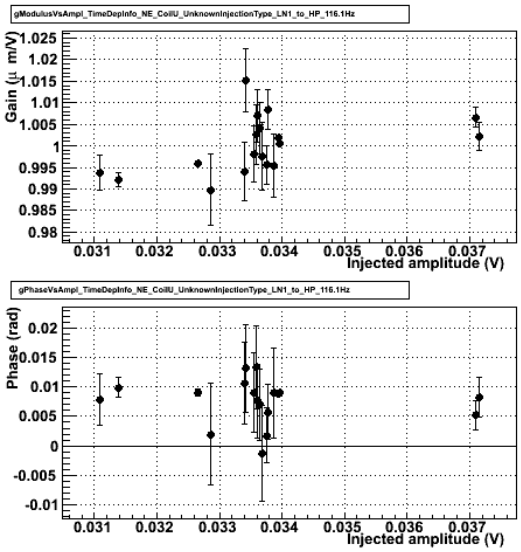

(b) 116.5 Hz

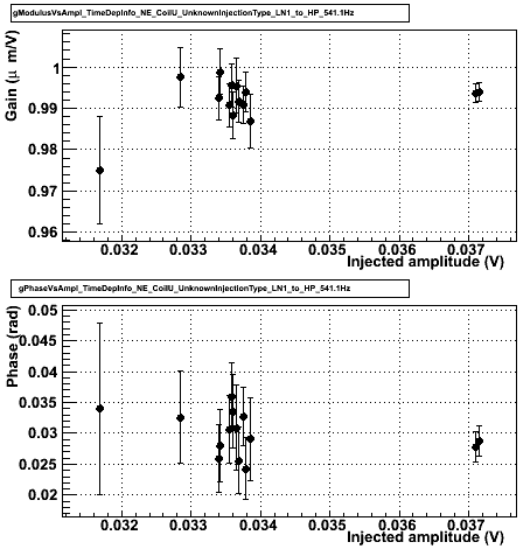

(c) 451.5 Hz

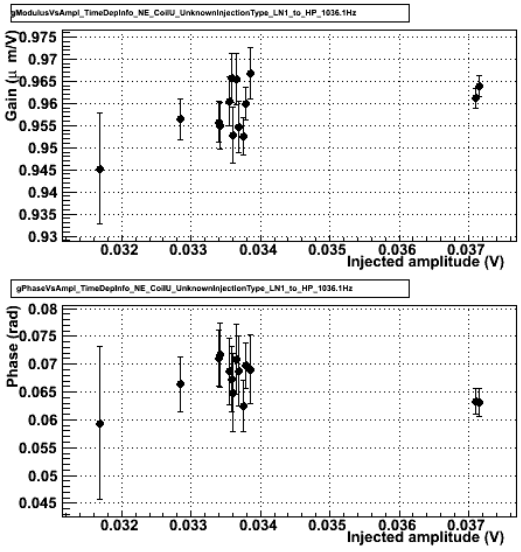

(d) 1036.5 Hz

Figure 30: ***Evolution as function of the signal amplitude of the measured actuation TF ratio (LN1/HP) for the up coil of the NE mirror*** *at four different frequencies. The amplitude in the x-axis is the amplitude of* $V1 : Ca\_NE\_RM\_CoilU$ *during the injections in LowNoise mode.*

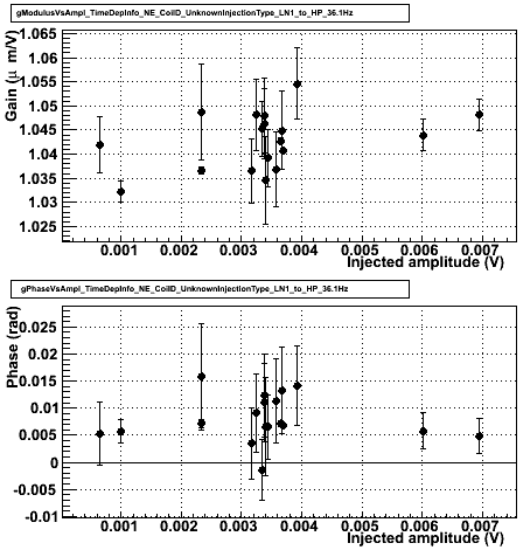

(a) 36.5 Hz

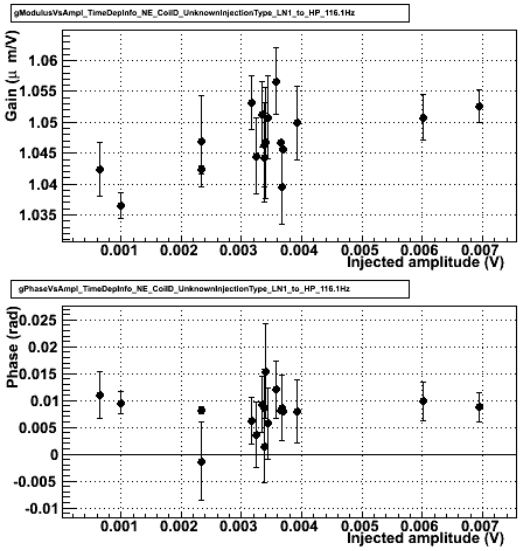

(b) 116.5 Hz

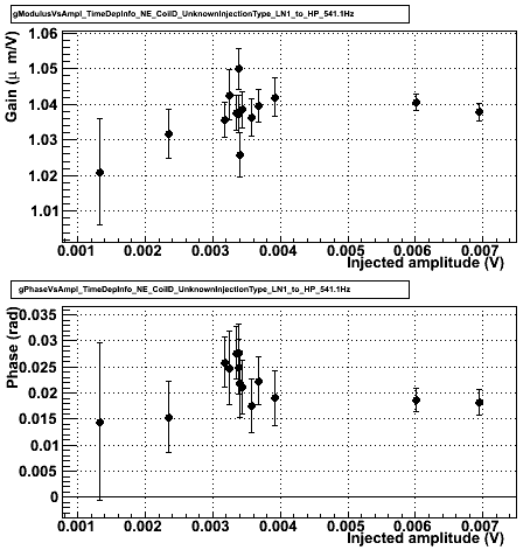

(c) 451.5 Hz

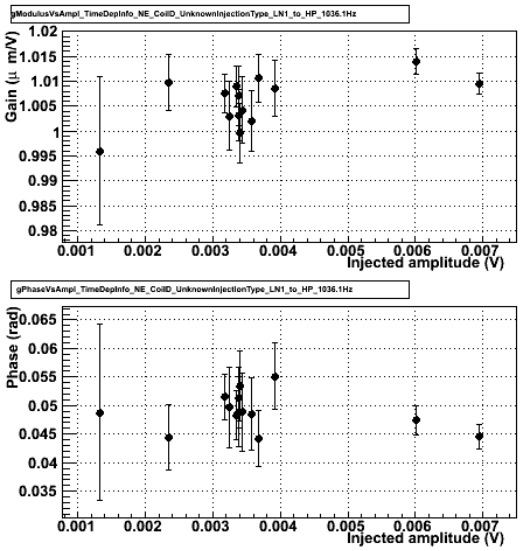

(d) 1036.5 Hz

Figure 31: ***Evolution as function of the signal amplitude of the measured actuation TF ratio (LN1/HP) for the down coil of the NE mirror*** *at four different frequencies. The amplitude in the x-axis is the amplitude of* $V1 : Ca\_NE\_RM\_CoilD$ *during the injections in LowNoise mode.*

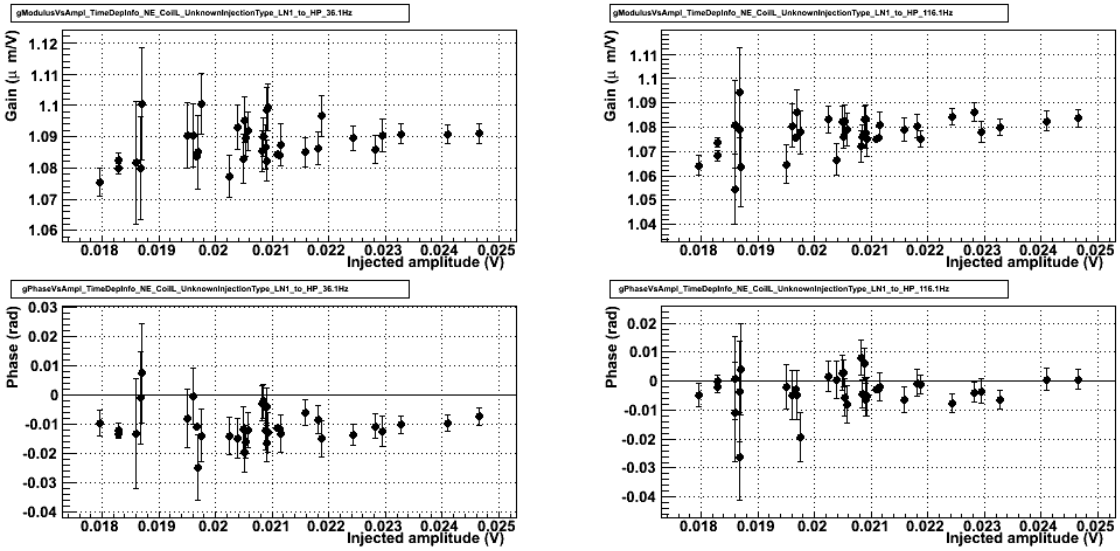

(a) 36.5 Hz (b) 116.5 Hz

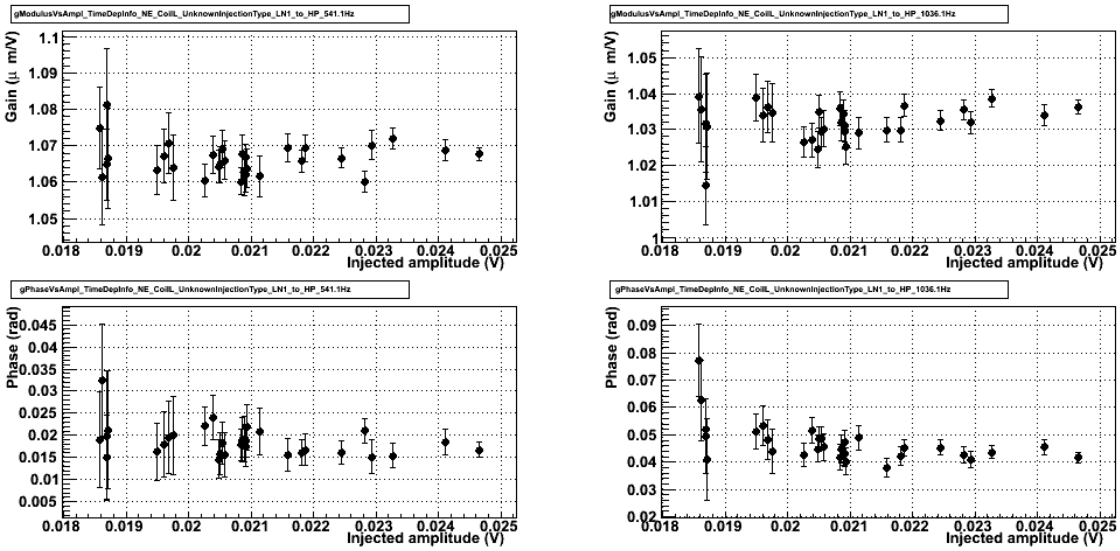

(c) 451.5 Hz (d) 1036.5 Hz

Figure 32: ***Evolution as function of the signal amplitude of the measured actuation TF ratio (LN1/HP) for the left coil of the NE mirror*** *at four different frequencies. The amplitude in the x-axis is the amplitude of* $V1 : Ca\_NE\_RM\_CoilL$ *during the injections in LowNoise mode.*

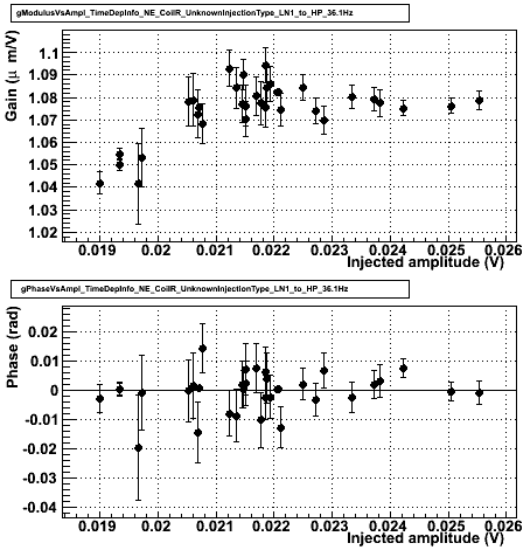

(a) 36.5 Hz

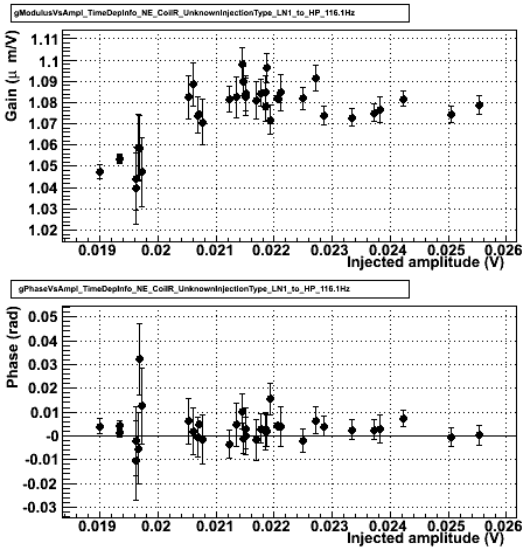

(b) 116.5 Hz

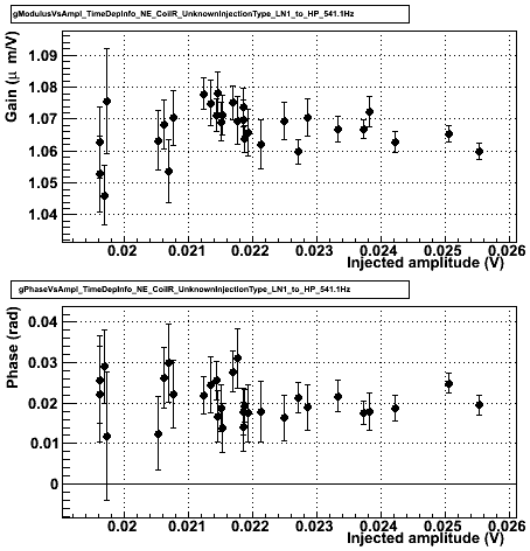

(c) 451.5 Hz

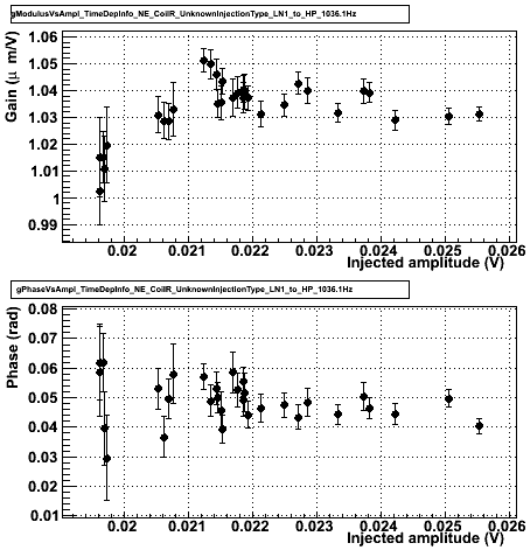

(d) 1036.5 Hz

Figure 33: ***Evolution as function of the signal amplitude of the measured actuation TF ratio (LN1/HP) for the right coil of the NE mirror*** *at four different frequencies. The amplitude in the x-axis is the amplitude of* $V1 : Ca\_NE\_RM\_CoilR$ *during the injections in LowNoise mode.*

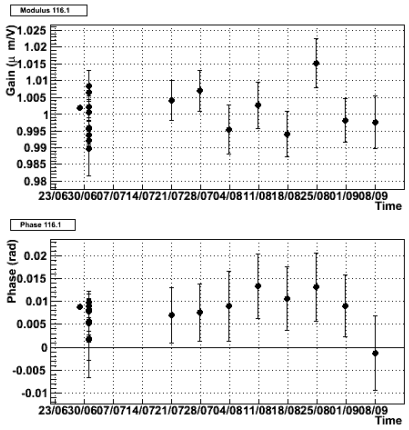

(a) Coil Up, 116.0 Hz

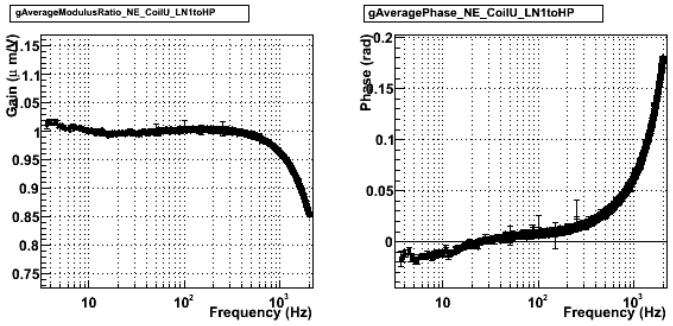

(b) Coil Up, averaged

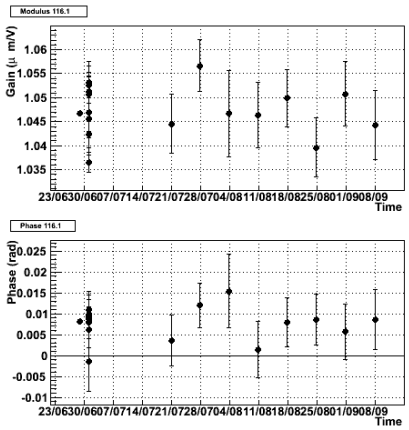

(c) Coil Down, 116.0 Hz

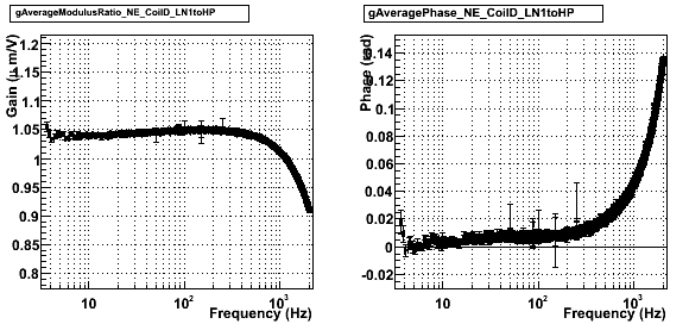

(d) Coil Down, averaged

Figure 34: ***Measured actuation TF ratio (LN1/HP) for the up and down coils of the NE mirror.***

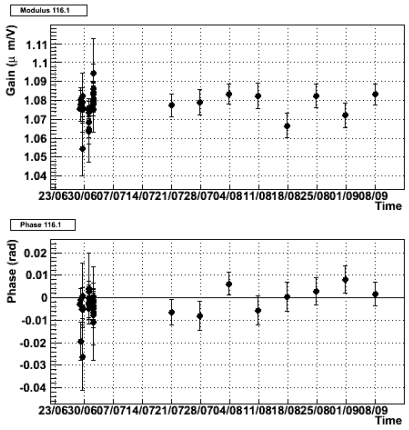

(a) Coil Left, 116.0 Hz

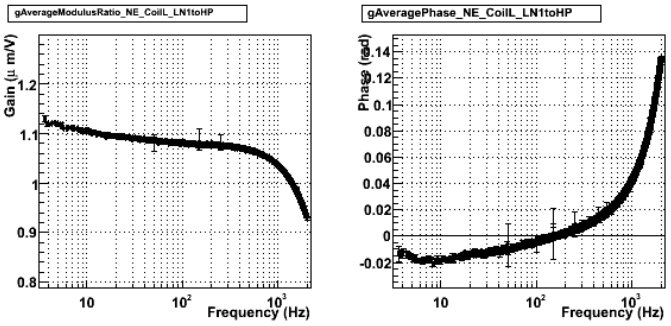

(b) Coil Left, averaged

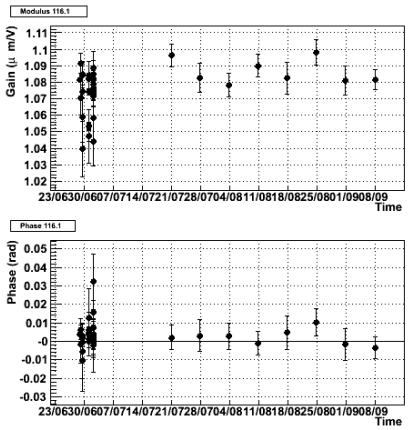

(c) Coil Right, 116.0

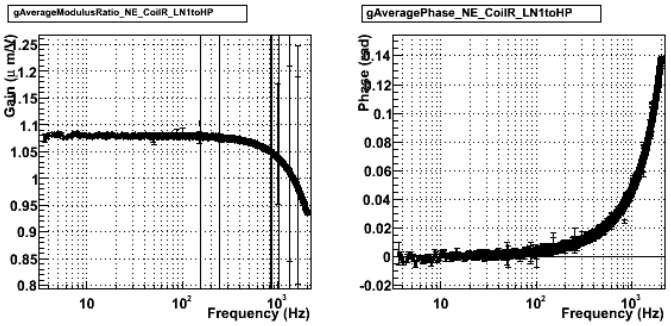

(d) Coil Right, averaged

Figure 35: ***Measured actuation TF ratio (LN1/HP) for the left and right coils of the NE mirror.***

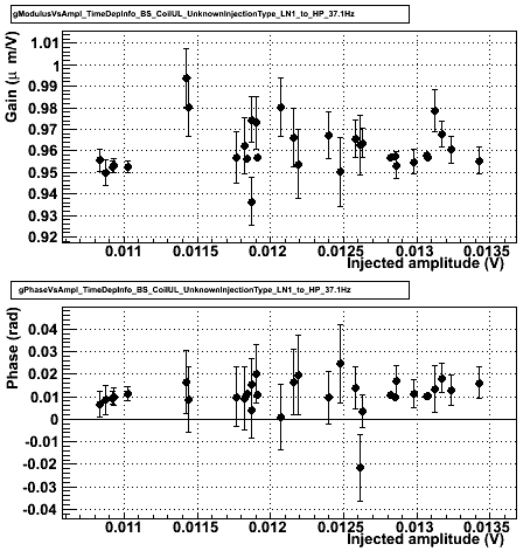

(a) 36.5 Hz

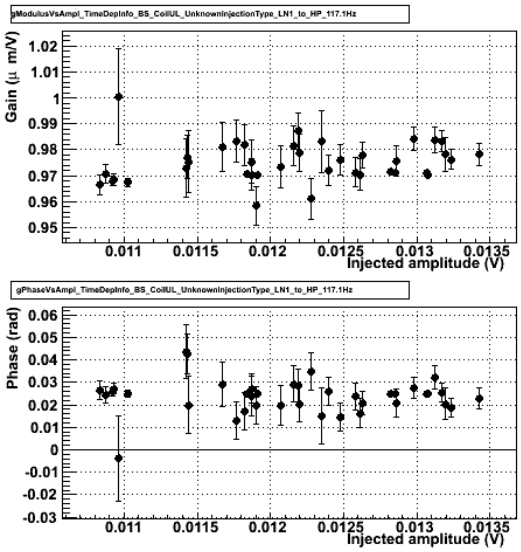

(b) 116.5 Hz

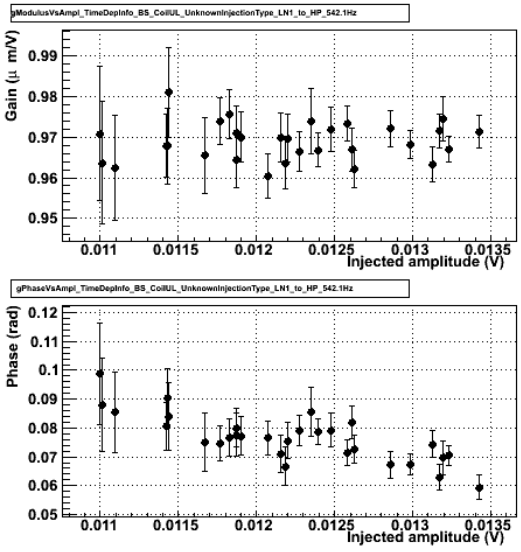

(c) 451.5 Hz

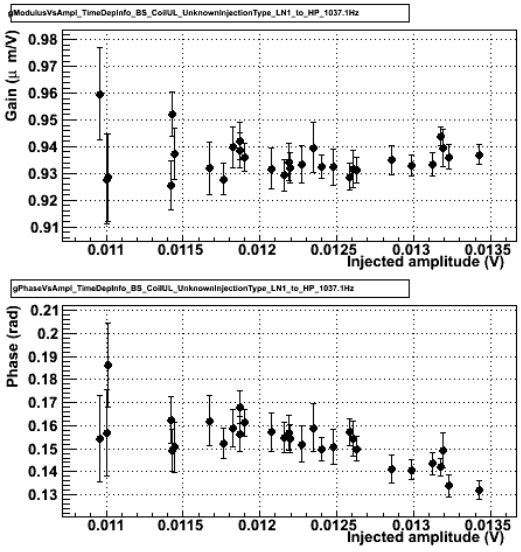

(d) 1036.5 Hz

Figure 36: ***Evolution as function of the signal amplitude of the measured actuation TF ratio (LN1/HP) for the up-left coil of the BS mirror*** *at four different frequencies. The amplitude in the x-axis is the amplitude of* $V1 : Ca\_BS\_RM\_CoilUL$ *during the injections in LowNoise1 mode.*

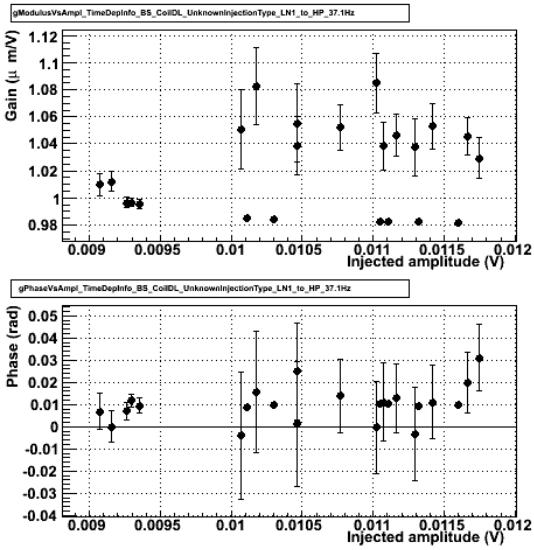

(a) 36.5 Hz

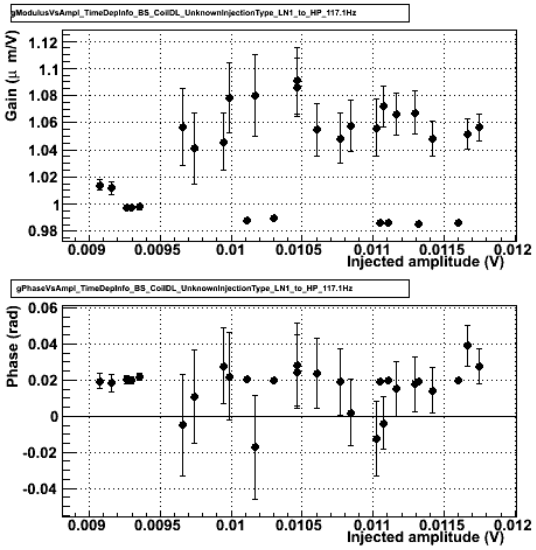

(b) 116.5 Hz

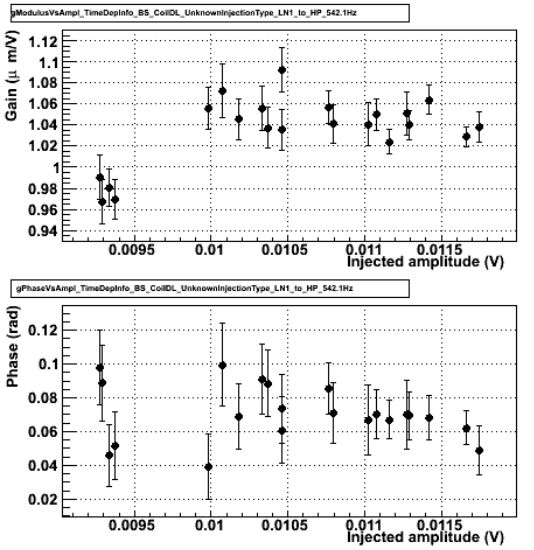

(c) 451.5 Hz

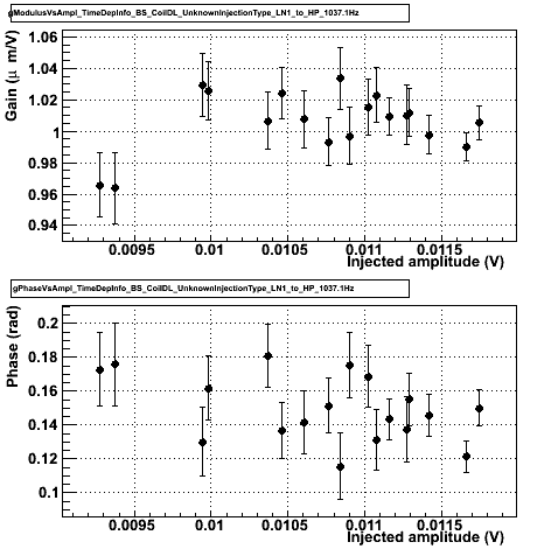

(d) 1036.5 Hz

Figure 37: ***Evolution as function of the signal amplitude of the measured actuation TF ratio (LN1/HP) for the down-left coil of the BS mirror*** *at four different frequencies. The amplitude in the x-axis is the amplitude of* $V1 : Ca\_BS\_RM\_CoilDL$ *during the injections in LowNoise1 mode.*

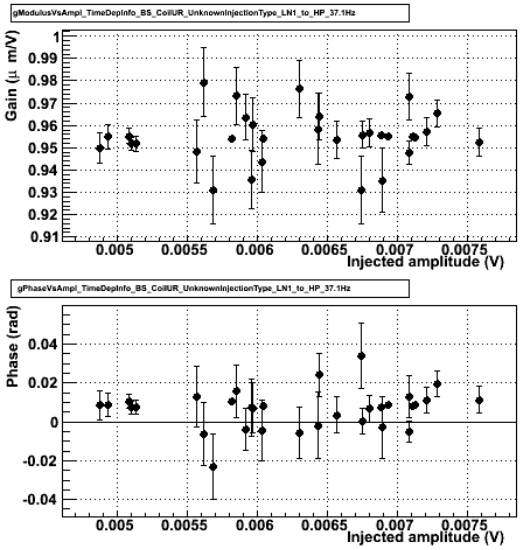

(a) 36.5 Hz

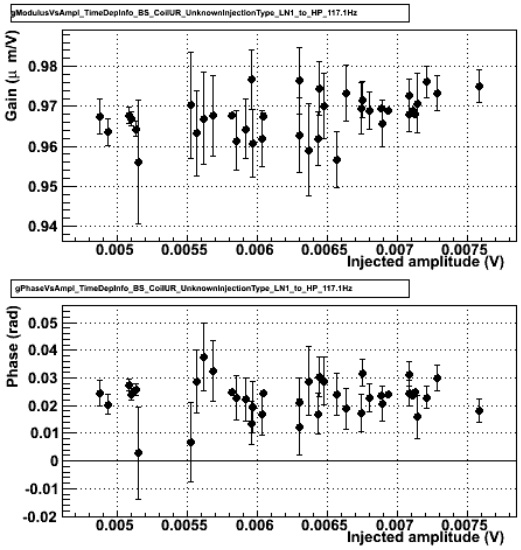

(b) 116.5 Hz

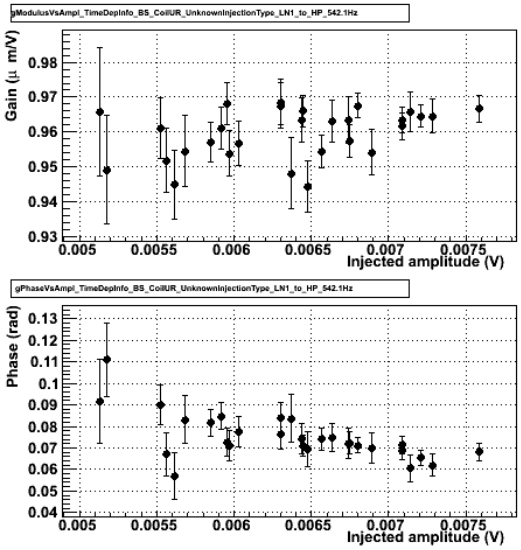

(c) 451.5 Hz

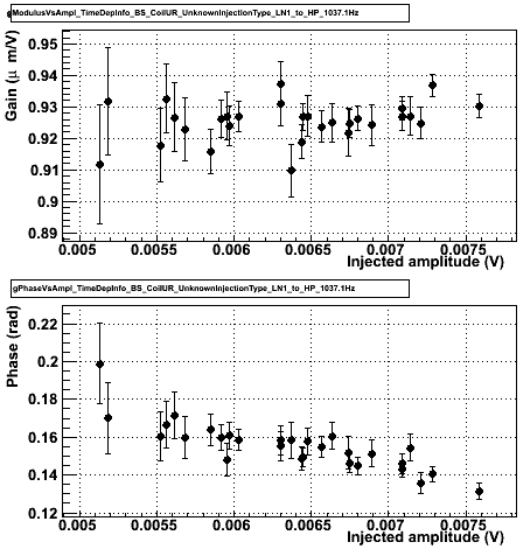

(d) 1036.5 Hz

Figure 38: ***Evolution as function of the signal amplitude of the measured actuation TF ratio (LN1/HP) for the down-left coil of the BS mirror*** *at four different frequencies. The amplitude in the x-axis is the amplitude of* $V1 : Ca\_BS\_RM\_CoilUR$ *during the injections in LowNoise1 mode.*

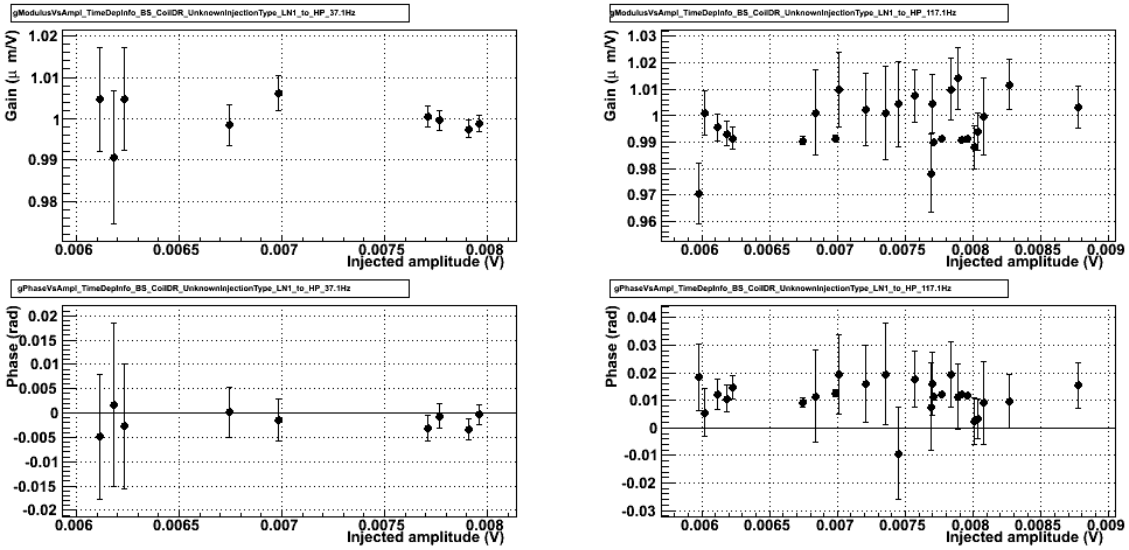

(a) 36.5 Hz

(b) 116.5 Hz

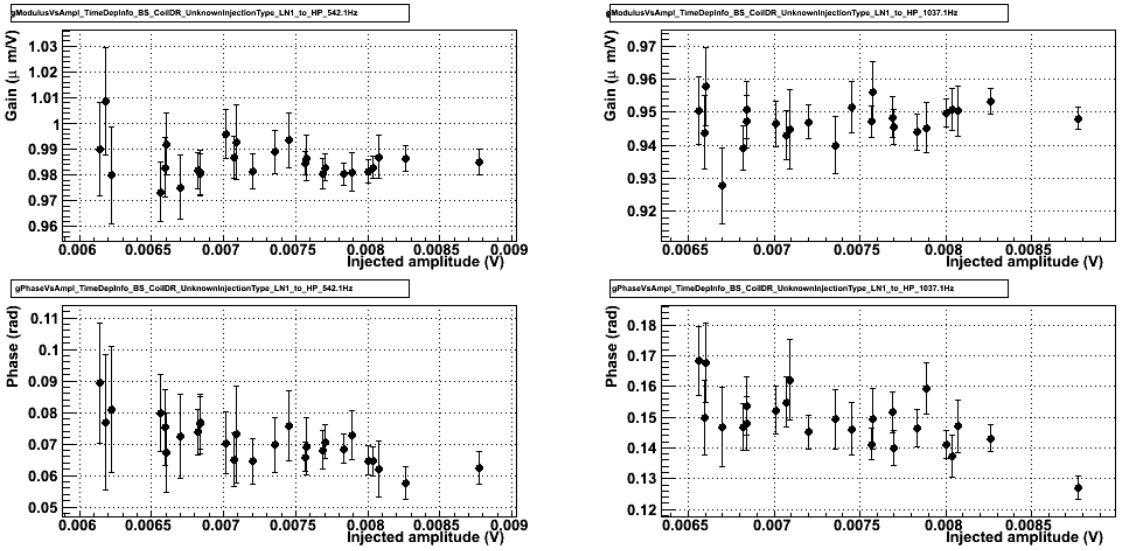

(c) 451.5 Hz

(d) 1036.5 Hz

Figure 39: ***Evolution as function of the signal amplitude of the measured actuation TF ratio (LN1/HP) for the up-left coil of the BS mirror*** *at four different frequencies. The amplitude in the x-axis is the amplitude of* $V1 : Ca\_BS\_RM\_CoilDR$ *during the injections in LowNoise1 mode.*

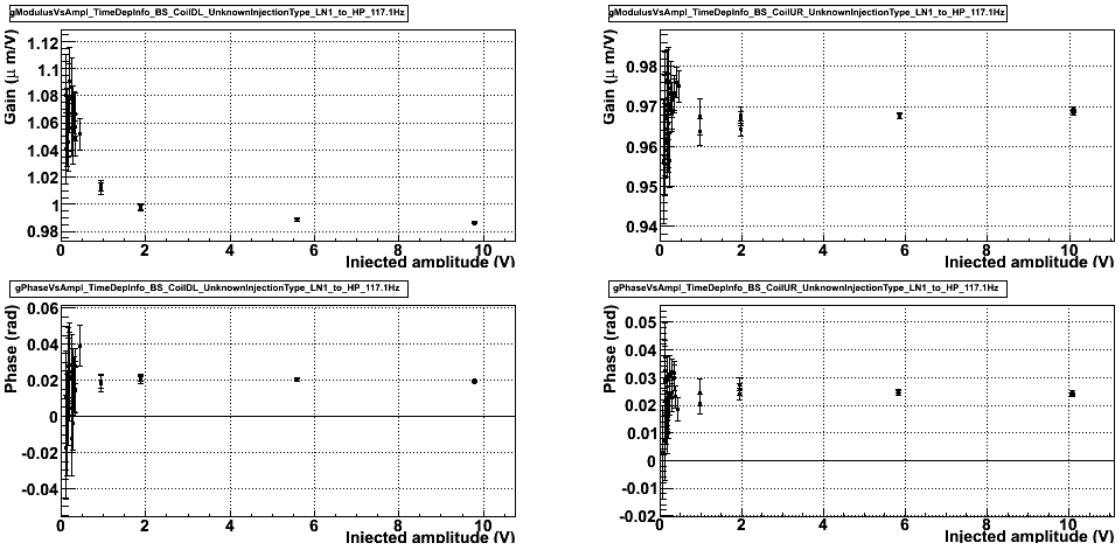

(a) Coil DL, 117 Hz

(b) Coil UR, 117 Hz

Figure 40: ***Evolution as function of the signal amplitude of the measured actuation TF ratio (LN1/HP) for the down-left and the up-right coils of the BS mirror*** *at 117 Hz. The amplitude in the x-axis is the amplitude of* $V1 : Ca\_BS\_RM\_\{CoilDL, CoilUR\}$ *during the injections* **in HighPower mode**.

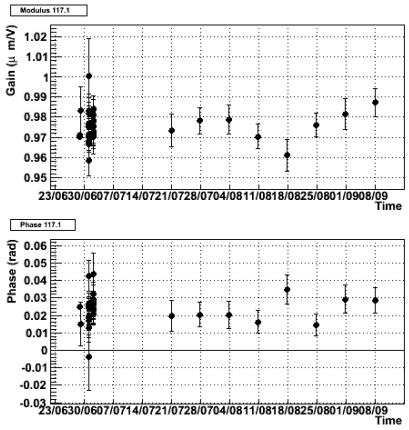

(a) Coil Up-Left, 117.0 Hz

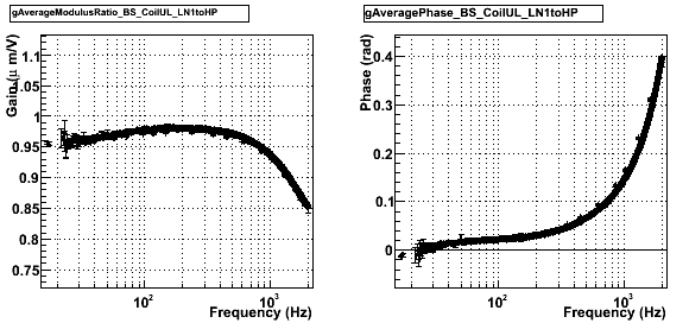

(b) Coil Up-Left, averaged

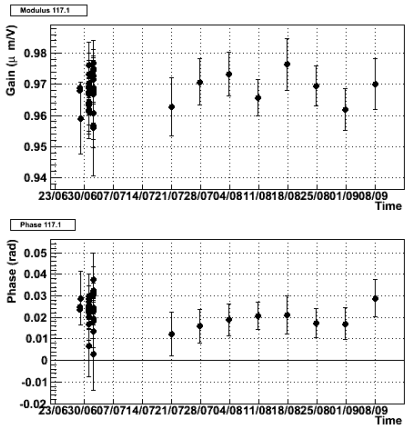

(c) Coil Up-Right, 117.0 Hz

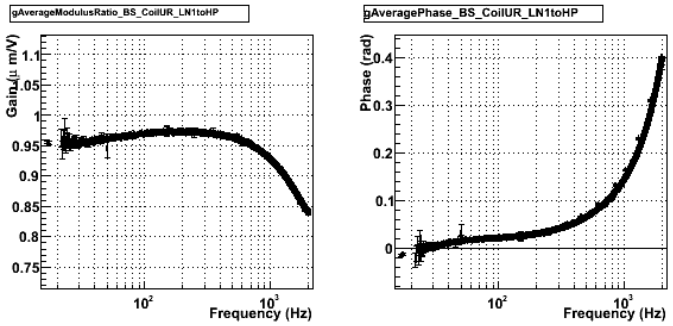

(d) Coil Up-Right, averaged

Figure 41: ***Measured actuation TF ratio (LN1/HP) for the up-left and up-right coils of the BS mirror.***

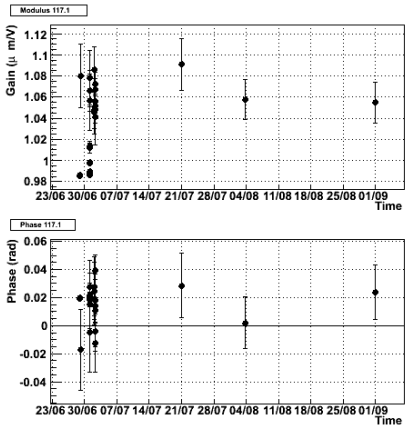

(a) Coil Down-Left, 117.0 Hz

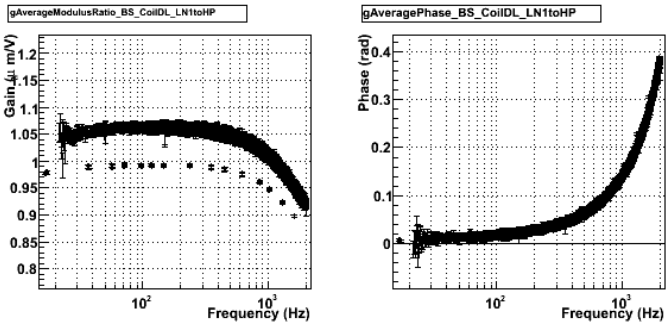

(b) Coil Down-Left, averaged

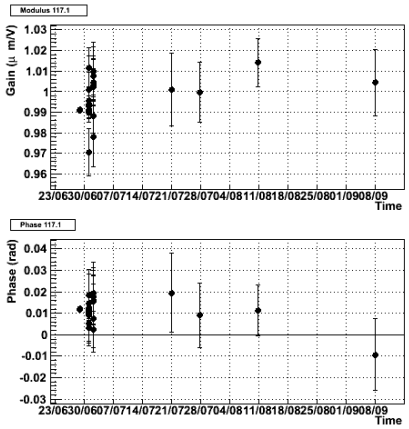

(c) Coil Down-Right, 117.0 Hz

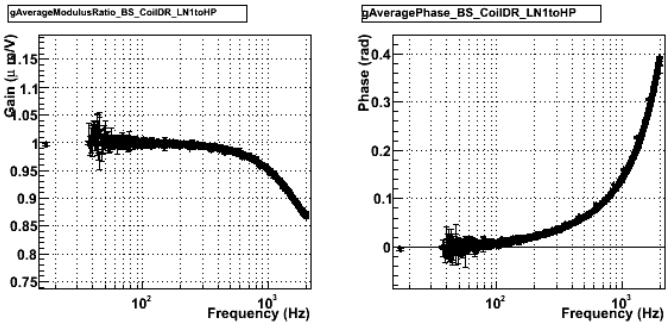

(d) Coil Down-Right, averaged

Figure 42: ***Measured actuation TF ratio (LN1/HP) for the down-left and down-right coils of the BS mirror.***

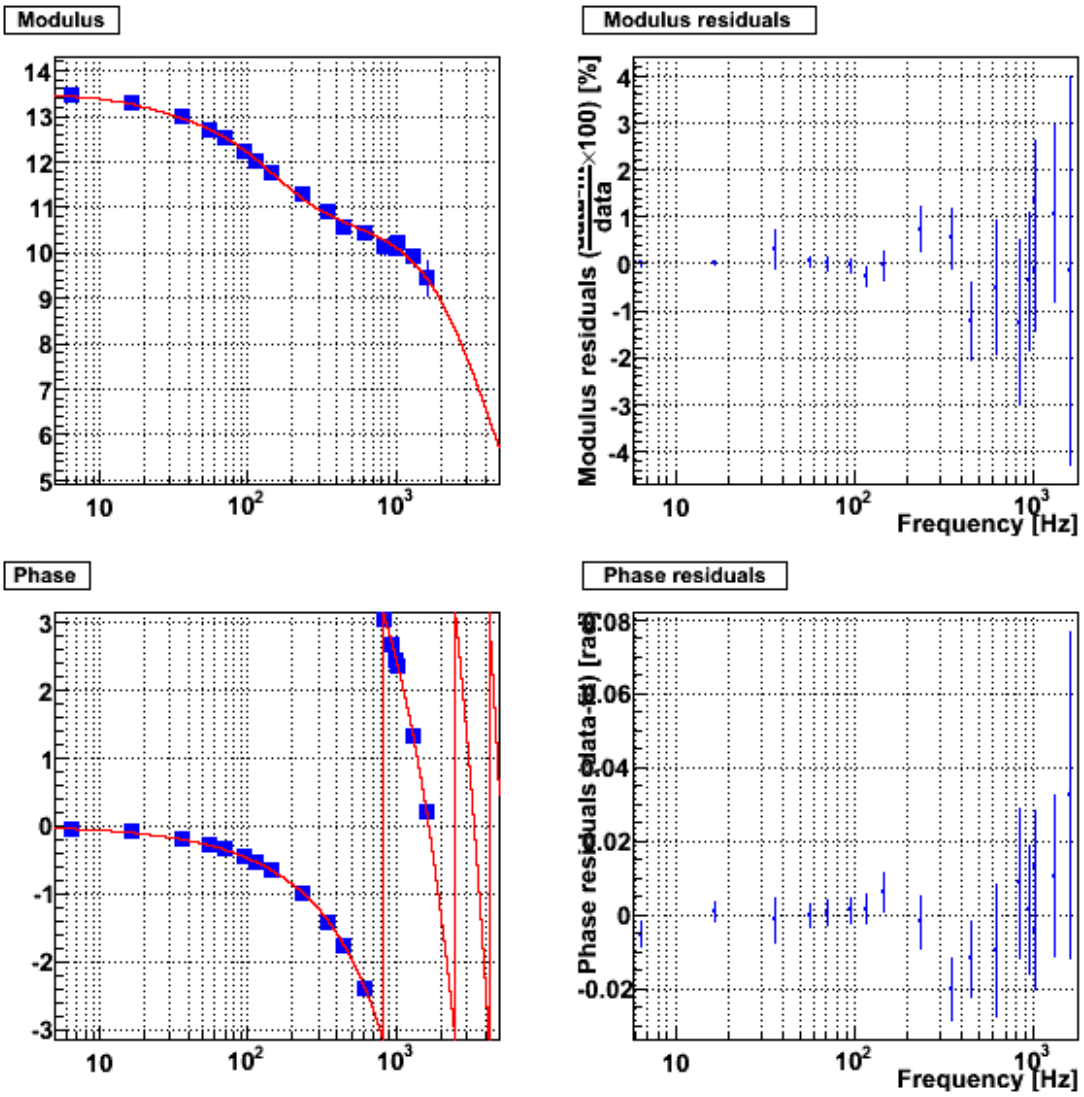

Figure 43: ***Measured actuation of the WE mirror using the U-D coils in LN1 mode****, fitted model and residuals.*

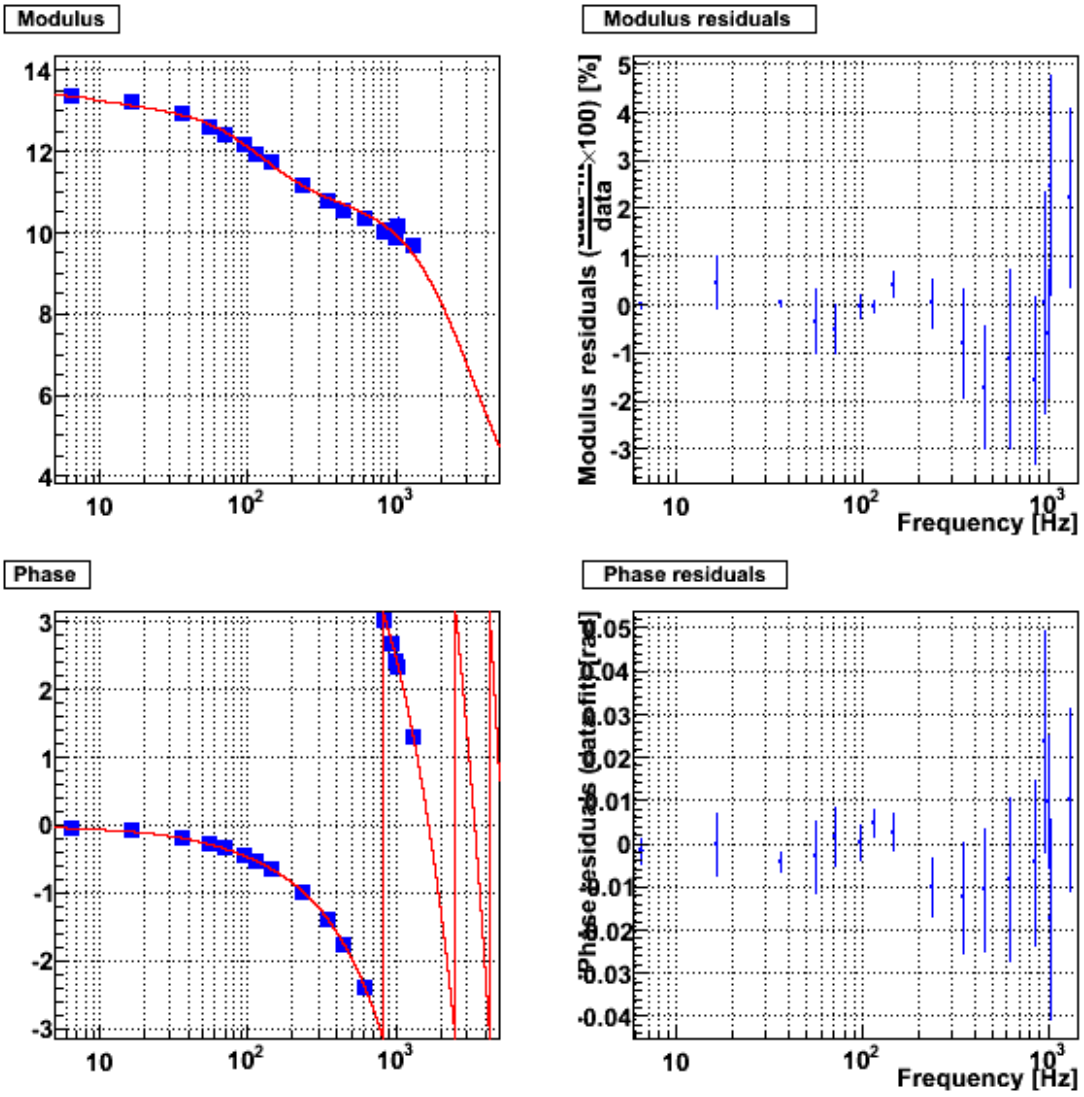

Figure 44: ***Measured actuation of the WE mirror using the L-R coils in LN1 mode****, fitted model and residuals.*

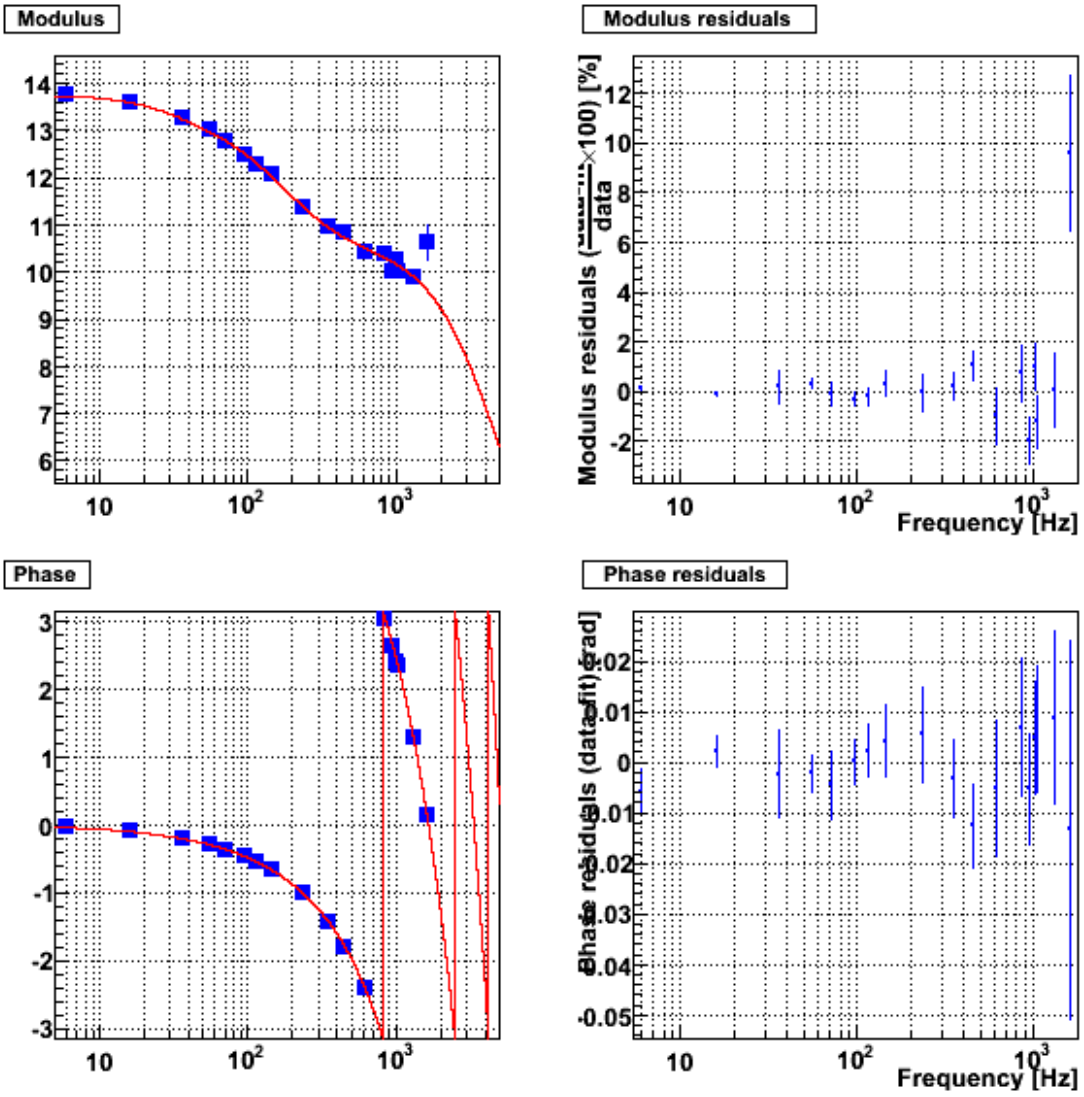

Figure 45: ***Measured actuation of the NE mirror using the U-D coils in LN1 mode****, fitted model and residuals.*

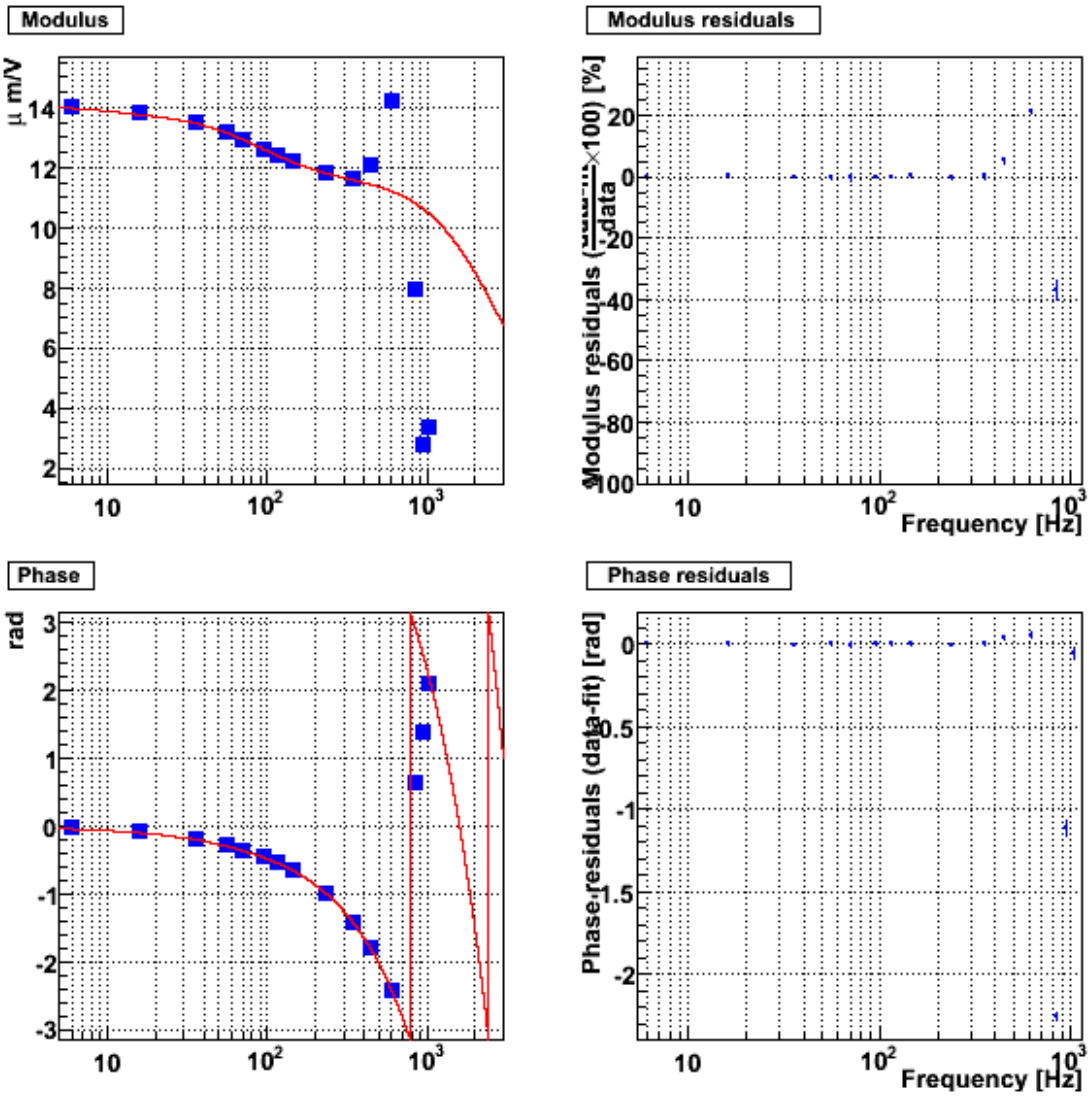

Figure 46: ***Measured actuation of the NE mirror using the L-R coils in LN1 mode****, fitted model and residuals. The data have been fitted below 400 Hz only.*

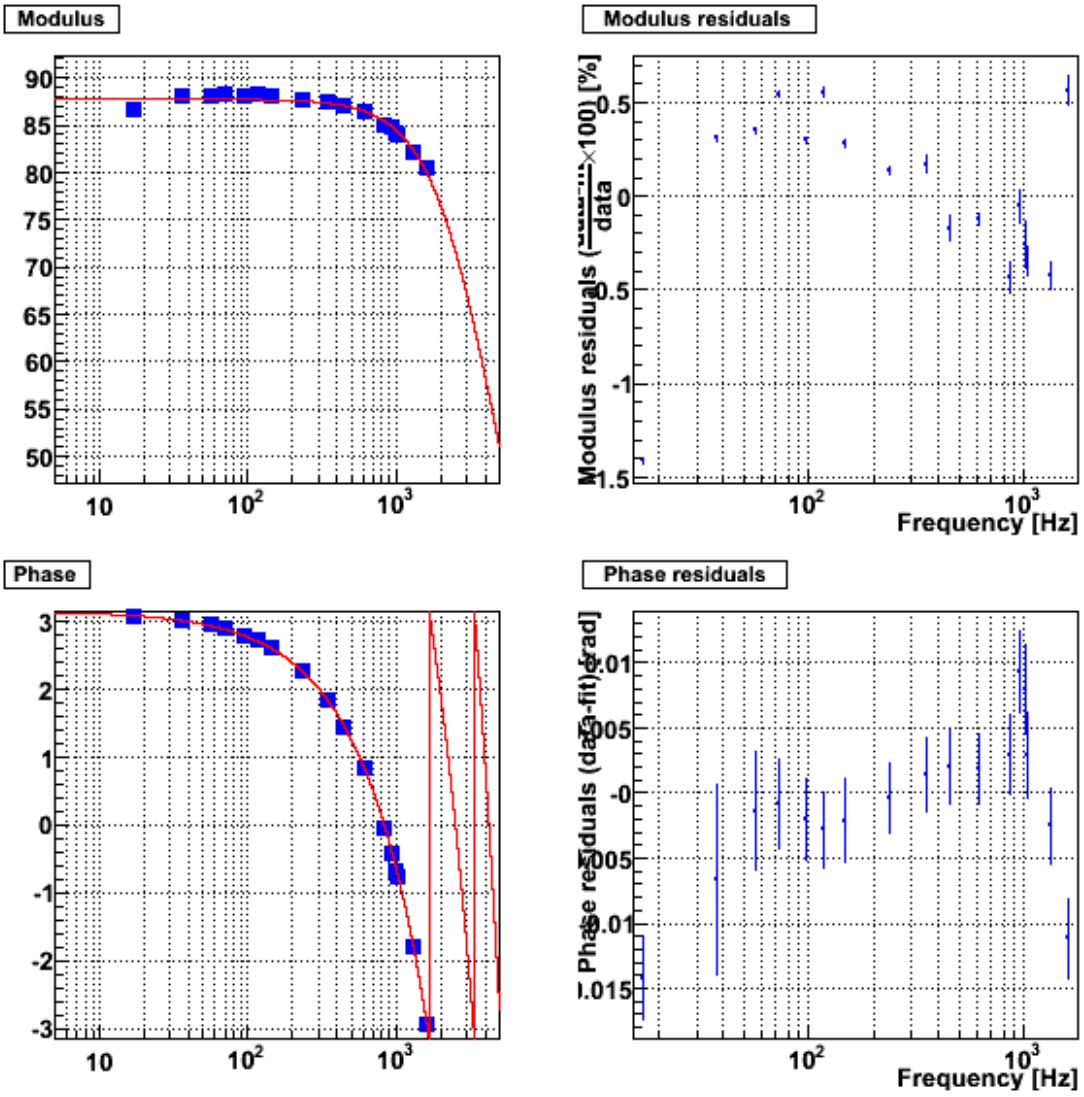

Figure 47: ***Measured actuation of the BS mirror using the four coils in LN1 mode****, fitted model and residuals.*

4 Calibration of the marionette actuation

The marionette actuation is defined as the TF (with modulus in m/V) from the correction signal to the induced mirror motion[19]. The time reference is the GPS time.

In the plots that are shown, the actuation is corrected for the mechanical model of the pendulum, defined as **two** 2nd order low-pass filters with $f_0 = 0.6\,\mathrm{Hz}$ and $Q = 1000$.

4.1 Description of the measurements

The calibration of the NE (U-D coils) and WE (U-D coils) mirror actuation in LN1 mode is used as reference to measure the NE and WE marionette actuations.

An intermediate step consists in measuring the Marionette/Mirror TF ratio. This is performed using the ITF in step 12, and measuring the ITF response in closed loop in two datasets:

- one injecting noise to the mirror actuation. It permits to measure the ITF response R_1 as function of the injected signal, in W/V,
- one injecting noise to the marionette actuation. It permits to measure the ITF response R_2 as function of the injected signal, in W/V.

Then, the ratio of R_2/R_1 gives the ratio of the responses of the marionette actuation to the mirror actuation. This ratio is then multiplied by the model of the mirror actuation (U-D coils, in LN1 mode) to obtain the marionette actuation. Only the points where the coherence is higher than 90% have been used to estimate R_1 and R_2.

This analysis assumes that the ITF response (in particular the optical gain) is stable between the two datasets. In principle this is the case since both datasets are taken within 3 minutes. Such data were taken at different times and monitored during VSR2. The stability of the measurements validate this hypothesis.

The injected noise has been white noise from a few Hz to ~ 200 Hz. Different amplitudes of the noise were injected in order to check the linearity of the response.

4.2 Calibration of the WE and NE marionettes

The measured ratio of the WE and NE marionette to mirror responses are shown figures 51 and 53 (the mirror and marionette actuations being corrected for their pendulum mechanical model). The monitoring of this ratio as function of time are shown at some frequencies

[19] The marionette longitudinal actuation is done through two coils (left and right). Emphasis filters are set in the DSP for both coil channels in order to compensate for de-emphasis filters used in the coil drivers. The resistance of the coil channel is $R \sim 16.5\,\Omega$ and its inductance is $L \sim 214\,\mathrm{mH}$: the L-R circuit results in a pole $R/(2\pi L)$ around $12 - -13\,\mathrm{Hz}$.

figures 48 and 50. The ratio is also shown as function of the injected amplitude for the WE measurements figure 49.

The obtained marionette TF is shown figures 52 and 54 along with the fitted model and residuals. The fits were performed between 9 Hz and 200 Hz. The fit parameters are given in the table 5. A 2nd order low-pass filter at 1 kHz has been arbitrarily added in order to have a non-divergent TF parameterization. Below 100 Hz, the residuals are flat, lower than 5% in modulus and better than 50 mrad in phase.

Note that the 4 μs timing systematic error are negligible for the marionettes: at 100 Hz, it corresponds to less than 3 mrad phase error.

4.3 Tables

	WE	NE
Gain (μm/V)	3.273 ± 0.010	6.43 ± 0.15
Raw delay (μs)	$(134.1) \pm 4.0)$	(1389.0 ± 3.2)
Delay (μs)	-15.2 ± 4.0	1239.7 ± 3.2
Φ_0 (rad)	0	0
Pole frequency (Hz)	14.702 ± 0.036	16.744 ± 0.081
Zero frequency (Hz)	0.5196 ± 0.0017	0.6726 ± 0.0089
Pole frequency (Hz)	0.6083 ± 0.0022	0.421 ± 0.015
Zero frequency (Hz)	35.18 ± 0.13	46.88 ± 1.0
Pole frequency (Hz)	47.74 ± 0.16	59.66 ± 1.28
Zero frequency (Hz)	–	212.29 ± 1.9
Complex zero f_0 (Hz)	-202.71 ± 0.76	-118.597 ± 0.048
Complex zero Q	0.6085 ± 0.0013	1.5013 ± 0.0014
2nd order low-pass	$f_0 = 1000\,\mathrm{Hz}$, $Q = 0.7$	
Pendulum	**Two** 2nd order low-pass filters: $f_0 = 0.6\,\mathrm{Hz}$, $Q = 1000$	
χ^2/ndf	3826.88/3417	3434.9/3492

Table 5: ***WE and NE marionette actuation parameterizations.*** *Fit computed from 9 Hz to 200 Hz. The χ^2/ndf of the fits are given. Residuals are within 5% in modulus and 50 mrad in phase up to 100 Hz. The raw delays are the delay measured using the raw delays from the mirror actuation measurements. The delay has been corrected for the PrCa and sensing delays to take as reference the correction channels (i.e. Sc_WE_zMar): delay = raw_delay − 100 − 49.3 μs. Applying these TFs to the correction channels Sc_WE_zMar should enable to estimate the induce motion at absolute GPS time.*

4.4 Figures

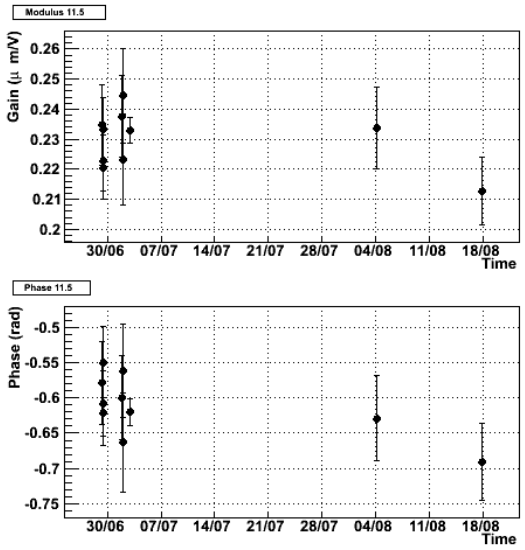

(a) 11.5 Hz

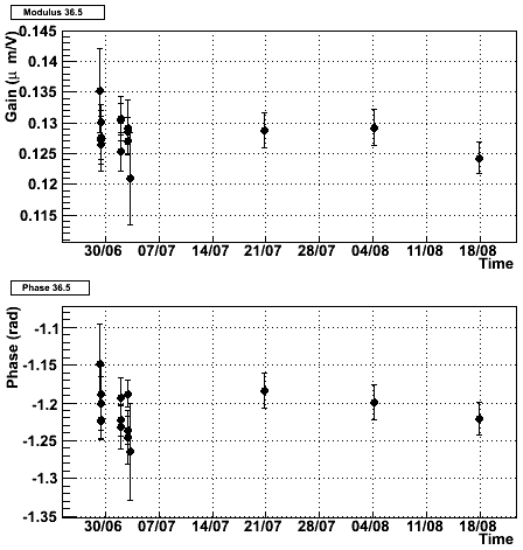

(b) 36.5 Hz

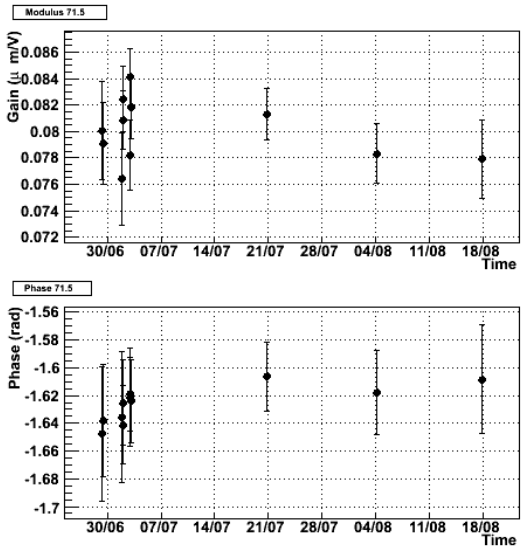

(c) 71.5 Hz

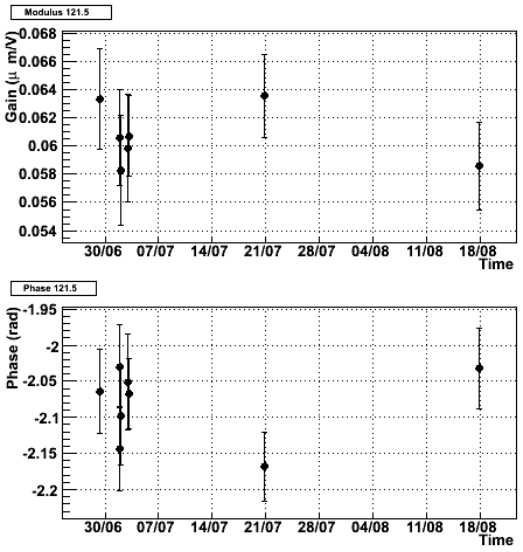

(d) 121.5 Hz

Figure 48: ***Measured WE marionette to mirror actuation (WE, U-D coils) TF ratio as function of time*** *at four different frequencies. The mirror and marionette actuations have been corrected for their pendulum mechanical models.*

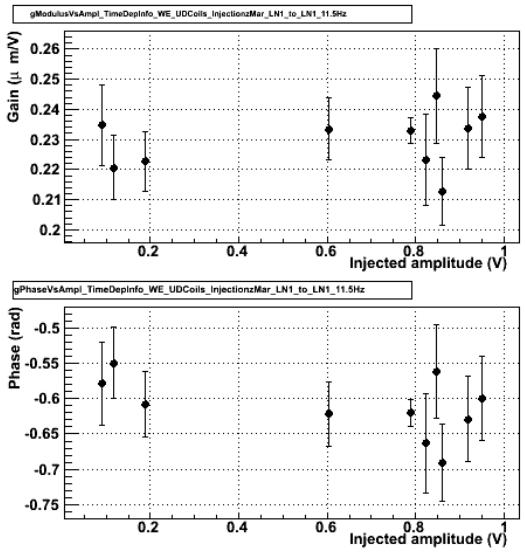

(a) 11.5 Hz

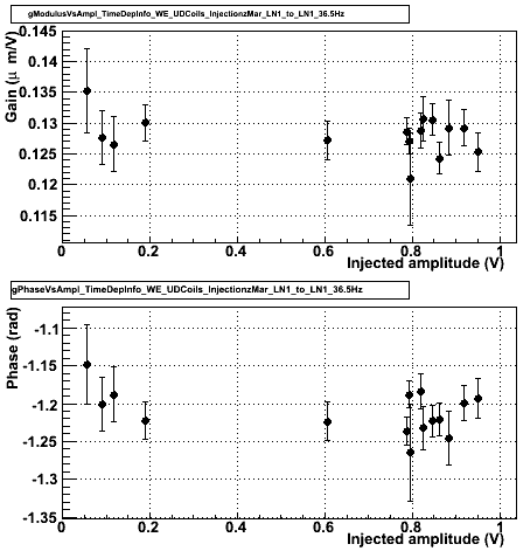

(b) 36.5 Hz

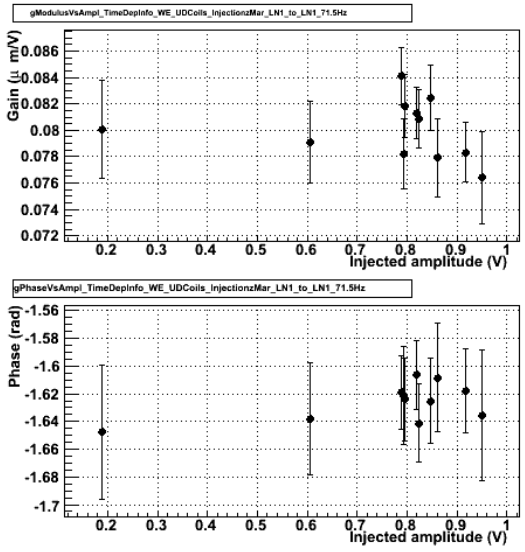

(c) 71.5 Hz

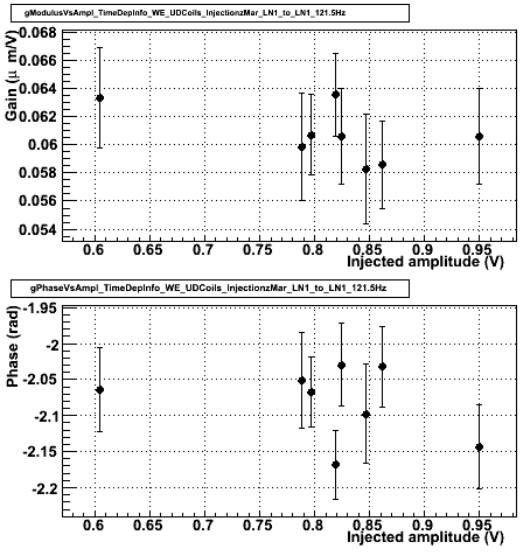

(d) 121.5 Hz

Figure 49: ***Measured WE marionette to mirror actuation (WE, U-D coils) TF ratio as function of amplitude of injected noise*** *at four different frequencies. The mirror and marionette actuations have been corrected for their pendulum mechanical models.*

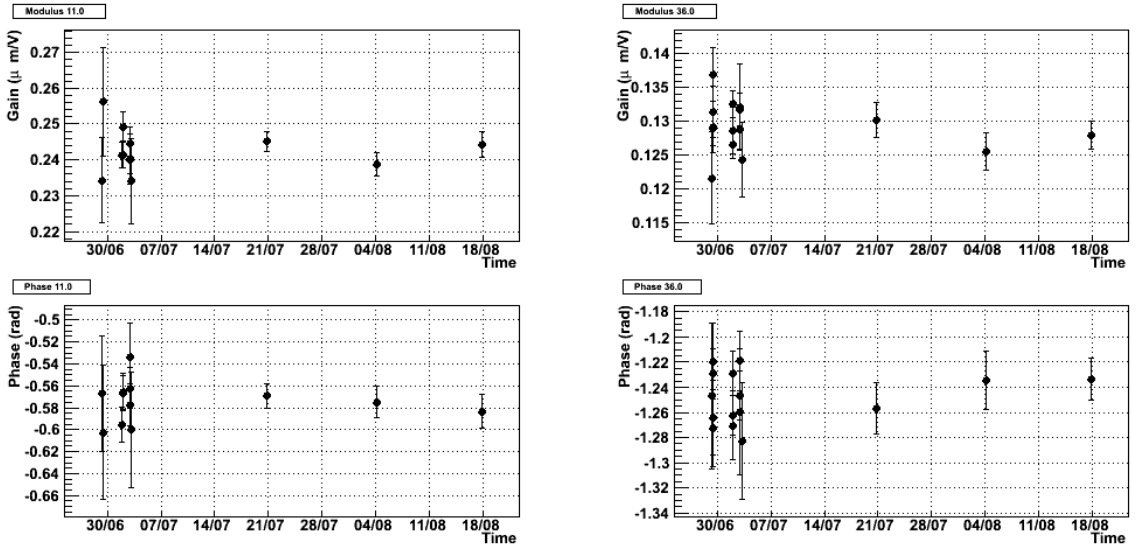

(a) 11.0 Hz

(b) 36.0 Hz

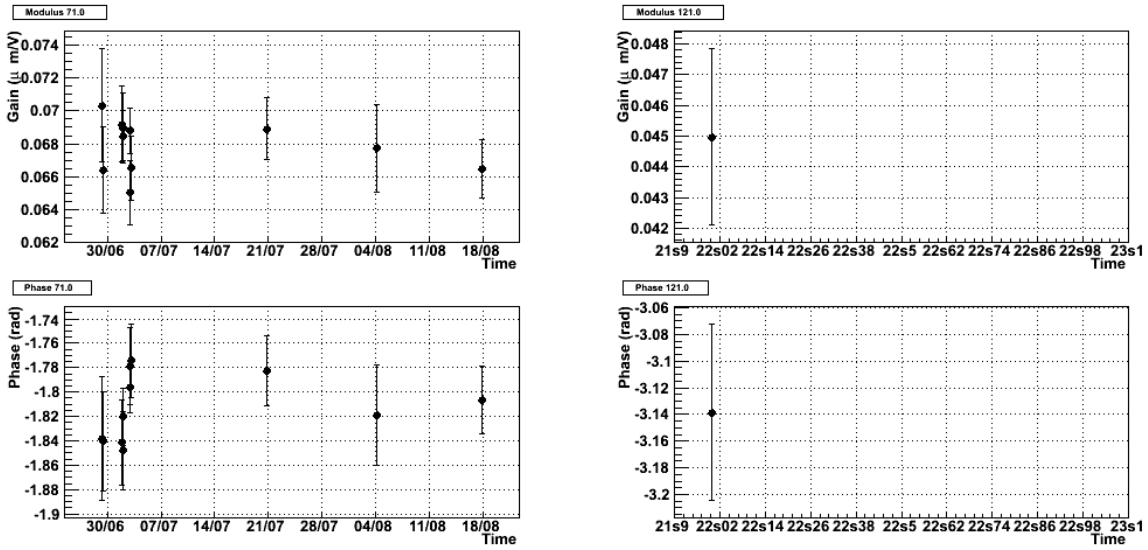

(c) 71.0 Hz

(d) 121.0 Hz

Figure 50: ***Measured NE marionette to mirror actuation (NE, U-D coils) TF ratio as function of time*** *at four different frequencies. The mirror and marionette actuations have been corrected for their pendulum mechanical models.*

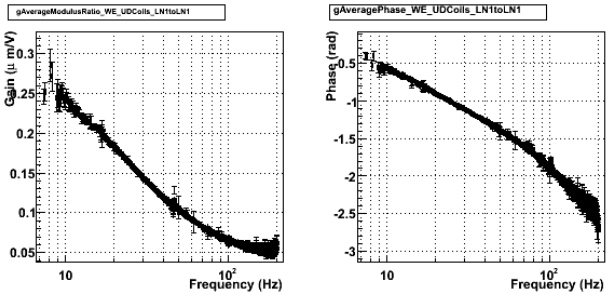

Figure 51: ***Averaged marionette to mirror actuation TF ratio of the WE suspension.*** *The mirror and marionette actuations have been corrected for their pendulum mechanical models.*

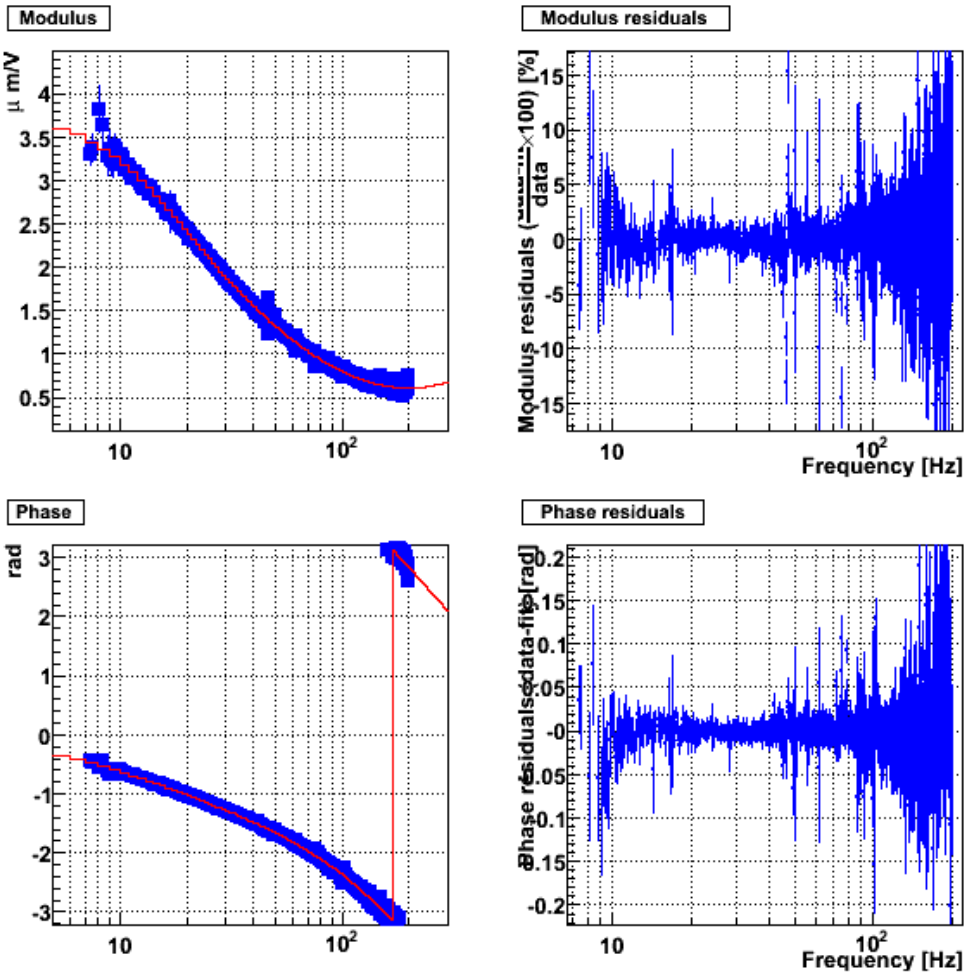

Figure 52: ***Measured WE marionette actuation TF****, fit and residuals.*

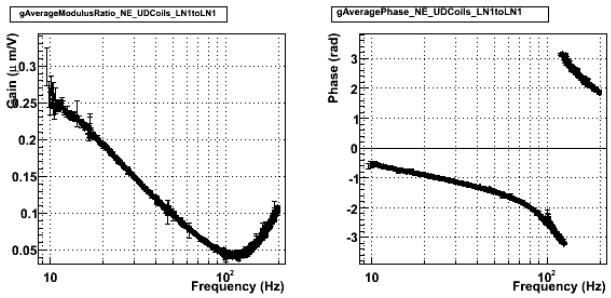

Figure 53: ***Averaged marionette to mirror actuation TF ratio of the NE suspension.***

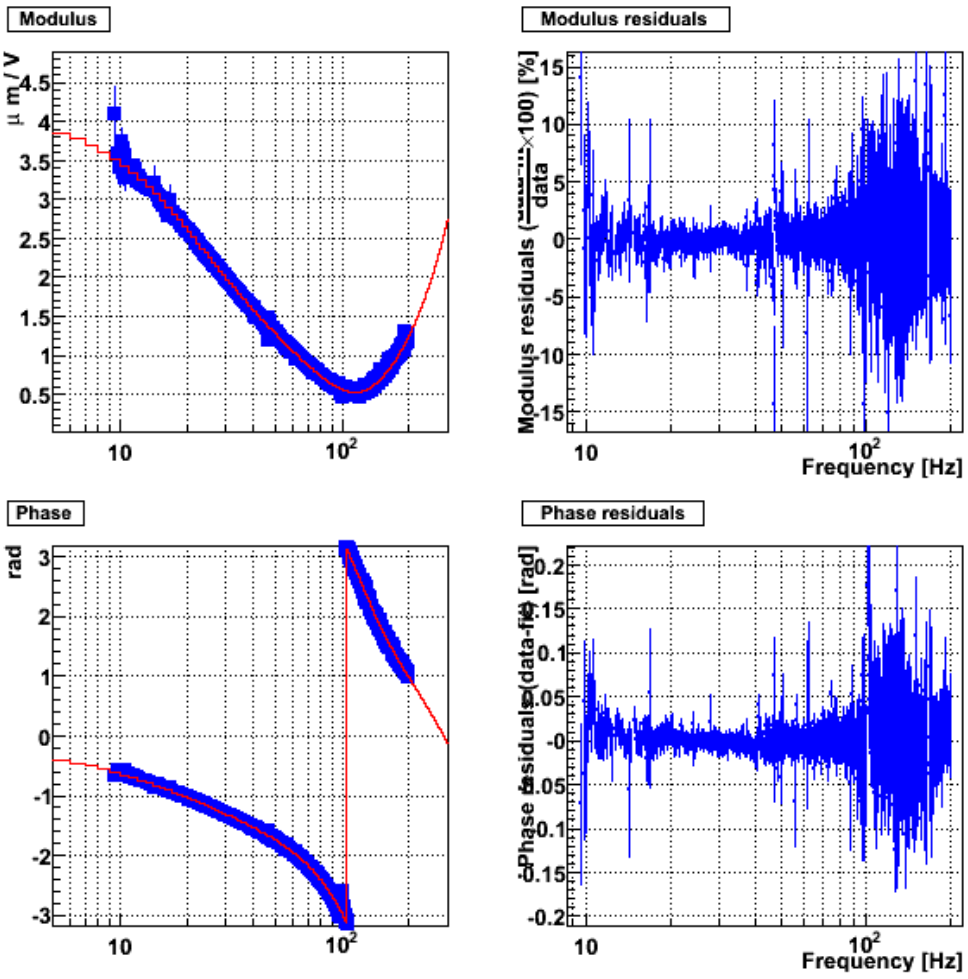

Figure 54: ***Measured NE marionette actuation TF****, fit and residuals.*

5 Conclusions

The first calibration for VSR2 has been computed with data from June 28th to September 1st 2009, including pre-run measurements and run periodic measurements.

The dark fringe readout has been calibrated, the timing being related to the absolute GPS time. The timing has been computed from the time series stored in FrVect setting the value of sample i at the time $startX[0] + i \times dx[0]$. The 20 kHz dark fringe channel models, given in the table 1, are understood from 1 Hz to 10 kHz within systematic errors of ± 4 μs. The 40 kHz dark fringe channel models, given in the table 2, are understood from 1 Hz to 10 kHz within systematic errors of $\pm 3\%$ in modulus, ± 30 mrad in phase and ± 4 μs. The time stability of the sensing response have been checked.

The mirror actuation in LN1 mode has been measured from 5 Hz to $\sim$1.5 kHz. The parameterizations are given in the tables 3 for the controls and 4 for the hardware injections. The delays are related to the absolute GPS time. Up to 1 kHz, the statistical errors are below 1%/10 mrad in modulus and phase respectively. The model residuals below 1.5 kHz are better than 2%/20 mrad.

The monitoring data reapeated every weeks or two weeks since the start of VSR2 show that the parameters have been stable within statistical errors from July to September 2009. The errors are dominated by systematic errors coming from the LN1/HP measurements: some coils show few percents dependence of the modulus ratio on the injected noise amplitude. A preliminary estimation of the systematic errors is $\sim 3\%$ on modulus. Observed phase variations are below 10 μs. More investigations are needed to better understand the observed variations.

Note that the PR mirror actuation has been measured yet.

The marionette actuation responses have been measured from 9 Hz to 200 Hz. The parameterizations are given in the table 5 for WE and NE. The delays are related to the absolute GPS time. The monitoring data during VSR2 and the different injected amplitudes did not show any variations within statistics. The systematic errors include the errors from the mirror actuation – $\sim 3\%$ in modulus and ~ 10 mrad in phase – and the residuals of the parameterizations: better than 5%/50 mrad, up to 100 Hz for WE and NE.

References

[1] S. Vilalte *Circuit Design of a Pulse Generator* (2003) VIR-0572A-09.

[2] N. Letendre, A. Masserot, B. Mours, *Virgo+ timing deployement* (2009) VIR-073B-08.

[3] B. Caron et al., Astroparticle Physics 10, 369-386 (1999), *SIESTA, a time domain, general purpose simulation program for the VIRGO experiment.*

[4] L. Rolland, F. Marion, B. Mours, *Mirror motion reconstruction for free swinging Michelson data* (2008) VIR-0112A-08.

[5] L. Rolland, F. Marion, B. Mours, *Mirror and marionette actuation calibration for VSR1* (2008) VIR-015A-08.

[6] A. Gennai, private discussion 2006

A Dark fringe ADC configuration

A.1 ADC configuration files -

The ADC configuration files can be found in the directory /virgoData/Adc7674.

Pr_B1 and Pr_B1p channels at 20 kHz - The configuration file of the ADC reading the Pr_B1 and Pr_B1p channels, sampled at 20 kHz, is PrB1_ADC0.cfg. The following lines define the digital anti-alias filter and sample frequency of the channels:

```
ADC7674_CHANNEL Pr_B1_d2_ACp  PrB1_ADC0 15 Butterworth_8_20dB  20000  0.0  0.5  volts
ADC7674_CHANNEL Pr_B1_d3_ACp  PrB1_ADC0  6 Butterworth_8_20dB  20000  0.0  0.5  volts

ADC7674_CHANNEL Pr_B1p_d2_ACp PrB1_ADC0  9 Butterworth_8_20dB  20000  0.0  0.5  volts
ADC7674_CHANNEL Pr_B1p_d2_ACq PrB1_ADC0 10 Butterworth_8_20dB  20000  0.0  0.5  volts
ADC7674_CHANNEL Pr_B1p_d2_DC  PrB1_ADC0  3 Butterworth_8_20dB  20000  0.0  0.5  volts

ADC7674_CHANNEL Pr_B1p_d1_ACp PrB1_ADC0 12 Butterworth_8_20dB  20000  0.0  0.5  volts
ADC7674_CHANNEL Pr_B1p_d1_ACq PrB1_ADC0 13 Butterworth_8_20dB  20000  0.0  0.5  volts
ADC7674_CHANNEL Pr_B1p_d1_DC  PrB1_ADC0 14 Butterworth_8_20dB  20000  0.0  0.5  volts

ADC7674_CHANNEL Ti_1PPS_GPSMaster PrB1_ADC0 11 Butterworth_8_20dB 20000 0.0 1.0 volts
```

Note that the slope of channel $Ti\_1PPS\_GPSMaster$ was 0.5 before September 8th 2009.

Pr_B1 channel at 40 kHz - The configuration file of the ADC reading the Pr_B1 channel at 40 kHz is $MoniDet.cfg$:

```
ADC7674_CHANNEL Pr_B1_d2_ACp_40K Moni_DET 0 Butterworth_8_20dB  40000  0.0  17.8  volts
                                                              # Shaping Mezzanine SN758
ADC7674_CHANNEL Pr_B1_d3_ACp_40K Moni_DET 1 Butterworth_8_20dB  40000  0.0  17.8  volts
                                                              # Shaping Mezzanine SN763
```

A.2 Additionnal information -

Some information about the channels are stored in the vectors and can be found in the raw data using such a command:

```
FrDump -i /virgoData/ffl/raw.ffl -f 936041082 -l 1 -t Pr_B1_d2_ACp -d 4
```

The comments stored in the power sensing readout vectors are listed here. The first part indicates the type of emphasis filter of the ADC board mezzanine and the mezzanine id number. The second part indicates the type of digital filter used in the ADC board. The delays introduced by the mezzanine anti-alias have been measured[20] at LAPP before their installation (within $\sim \pm 0.15\,\mu$s) and are also given in the following list:

- $Pr\_B1\_d2\_ACp$: `[V1-2CnN__Flat_AA@100kHz-132][Butterworth_8_20dB]`, $5.72\,\mu$s.
- $Pr\_B1\_d3\_ACp$: `[V1-2CnN__Flat_AA@100kHz-151][Butterworth_8_20dB]`, $5.71\,\mu$s.
- $Pr\_B1\_d2\_ACp\_40K$: `[V1-2C_Sh_2/12_AA@100kHz-758][Butterworth_8_20dB]`, ?.
- $Pr\_B1\_d3\_ACp\_40K$: `[V1-2C_Sh_2/12_AA@100kHz-763][Butterworth_8_20dB]`, ?.
- $Pr\_B1p\_d1\_DC$: `[V1-2CnN__Flat_AA@100kHz-82] [Butterworth_8_20dB]`, $5.78\,\mu$s.
- $Pr\_B1p\_d2\_DC$: `[V1-2CnN__Flat_AA@100kHz-155][Butterworth_8_20dB]`, $5.68\,\mu$s.
- $Pr\_B1p\_d1\_ACp$: `[V1-2CnN__Flat_AA@100kHz-181][Butterworth_8_20dB]`, $5.66\,\mu$s.
- $Pr\_B1p\_d2\_ACp$: `[V1-2CnN__Flat_AA@100kHz-172][Butterworth_8_20dB]`, $5.72\,\mu$s.
- $Pr\_B1p\_d1\_ACq$: `[V1-2CnN__Flat_AA@100kHz-153][Butterworth_8_20dB]`, $5.63\,\mu$s.
- $Pr\_B1p\_d2\_ACq$: `[V1-2CnN__Flat_AA@100kHz-150][Butterworth_8_20dB]`, $5.71\,\mu$s.
- $Ti\_1PPS\_GPSMaster$: `[V1-2CnN__Flat_AA@100kHz-83] [Butterworth_8_20dB]`, $5.68\,\mu$s.

[20] The measurement results can be found at LAPP in /virgoData/AdcTF/Results, in subdirectories per mezzanine serial number.

B Filter definitions

The definitions of the different filters used in the calibration prameterizations are given in this appendix.

B.1 Simple pole

A pole at frequency f_p is described as:

$$H(f) = \frac{1 - \mathrm{j}x}{1 + x^2}$$

where $x = \frac{f}{f_p}$.

The frequency f_p should be positive to have a stable filter.

B.2 Simple zero

A zero at frequency f_0 is described as:

$$H(f) = 1 + \mathrm{j}x$$

where $x = \frac{f}{f_0}$.

B.3 2nd order low-pass filter (complex pole)

A 2nd order low-pass filter at frequency f_0 with quality factor Q is described by:

$$H(f) = \frac{-f_0^2(f^2 - f_0^2) - \mathrm{j}\frac{f_0^3 f}{Q}}{(f^2 - f_0^2)^2 + (\frac{f f_0}{Q})^2}$$

The frequency f_0 should be positive to have a stable filter.

B.4 Complex zero

A complex zero at frequency f_0 with quality factor Q is described as the inverse of a 2nd order low-pass filter:

$$H(f) = \frac{1}{\frac{-f_0^2(f^2 - f_0^2) - \mathrm{j}\frac{f_0^3 f}{Q}}{(f^2 - f_0^2) + (\frac{f f_0}{Q})^2}}$$

B.5 8th order Butterworth filter

A 8th order Butterworth filter with a cut-off frequency f_0 is defined as:

$$H(s) = \frac{1}{(s^2 + 0,3902s + 1)(s^2 + 1,1111s + 1)(s^2 + 1,6629s + 1)(s^2 + 1,9616s + 1)}$$

where $s = \mathrm{j} \times \frac{f}{f_0}$.

C ADC and DAQ signal processing and timing

In this section, the way the signal is processed in the ADC and DAQ is explained. In particular, the way the data are time-flagged in the ADC and then stored in the frames is highlighted.

A synoptic of the processing is given in figure 55. A first thing to note is that there are different "clocks":

- 800 kHz clock: it is the clock used to sample the signal in the ADC. This clock is synchronised on the IRIG-B signal from the GPS receiver.
- 20 kHz clock: a sub-clock is created in the ADC board in order to subsample the 800 kHz signal to a 20 kHz signal.
- 10 kHz clock: defines the frequency for the ADC board to create and send the packets of data to the DAQ.

The 3 clocks are represented in the first line of the figure.

C.1 Timestamps

C.1.1 Timestamp set in the ADC board

In the ADC board, the signal is first sampled at 800 kHz. It then passes through a DSP where some filter can be applied. The signals of four DSPs are sent to one FPGA where some subsampling can be applied. After the FPGA, the signal is sent to the DAQ through an optical fiber by packets containing 100 μs (10 kHz) of data. Each packet contains a time stamp which is the time of the first sample of the ADC board. In practice, it is the time when the first sample is out of the FPGA: this means that it is 2.7 μs more than the real time of the sample that was frozen in the ADC: $t_{ADC} = t_{sample} + 2.7\ \mu$s.

C.1.2 Timestamp set in the DAQ

Concerning the dark fringe readout ADC board (at 20 kHz), the DAQ has a parameter, $PAGE\_DELAY$ set to 50. It means that the timestamps t_{ADC} of the packets received from the ADC board are modified: $t_{DAQ} = t_{ADC} - 50\ \mu$s.

C.1.3 Writing the data in frame with the FrameBuilder

When writing the data into the frames, the FrameBuilder uses the timestamp from the DAQ t_{DAQ} to check if the new packet is in a new frame or not (when the time passes over an integer number of seconds). The data are put in FrVect objects. In the data, the first sample of the first packet of the new frame is stored with the time of the frame $frame->GTimeS$. The following samples of a FrVect $vect$ have the time $frame->GTimeS + i \times vect->dx[0]$ where i is the sample number, starting at 0.

C.2 Sampling signals at 800 kHz

When sampling a signal at 800 kHz, all the samples after the ADC are output. The 10 kHz clock defines a new packet at t_0. The first sample, number 0, is the sample coincident with the 10 kHz clock. Thus the ADC gives a timestamp $t_0 + 2.7$ μs to the data of this packet. The DAQ then gives it a timestamp $t_{DAQ} = t_0 + 2.7 - 50$ μs. The FrameBuilder uses this timestamp t_{DAQ} to put the packet in a new frame (if the time is after an integer number of seconds) or in the same frame as the previous packet.

As a consequence (see figure 55), the net effect is that the data with the first sample frozen at t_0 are stored in the packet starting at $t_0 - 100$ μs: the 800 kHz data are advanced by 100 μs.

C.3 Sampling signals at 20 kHz

When sampling a signal at 20 kHz, the 800 kHz signal sampled by the ADC are subsampled in the DSP of the ADC board. The subsampling is done picking 1 sample out of 40: the 39th of the corresponding packet. The 10 kHz clock defines a new packet at t_0. The first sample, number 0, is the 30th 800 kHz sample. Thus the ADC gives a timestamp $t_0 + 48.75 + 2.7 \sim t_0 + 51.3$ μs to the data of this packet. The DAQ then gives it a timestamp $t_{DAQ} = t_0 + 51.3 - 50 = t_0 + 1.3$ μs. The FrameBuilder uses this timestamp t_{DAQ} to put the packet in a new frame (if the time is after an integer number of seconds) or in the same frame as the previous packet.

As a consequence (see figure 55), the net effect is that the data with the first sample frozen at $t_0 + 48.75$ μs are stored in the packet starting at t_0 μs: the 20 kHz data are advanced by 48.75 μs.

C.4 Sampling signals at different frequencies

When two signals are sampled at different frequencies, the timestamp of the 10 kHz packet of data is based on the time of the first sample of the signal with the highest sampling rate.

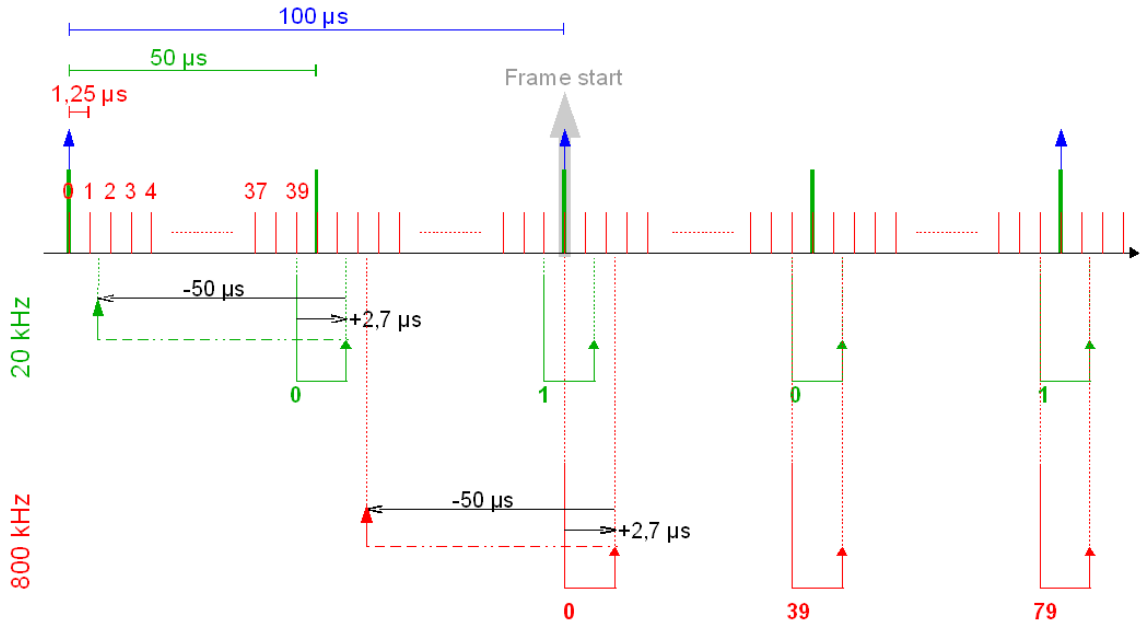

Figure 55: ***Synoptic of the timing processing including the digital part of the ADC and the DAQ*** *for the sampling at 20 kHz and 800 kHz.*